Title
Development of RNA Sensors for Cyclic Dinucleotide Second Messengers in Bacteria

Author
Kellenberger, Colleen Ann

Publication Date
2014

Peer reviewed|Thesis/dissertation

Development of RNA Sensors for Cyclic Dinucleotide Second Messengers in Bacteria

By

Colleen Ann Kellenberger

A dissertation submitted in partial satisfaction of the

requirements for the degree of

Doctor of Philosophy

in

Chemistry

in the

Graduate Division

of the

University of California, Berkeley

Committee in charge:

Professor Ming C. Hammond, Chair
Professor Carolyn R. Bertozzi
Professor Daniel A. Portnoy

Fall 2014

Abstract

Development of RNA Sensors for Cyclic Dinucleotide Second Messengers in Bacteria

by

Colleen Ann Kellenberger

Doctor of Philosophy in Chemistry

University of California, Berkeley

Professor Ming C. Hammond, Chair

Second messengers are intracellular signaling molecules that enable cells to respond to environmental changes by relaying signals received at the cell surface to enact downstream physiological effects. A recently expanded class of second messengers in bacteria are the cyclic dinucleotides, which include cyclic di-GMP (cdiG), cyclic di-AMP (cdiA), and 3′,3′ cyclic AMP-GMP (cAG). In bacteria, these messengers regulate processes ranging from chemotaxis and sporulation to antibiotic resistance and virulence. Recent studies have found that bacterial cyclic dinucleotides, as well as a mammalian 2′,3′ cAG homolog, trigger the innate immune response upon detection in the mammalian cell cytosol. However, many components and roles of cyclic dinucleotide signaling remain unidentified or poorly understood. A clear understanding of cyclic dinucleotide signal transduction would further the pursuit of these signaling pathways as therapeutic targets and the effects of using cyclic dinucleotides as small molecule adjuvants. Herein, novel strategies for cyclic dinucleotide detection are reported that use that natural ability of riboswitch RNAs to discriminate between these nucleotide-based messengers.

First, a microfluidic electrophoretic mobility shift assay (μMSA) is presented that enables highly sensitive and rapid detection of cdiG *in vitro*. This method takes advantage of the ligand-induced conformational change of a natural cdiG GEMM-I class riboswitch aptamer, termed Vc2. This same aptamer was then converted to a fluorescent biosensor for live-cell imaging by fusing it to the Spinach aptamer, an RNA mimic of GFP. This Vc2-Spinach RNA-based biosensor senses low levels of endogenous cdiG in *Escherichia coli* and responds to increased levels of cdiG upon coexpression of a heterologous cdiG synthase. A similar Spinach-based strategy was used to develop a cdiA RNA-based biosensor through fusion to riboswitches from the recently reported ydaO class. This cdiA sensor is the first tool for live cell imaging of cdiA and provided the first demonstration of the Spinach system in *Listeria monocytogenes*, an important gram-positive intracellular pathogen. Finally, as no known biosensor existed for 3′,3′ cAG, rational engineering of a cdiG aptamer led to the discovery of a subclass of GEMM-I riboswitches in *Geobacter* species that is naturally specific for 3′,3′ cAG. Further analysis revealed that this novel riboswitch subclass, which represents the first

known effector for this messenger, is important in regulating the process of extracellular electron transfer in *Geobacter* and these riboswitches were used to develop the first biosensor specific for 3′,3′ cAG. It is envisioned that the use of these cyclic dinucleotide-specific sensors can be used to further identify unknown components in the signal transduction of these important regulatory molecules.

Dedicated to my family – past, present, and future.

TABLE OF CONTENTS

ACKNOWLEDGEMENTS

This work would not have been possible without the support of many people. First, I would like to thank my adviser, Dr. Ming Hammond for all of her guidance over the past five years and for helping to develop me into the scientist I am. Additionally, my fellow graduate students in the Hammond lab, Scott, Tania, Cindy, Zach, and Yichi have all contributed to useful discussions and I thank them for making the lab such a great environment. I especially thank Scott Hickey for being my cohort from the beginning and let's just hope Love-to-Pour remains in good hands.

Many collaborators have provided key expertise and insight into areas we would have never expected to enter at the onset of this project. Our microfluidic chip collaborators, Peter Y. Pan and Dr. Amy Herr, have saved us from many painstaking hours of standard gel electrophoresis. Our *Listeria* and cyclic di-AMP project collaborators, Dr. Chen Chen and Dr. Dan Portnoy, have enabled us to foray into interesting experiments in microbiology. I owe a special thanks to Dan for an afternoon of discussing career choices and for letting me into his group meetings to try and bend my mind toward microbiology. Also, I was very fortunate to have received a National Defense Science and Engineering Graduate (NDSEG) Fellowship, which has supported a great deal of this research.

Finally, I owe everything to my family for getting me where I am today. To my parents, Kathy, Gregg, and Becca, I am endlessly grateful for their support and their ever-present willingness to listen. My brother, Kevin, and his wife, Stefanie, keep me laughing. My support network of Aunts, Uncles, and cousins is incredible and I am incredibly grateful for my godmother Aunt MaryBeth, who was one of my first inspirations to go into science. Lastly, I cannot thank enough the endless support of my fiancé, Dr. Geoffrey Feld, and his dog(tor) Patton, with whom I look forward to beginning a new adventure in North Carolina.

CHAPTER 1

An Introduction to Cyclic Dinucleotide Second Messengers

Although bacteria are often portrayed negatively due to the low percentage that cause disease, these microorganisms play an extensive number of roles including many that are beneficial to health or the environment. For instance, recent studies have found that the human intestinal microbiome consists of over a trillion bacterial cells, comprising at least 1,000 different species, and that several of these species are required for their production of essential vitamins or for absorption of iron from the intestine (Kim et al., 2013; Wallace and Redinbo). However, even these organisms are forced to adapt their behaviors to endure in altered environmental conditions, such as when the intestine is infected by the bacterial pathogen *Vibrio cholerae* and commensal bacterial populations must acclimate to a change in water and electrolyte flux or else be eliminated (Pukatzki and Provenzano, 2013). Bacteria in general are often faced with distinctly contrasting settings to which they must adapt their behavior in order to survive, which range from the intestinal microbiota evolving to the diet of the human host, to the *Vibrio cholerae* transitioning from survival in estuaries to colonization of the human gut, where it begins the intensive multiplication that leads to cholera.

At the center of a bacterium's ability to adapt are signal transduction pathways, which enable the cell to respond to a change in the cellular environment to enact a change in cell lifestyle. These pathways consist of a primary signal that triggers a series of molecular interactions or modifications that leads to an alteration in gene regulation. However, this process is often complicated by the fact that the primary signal in the environment, often in the form of a small molecule or peptide, is unable to pass through the cell membrane. To circumvent this issue, many cells use membrane-bound receptors that directly or indirectly alter the concentration of a freely diffusible second messenger inside the cell. Second messengers then propagate the signal by binding to a vast array of effector targets, including enzymes, transcription factors, and other allosteric regulators such as riboswitch RNAs.

A recently expanded class of second messengers in bacteria are the cyclic dinucleotides, which include 3′-5′, 3′-5′ cyclic di-GMP (cdiG), cyclic di-AMP (cdiA), and cyclic AMP-GMP (3′,3′ cAG) (Figure 1.1). These messengers are present in diverse bacterial species and regulate important processes including chemotaxis, biofilm formation, and bacterial pathogenicity (Danilchanka and Mekalanos, 2013). For example, while in the environmental bacterium *Gluconacetobacter xylinum* cdiG activates the production of cellulose (Ross et al., 1987), increased cdiG levels in the pathogenic bacterium *Vibrio cholerae,* and in many other bacteria (Table 1.1), transition bacteria from a motile to a sessile, biofilm-forming state (Krasteva et al., 2010). However, due to the highly integrated role second messengers play as intermediates in numerous signaling pathways, many of the components and mechanisms involved in second messenger signaling remain poorly understood. Countless questions remain about the central regulatory roles of cyclic dinucleotides, especially with regard to cdiA and cAG, which were just discovered as natural molecules within the past five years. Discussed below is an overview of the current known factors involved in cyclic dinucleotide signaling, along with a summary of current tools and their limitations for studying cyclic dinucleotide biology.

1.1 Discovery of cyclic dinucleotide second messengers

Benziman and coworkers discovered the first cyclic dinucleotide second messenger, cyclic di-GMP (cdiG), which they reported activates cellulose synthesis in the bacterium *Gluconacetobacter xylinum*, an important biological resource for lignin-free cellulose (Ross et al., 1987). Since then, cdiG synthesis and degradation enzymes have been identified as nearly ubiquitous in bacteria, with especially high abundance in gram-negative Proteobacteria, including *Vibrio cholerae* and *Yersinia pestis*, the causative agents of the devastating diseases such as cholera and plague, respectively (Römling et al., 2013). Surprisingly, while cdiG regulatory factors are not predicted to be in Archaea, a cdiG synthase was identified in the eukaryote *Dictyostelia* (Chen and Schaap, 2012; Seshasayee et al., 2010).

The second messenger cyclic di-AMP (cdiA) was discovered serendipitously in the crystal structure of the DNA integrity scanning protein (DisA) from *Bacillus subtilis*, where a single molecule of cdiA was identified at each of the four dimer interfaces of this octameric complex (Witte et al., 2008). Further study revealed that DisA synthesizes cdiA as it scans along DNA, but that synthase and scanning activity are arrested upon encountering a DNA lesion, thus delaying *B. subtilis* sporulation (Witte et al., 2008). Bioinformatic analysis predicts that this messenger is also widespread in bacteria, especially in gram-positive bacteria of the phyla Firmicutes and Actinobacteria that encompass many bacterial pathogens, including the causative agents of listeriosis Staph infections, and Chlamydia, and in a subset of archaea of the phylum Euryarchaeota (Corrigan and Gründling, 2013).

The final cyclic dinucleotide second messengers, 3′-5′,3′-5′ cyclic AMP-GMP (3′,3′ cAG) along with the mammalian analog 2′-5′,3′-5′ cyclic AMP-GMP (2′,3′ cAG) were discovered in searching for pathogenesis determinants in bacteria and eukaryotes (Davies et al., 2012; Wu et al., 2013). First, 3′,3′ cAG was found in *Vibrio cholerae* as the product of the enzyme dinucleotide cyclase *Vibrio* (DncV) (Davies et al., 2012). This enzyme, while it can produce cdiA, cdiG, and 3′,3′ cAG *in vitro*, preferentially synthesizes 3′,3′ cAG both *in vitro* and *in vivo* and its expression is important for *Vibrio cholerae* pathogenesis (Davies et al., 2012). Furthemrore, the first mammalian cyclic dinucleotide analog, 2′,3′ cAG (also known as cGAMP), was isolated as the compound that activates the innate immune response in metazoans upon viral DNA infection (Sun et al., 2013; Wu et al., 2013). Contrary to cdiG and cdiA, early bioinformatics analyses searching for signaling components related to either analog of cAG indicate that their synthases have limited homology in bacteria and eukaryotes, as discussed in the next section. While these four purine-based molecules comprise the class of currently known bacterial second messengers, it remains to be seen whether other structural analogs will be discovered to play a role in bacterial or eukaryotic signaling.

1.2 Cyclic dinucleotide signaling in bacteria

Synthesis and Degradation

As cdiG is the longest-studied cyclic dinucleotide, it can serve as a model for signal transduction by cyclic dinucleotides in bacteria (Figure 1.2). In response to

various environmental cues, such as blue light (Gomelsky and Klug, 2002), nitric oxide (Liu et al., 2012; Plate and Marletta, 2012), or quorum sensing molecules (Deng et al., 2012), levels of cdiG are regulated by diguanylate cyclases and phosphodiesterases, which synthesize and degrade cdiG, respectively. Diguanylate cyclases (DGCs) contain a conserved GGDEF amino acid motif and synthesize cdiG from two GTP molecules as a homodimeric complex. Alternatively, cdiG is hydrolysed into pGpG or two 5′-GMP molecules by phosphodiesterases (PDEs) with a conserved EAL or HD-GYP domain, respectively (Römling et al., 2013). Notably, GGDEF, EAL, and HD-GYP domain-containing proteins are highly abundant in many bacteria; however, the latter two remain largely uncharacterized. The first report that the GGDEF amino acid sequence could confer cdiG synthase activity (Ausmees et al., 2001) opened the door to the enticing possibility of widespread cdiG signaling, as bioinformatics studies have found a total of 11,248 GGDEF and/or EAL domain proteins from 618 out of 867 fully-sequenced prokaryote genomes (Seshasayee et al., 2010).

The high multiplicity of these proteins begs the question for the necessity of such an array, and furthermore how these enzymes interact to regulate overall cdiG levels. One hypothesis is that they are expressed differentially in response to various environmental cues or due to regulation by various transcription factors, such as the RpoS transcription factor in *E. coli* (Sommerfeldt et al., 2009). Tight control of the overall cdiG pool seems to partially be regulated by localization and specificity of proximal effectors that interact with each other (Hobley et al., 2012; Kulasekara et al., 2006). Also of interest is that many proteins (>34%) contain GGDEF and EAL or HD-GYP domains arranged in tandem (Seshasayee et al., 2010). In these proteins, there are cases of bifunctionality, where activity of either domain is regulated by environmental factors, interaction with protein partners (Boles and Mccarter, 2002; Ferreira et al., 2008; Tarutina et al., 2006), or loss of activity of one domain, where either the DGC or PDE has become inactive through mutation of the conserved catalytic domain (Christen et al., 2005; Römling et al., 2013). In these inactive proteins, cdiG or GTP often bind to the degenerate domain to regulate enzymatic activity (Christen et al., 2005), although these tandem proteins remain largely unstudied.

Cyclic di-AMP signaling appears to share a similar regulatory network as cdiG (Figure 1.3). The messenger cdiA is synthesized from two molecules of ATP by diadenylate cyclases (DACs), which contain a conserved DisA_N domain, and is hydrolyzed into pApA by cdiA-specific PDEs, termed GdpP (GGDEF domain containing PDE) (Corrigan and Gründling, 2013). In contrast to cdiG, environmental signals that control cdiA levels remain unidentified and also DACs are typically present in only one copy per bacterial genome (Corrigan and Gründling, 2013), with the notable exception of *Bacillus subtilis*, which contains three confirmed DACs. It is interesting that cdiA-specific phosphodiesterases also contain a modified GGDEF domain, indicating another role of degenerate GGDEF domains, although enzymatic activity lies within the phosphoesterase DHH domain (Rao et al., 2010). It is believed that another class of cdiA phosphodiesterases might exist since GdpP-type proteins have only been found in bacteria of the phyla Firmicutes and Tenericutes, yet not in Actinobacteria where many DACs have been predicted. Attempts to delete the diadenylate cyclase gene in

Streptococcus pyogenes or *Listeria monocytogenes* grown in rich media have previously been reported unsuccessful (Kamegaya et al., 2011; Witte et al., 2013; Woodward et al., 2010), indicating that cdiA is essential under these conditions.

The only confirmed synthase for bacterial 3',3' cAG is the enzyme DncV found in the 7th pandemic El Tor biotype of *V. cholerae* (Figure 1.4) (Davies et al., 2012). This enzyme is encoded in a genomic island that distinguishes the most recent pandemic from previous, classical strains. DncV has homologs with 20% sequence similarity encoded in the pathogenic islands of many other pathogenic bacteria, but their 3',3' cAG synthase activity has yet to be demonstrated (Davies et al., 2012). The mammalian 2′,3′ cAG synthase, cGAS, produces this messenger in response to the presence of cytosolic DNA in mammalian cells (Sun et al., 2013). The cGAS enzyme has been predicted to have appeared as early as the choanoflagellate *Monosiga brevicollis*, although the DNA sensing function of this messenger in invertebrates is unclear (Wu et al., 2014). Intriguingly, both DncV and cGAS have homology to human oligoadenylate cyclases and are in the class III nucleotidyl transferase superfamily of proteins (Wu et al., 2014), raising speculation about how the most recent strain of *V. cholerae* acquired this synthase with metazoan homology. As of yet, no specific cAG-specific phosphodiesterases have been identified for either analog.

Effectors and Outputs

Fluctuating levels of cdiG and cdiA are detected and transduced in the cell by effectors at both the protein and the RNA level (Figures 1.2 and 1.3). While cyclic dinucleotide binding proteins are quite diverse, they can generally be classified into allosteric, inhibitory and transcriptional regulators. RNA effectors consist of cyclic dinucleotide-binding riboswitches, which are allosteric regulators typically found in the 5′ untranslated region (UTR) of mRNAs that are able to regulate expression of the downstream gene through binding a small molecule. The processes regulated by protein and RNA effectors overlap, indicating multiple modes of regulating a signal output.

Cyclic di-GMP protein effectors are highly diverse and include PilZ domain proteins, degenerate GGDEF or EAL proteins, and transcriptional regulators belonging to many different classes (e.g., CRP/FNR-type in *Xanthamonas* and *Burkholderia*, and GsgD/LuxR-type in *Vibrio*) (Römling et al., 2013). Binding of cdiG to these proteins leads to regulatory changes in several essential processes including bacterial motility, chemotaxis, biofilm formation, and cell differentiation. Additionally, cdiG levels regulate many different aspects of bacterial virulence, including expression of virulence regulators, host cell invasion, cytotoxicity, secretion of virulence factors, and host cell adherence (Ahmad et al., 2011; Kulasekara et al., 2006; Lee et al., 2007; Römling et al., 2013; Tischler and Camilli, 2004). Yet, it is likely that many more cdiG effectors exist but have evaded bioinformatic prediction since the number of enzymes involved in cdiG metabolism still exceeds the number involved in receiving cdiG signals (Römling et al., 2013). Further complicating cdiG signaling is that even cdiG receptors come in binding competent and incompetent forms (i.e., "active" and "degenerate" forms), for example the eponymous PilZ protein from *Pseudomonas aeruginosa* is unable to bind cdiG (Li et

al., 2009). Further elucidation of cdiG signaling effectors will clarify the extensive regulatory networks of this molecule, allowing these pathways to be targeted in manipulating bacterial virulence.

Relatively few cdiA protein effectors have been identified, but the currently characterized receptors are quite distinct in their regulatory domains. These receptors are thus far limited to *Listeria monocytogenes*, *Mycobacterium smegmatis*, *Staphylococcus aureus*, and *B. subtilis*, where cdiA binds to proteins involved in central metabolism, ion transporters, cell wall homeostasis, and DNA integrity and sporulation (Corrigan and Gründling, 2013; Sureka et al., 2014). However, many of these processes though have missing links between the relative cdiA levels and factors leading to a given output. Further study is necessary to identify these unknowns and gain insight into the other processes are regulated by this essential signaling molecule.

Riboswitches offer an alternative method of gene regulation through a ligand-induced conformational change of the mRNA that alters either transcription or translation of the downstream gene. Three classes of riboswitches for cdiG and cdiA have recently been reported that bind these ligands with high specificity and affinity. Two different classes of GEMM (Genes for the Environment for Membranes and for Motility) riboswitches bind cdiG and are located upstream of many genes involved in pili and flagella formation, chemotaxis, chitin binding, and many other signal transduction components. The ydaO class of riboswitches binds specifically to cdiA and regulates the expression of genes involved in cell wall metabolism, ion transporters, and other broad signaling pathways (Nelson et al., 2013). Similar to the distribution of cdiG and cdiA metabolism enzymes, GEMM and ydaO riboswitches are both widespread throughout bacteria, with high prevalence in gram-negative and gram-positive bacteria, respectively (Block et al., 2010; Nelson et al., 2013; Sudarsan et al., 2008; Weinberg et al., 2007).

Although no receptors have yet been found for 3′,3′ cAG, it is known that expression of its synthase DncV leads to increased virulence, decreased chemotaxis, and increased fatty acid biosynthesis in *V. cholerae* (Davies et al., 2012). The latter two of these outputs have further been shown to play roles in bacterial virulence, where decreased chemotaxis has been correlated with a hyperinfective state (Butler et al., 2006) and fatty acids appear to regulate the activity of the ToxT virulence factor in *V. cholerae* (Lowden et al., 2010). Identification of effectors and other outcomes of 3′,3′ cAG signaling will provide further insight into the overall significance of this signaling molecule.

1.3 Cyclic dinucleotide signaling in eukaryotes

While traditionally only thought of as bacterial signaling molecules, roles for cyclic dinucleotides in eukaryotic cell signaling are beginning to emerge (Schaap, 2013). First, 2′,3′ cAG is the first cyclic dinucleotide that appears to be specific to eukaryotic signaling (Ablasser et al., 2013; Diner et al., 2013; Gao et al., 2013a). In response to cytosolic detection of dsDNA, cGAS produces 2′,3′ cAG, which binds to the endoplasmic reticulum-associated adaptor STimulator of INterferon Genes (STING) and triggers the innate immune response through activation of kinases TBK1 and IKK that

subsequently activate type-I interferon transcription factors including IRF3, STAT6, and NF-κB (Sun et al., 2013). Previous discoveries had identified that secretion of cdiA by the intracellular pathogen *Listeria monocytogenes* into the host cell cytosol triggered the same immune response (Woodward et al., 2010), and further studies confirmed this possible for all three bacterial cyclic dinucleotides (Burdette et al., 2011; Diner et al., 2013). Recent studies however, raised controversy over the relative affinities of STING for bacterial cyclic dinucleotides versus 2′,3′ cAG (Gao et al., 2013a; Zhang et al., 2013b), but crystal studies show that only 2′,3′ cAG and 3′,3′ cAG, but not cdiG, are able to elicit a significant conformational change upon binding STING (Gao et al., 2013b; Zhang et al., 2013b). Further study is required to fully elucidate the roles bacterial cyclic dinucleotides versus 2′,3′ cAG in innate immune signaling in different species (Hansen et al., 2014).

Roles of cyclic dinucleotides outside of the innate immune response include a developmental transition in Dictyostelia and a possible role in gating the pacemaker current in mammalian cells (Chen and Schaap, 2012; Lolicato et al., 2014). First, the social amoeba *Dictyostelia discoideum* uses cdiG as an intercellular signal to transition from a motile slug to a fruiting body (Chen and Schaap, 2012). These amoebas contain a DGC, DgcA, expressed at the tip of the slug and disruption of this gene prevents stalk formation to form the fruiting body. Addition of cdiG to the media restores the ability of fructification, but interestingly, no other components of cdiG signaling have been identified in the organism, raising the question of how this cdiG signal is identified and transduced.

Additionally, cyclic dinucleotides are able to bind the hyperpolarization-activated cyclic nucleotide-gates (HCN) channel important in regulating the pacemaker current in sinoatrial node cells (Lolicato et al., 2014). In modeling studies of the HCN channel, it was discovered that a cyclic dinucleotide would likely bind to an inhibitory site in this voltage-gated channel, thus reducing the pacemaker current. Electrophysiology studies confirmed that all four cyclic dinucleotides are capable of this pace reduction, and subsequent studies were aimed at identifying other compounds that had potential for clinical use (Lolicato et al., 2014). It remains to be determined, however, whether this inhibitory activity is physiologically relevant and whether cyclic dinucleotides are actually present in this cell type.

1.4 Detection of cyclic dinucleotides

As detailed above, many questions remain with regard to cyclic dinucleotide regulation, yet a comprehensive understanding of cyclic dinucleotide signaling requires methods for detecting how the levels of these molecules are changed under different conditions. Several methods for *in vitro* detection of cyclic dinucleotides are available, yet *in vivo* methods of cyclic dinucleotide measurement only exist for cdiG. To date, only intracellular levels of cdiG and cdiA have been measured, with concentrations ranging from <50 nM to low micromolar for cdiG and low micromolar concentrations of cdiA (Corrigan et al., 2011; Hengge, 2009; Oppenheimer-Shaanan et al., 2011), thus sensitive and dynamic detection methods are required. Current methods and their

limitations are described below, as well as an outlook for cyclic dinucleotide detection using a novel, RNA-based approach.

In vitro *detection of cdiG*

The most widely used method for cyclic dinucleotide detection uses high performance liquid chromatography coupled mass spectrometry (HPLC-MS), which can be applied to study any cyclic dinucleotide. This method is sensitive (limit of detection ~ 2 nM for cdiG) (Simm et al., 2009; Spangler et al., 2010), yet typically requires sample purification prior to HPLC, is low-throughput, and requires liquid chromatography methods with high-resolving power to separate the structurally similar cyclic dinucleotides. This method has been used extensively for cdiG (Simm et al., 2009; Spangler et al., 2010), and has been used to determine that cdiA (Woodward et al., 2010) and 2',3' cAG (Wu et al., 2013) were immunostimulatory molecules, and to prove that 3',3' cAG was the predominant product of DncV *in vitro* and *in vivo* (Davies et al., 2012).

Many methods for cdiG detection take advantage of its distinct ability to form highly H-bonded structures called G-quadruplexes. Quadruplex formation requires certain monovalent or divalent cations and only occurs in the presence of at least low micromolar levels of cdiG, thus inherently limiting the sensitivity of these assays (Nakayama et al., 2011). One such method uses circular dichroism (CD) to monitor levels of cdiG (Stelitano et al., 2013). G-quadruplexes formed by cdiG are optically active due to the hyperchromic effect of the four stacked bases, which leads to an increased CD signal. Formation of the cdiG dimer is fast (within 5 min), allowing the enzymatic activities of DGCs and PDEs (PleD and RocR, respectively in Stelitano et al., 2013) to be monitored in real-time.

Other G-quadruplex-based intercalation methods include a thiazole orange dye and a peroxidation-based colorimetric assay (Nakayama et al., 2011, 2012a). Thiazole orange dye fluoresces upon intercalation into cdiG G-quadruplexes and this method has been used to examine the activity of the *Pseudomonas fluorescens* diguanylate cyclase WspR and the levels of cdiG from *E. coli* cell lysates (Nakayama et al., 2011). The peroxidation assay takes advantage of the propensity of hemin to be oxidized when it pi-stacks with a G-quadruplex. Formation of the G-quadruplex is favored in this assay through the addition of the proflavin intercalator, and then cdiG levels are measured based on the subsequent oxidation by hemin of the colorless compound 2,2'-azino-bis(3-ethylbenzothiazoline-6-sulfonic acid) (ABTS) to a colored, radical cation state. Though this method is complex and indirect, it was successfully used to compare cdiG levels from *E. coli* cell lysates that had either a DGC or PDE overexpressed (Nakayama et al., 2012a).

Although cdiA and cAG do not form canonical G-quadruplex structures, small molecule probes have been developed to detect them *in vitro* using their base-stacking capabilities. For cdiA, the coralyne dye, which is known to form complexes with linear polyA oligonucleotides, is able to form a fluorescent complex when bound to cdiA multimers (Zhou et al., 2014). Additionally, the molecule 3',3' cG(d2AP)MP, which is a

2-aminopurine cAG analog, can intercalate with mixtures of cdiG and 3',3' cAG, resulting in fluorescence quenching (Roembke et al., 2014). Both assays were used to monitor the activities of a DGCs and DACs as well as phosphodiesterases, though in the case of 3',3' cG(d2AP)MP, the intercalator is also cleaved by PDEs.

Overall, intercalation-based methods suffer from poor sensitivity due to the relatively high ligand concentrations required to form these complexes. As many different stoichiometries of intercalation and G-quadruplex formation can exist, these methods are not a direct measurement of ligand concentration. Additionally, intercalation-based methods often require stringent protein purification as cyclic dinucleotide binding proteins co-elute with cyclic dinucleotides and they must be removed for biochemical analysis. Due to the tight regulation of cyclic dinucleotides, for example, the regulation of cdiG by many metabolic enzymes, *in vitro* methods that can detect submicromolar changes in cdiG concentration are required in order to understand these complex signaling pathways.

Detection of cyclic dinucleotide-protein interactions

Other *in vitro* methods are aimed at studying specific protein-ligand interactions. Several cyclic dinucleotide analogs, such as fluorescent, biotinylated, and magnetic bead-coupled molecules, have been synthesized or are available from commercial vendors. These analogs have been used to analyze binding of various cdiG protein receptors (Luo et al., 2012) and also in affinity pull-down assays to identify novel cdiA-binding proteins (Corrigan et al., 2013). One complication with these analogs is that the modification to the cyclic dinucleotide might not always be tolerated by the interacting biomolecule (Luo et al., 2012), thus potentially producing many false negatives and inhibiting the discovery of otherwise active binding partners.

A high-throughput method for identification and characterization of proteins that bind cyclic dinucleotides is Differential Radial Capillary Action of Ligand Assay (DRaCALA), where radiolabeled ligand is incubated with a protein of interest, then is applied to nitrocellulose to examine the interaction (Roelofs et al., 2011). If the protein binds to ligand, the interaction of the protein with nitrocellulose will cause the radioactive signal to remain localized, but unbound ligand will diffuse on the membrane through capillary action, causing the radioactive signal to disperse. This is a high sensitivity, high throughput assay that was successfully used to identify a novel cdiG binding domain in proteins, termed GIL (Fang et al., 2014; Roelofs et al., 2011). While this method is able to be used with crude cell lysates, one limitation of this method is that it is can only detect protein-ligand interactions and would not be able to examine RNA-binding motifs, such as with riboswitches or any undiscovered non-coding RNAs that interact with cyclic dinucleotides.

Live cell imaging techniques

Live cell imaging techniques for cyclic dinucleotides are powerful, yet their development can be challenging. Besides work published herein, the only *in vivo* techniques reported are protein-based Förster Resonance Energy Transfer (FRET) sensors (Christen et al., 2010; Ho et al., 2013), as no small molecule reporters that

selectively react with cyclic dinucleotides have yet been developed. To date three biosensors have been engineered by fusing fluorescent proteins to natural PilZ-domain cdiG protein receptors. These sensors display a range of affinities (dissociation constants (K_d): 0.12-2.1 μM) and have been used to monitor dynamics of cdiG in live cells. For example, the seminal cdiG biosensor based on the YcgR effector from *Salmonella enterica*, was used to show the asymmetrical distribution of cdiG during cell division in *Caulobacter crescentus* and *Pseudomonas aeruginosa*. Interestingly, all three are turn-off sensors, as they undergo a loss of FRET as cdiG binds.

Outlook

As described here, detection methods for sensitive, high throughput, and especially live cell imaging of cyclic dinucleotides remain underdeveloped. An area that has long remained unexplored for small molecule detection is the use of the highly discriminatory recognition of specific small molecules by RNA. As mentioned previously, riboswitches are natural small molecule receptors that use allosteric regulation to affect gene control. Previously, riboswitches have been used as small molecule reporters through fusion of the riboswitch sequence to a reporter gene, such as lacZ or GFP (Fowler et al., 2010; Topp et al., 2010), which bind sensitively and specifically to the small molecule, but dynamic regulation of these reporters is lost once the protein has been expressed and reduction of signal is no longer dependent on ligand concentration.

Highly sensitive and specific riboswitches for cdiG and cdiA have been reported (Nelson et al., 2013; Sudarsan et al., 2008), but these RNAs remain largely unexplored as small molecule sensors. Herein are described distinct methods for sensitive, high throughput and live cell imaging of cyclic dinucleotides using RNA aptamers. The first method presented in Chapter 2 focuses on sensitive *in vitro* detection of cdiG using an electrophoretic mobility shift assay (EMSA) that can be adapted for microfluidic analysis with high-throughput capabilities. Chapters 3-5 focus on novel live cell imaging of each specific bacterial cyclic dinucleotide using riboswitch aptamers coupled to the Spinach aptamer, an RNA mimic of GFP (Paige et al., 2011, 2012). It is envisioned that these specific sensors will further our comprehension of the signal transduction pathways of these critical second messengers, allowing for understanding and manipulation of processes including bacterial pathogenicity.

1.5 Figures

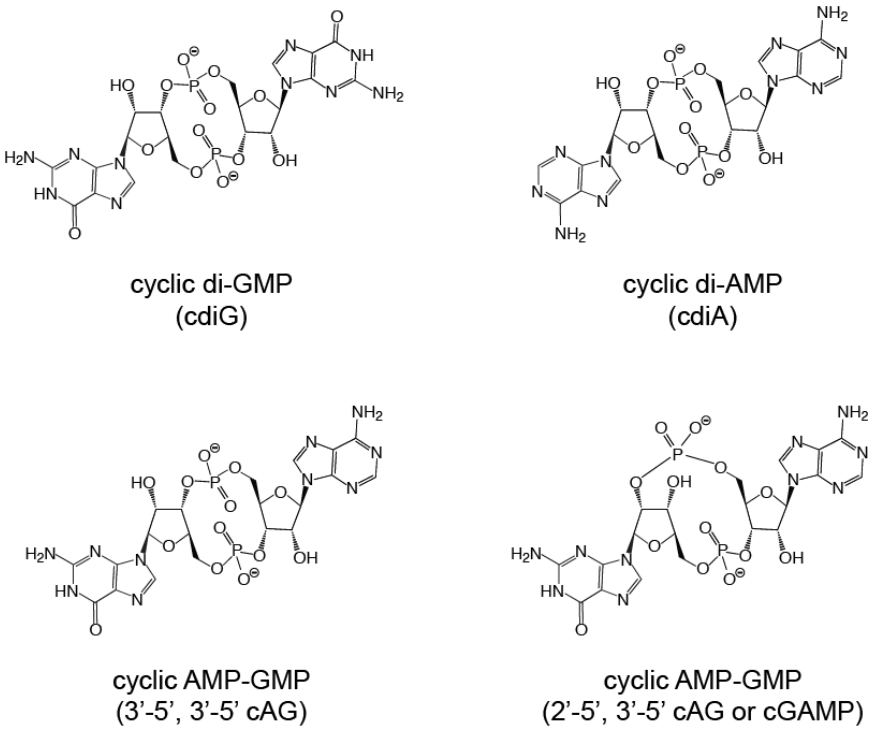

Figure 1.1 Chemical structures of cyclic dinucleotide second messengers.

Organisms known to have cdiG

Gluconacetobacter xylinus
Bacillus subtilis
Caulobacter crescentus
Clostridium difficile
Escherichia coli
Pseudomonas aeruginosa
Vibrio cholerae
Xanthomonas campestris
many others

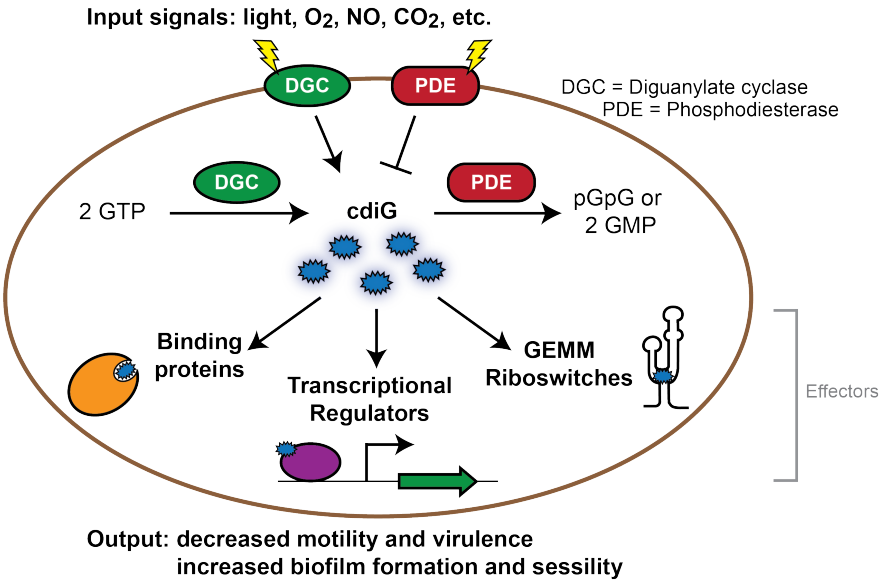

Figure 1.2 Model of cdiG signaling in bacteria.

Organisms known to have cdiA

Bacillus subtilis
Chlamydia trachomatis
Listeria monocytogenes
Mycobacterium tuberculosis
Staphylococcus aureus
Streptococcus pyogenes
several others

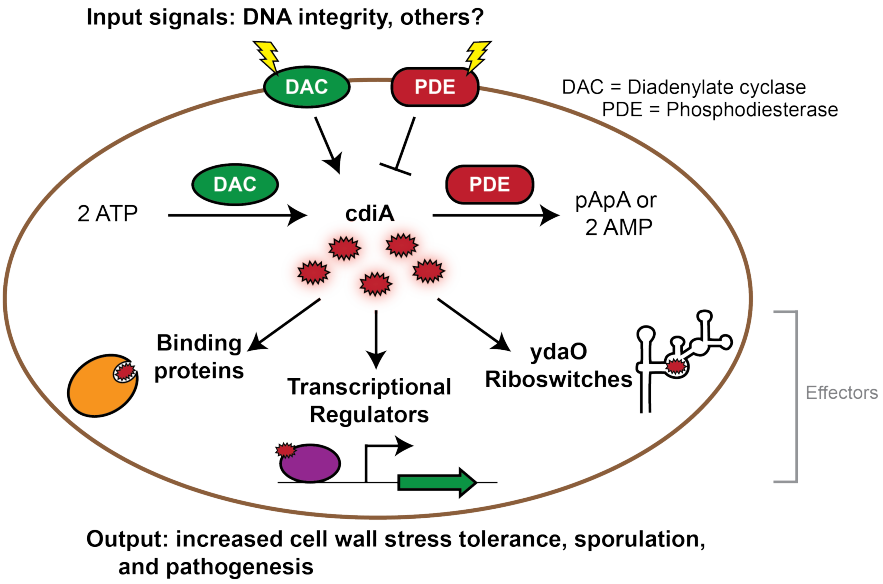

Figure 1.3 Model of cdiA signaling in bacteria.

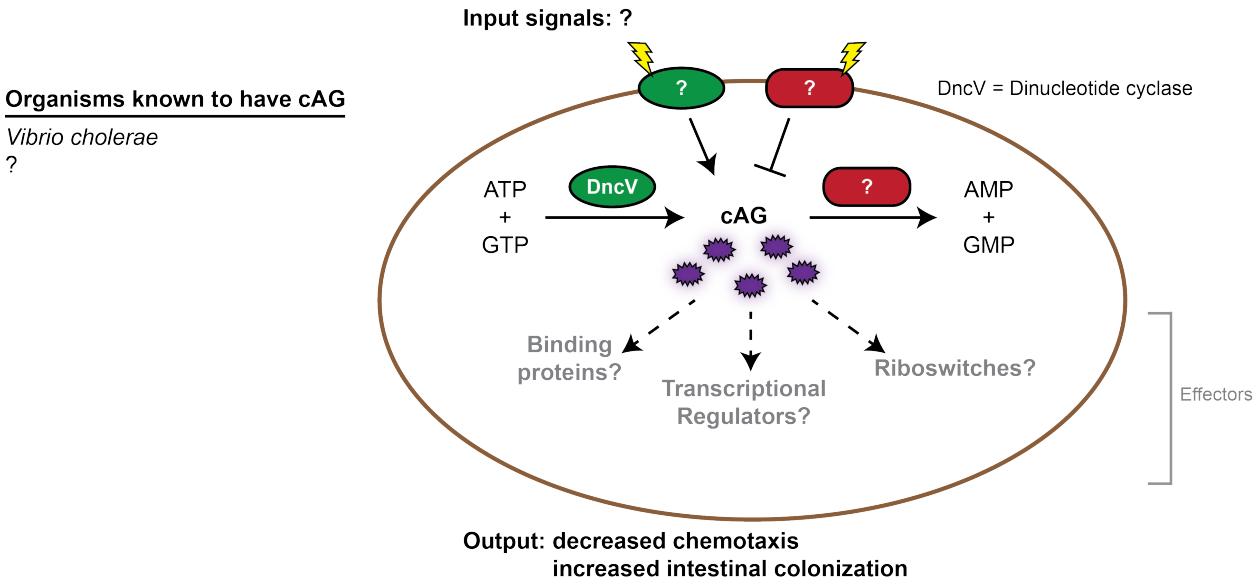

Figure 1.4 Model of 3′,3′ cAG signaling in bacteria.

Table 1.1 List of cyclic dinucleotide-regulated activities in bacteria.

Signaling molecule	Organism	Regulation	Reference
Cyclic di-GMP*	*Caulobacter crescentus*	• Cell cycle progression	(Abel et al., 2013)
		• Flagellar activity	(Christen et al., 2007)
	Clostridium difficile	• Flagellar synthesis	(Sudarsan et al., 2008)
	Escherichia coli	• Motility	(Ryjenkov et al., 2006)
		• Cellulose synthesis	(Weber et al., 2006)
	Gluconacetobacter xylinus	• Cellulose synthesis	(Ross et al., 1987)
	Klebsiella pneumoniae	• Biofilm formation	(Wilksch et al., 2011)
		• Oxidative stress response • Virulence	(Huang et al., 2013)
	Pseudomonas aeruginosa	• Twitching motility	(Kazmierczak et al., 2013)
		• Biofilm formation/quorum sensing	(Habazettl et al., 2011)
	Pseudomonas fluorescens	• Cell adhesion	(Chatterjee et al., 2014)
	Vibrio cholerae	• Intestinal adhesion	(Sudarsan et al., 2008)
		• Virulence gene expression • Biofilm formation	(Krasteva et al., 2010)
	Xanthomonas campestris	• Biofilm formation	(Lu et al., 2012)
		• Bacterial virulence • Global transcription regulation	(Chin et al., 2010)
Cyclic di-AMP	*Bacillus subtilis*	• Bacterial sporulation • Sensing of DNA integrity	(Oppenheimer-Shaanan et al., 2011)
	Listeria monocytogenes	• Activation of host innate immune response	(Woodward et al., 2010)
		• Cell wall stability and growth	(Witte et al., 2013)
		• Central metabolic balance	(Sureka et al., 2014)
	Mycobacterium smegmatis	• Fatty acid synthesis	(Zhang et al., 2013a)
	Staphylococcus aureus	• Amount of cross-linked peptidoglycan • Cell size	(Corrigan et al., 2011)
3′,3′ Cyclic AMP-GMP	*Vibrio cholerae*	• Intestinal colonization • Chemotaxis • Fatty acid biosynthesis	(Davies et al., 2012)

*For more comprehensive lists of c-di-GMP regulatory effects, see the following reviews: (Hengge, 2009; Kalia et al., 2012; Krasteva et al., 2012; Römling et al., 2013)

CHAPTER 2

A Minimalist Biosensor: Quantitation of Cyclic Di-GMP Using Conformational Change of a Riboswitch

2.1 Abstract

Cyclic di-GMP (cdiG) is a bacterial second messenger important in regulating a wide variety of cellular processes, such as the transition from a motile to a sessile lifestyle. Many questions remain about the role and regulation of this small molecule, but current methods of detection are limited. We take advantage of a natural, high affinity receptor of cdiG, the Vc2 GEMM-I class riboswitch aptamer, to develop highly sensitive and rapid detection methods based on electrophoretic mobility shift assays (EMSAs). At first, a tetraloop mutant of the aptamer (A33U Vc2) was shown to display a more dramatic mobility shift than the WT aptamer upon ligand binding. This A33U Vc2 aptamer was used to develop an EMSA that detects high picomolar levels of cdiG, but the assay requires nearly 4 days to complete. Through optimization of the binding reaction parameters and conversion to a microfluidic mobility shift assay (μMSA), the assay time was decreased to 30 min total while maintaining low nanomolar sensitivity, demonstrating the utility of the μMSA assay as a rapid and sensitive method of detecting unlabeled cdiG.

2.2 Introduction

Cyclic di-GMP (cdiG) is a ubiquitous signaling molecule in bacteria that plays a role in bacterial virulence, motility and biofilm formation (Hengge, 2009). The molecule was first discovered by Benziman and coworkers in 1987 and since has been the subject of extensive research, yet many questions remain about the components and mechanisms of signaling (Düvel et al., 2012; Massie et al., 2012; Ross et al., 1987). Recently, cdiG and the other natural cyclic dinucleotides were shown to trigger an innate immune response in mammalian cells and thus, cdiG is also a promising small molecule adjuvant (Burdette et al., 2011; Svindland et al., 2012). In order to make further advances in studying cdiG biology though, it is necessary that facile and accurate methods exist for detecting small changes in the concentration of this second messenger.

Key areas of cdiG signaling that remain poorly understood include input signals that lead to cdiG-dependent regulation, temporal resolution of cdiG signaling, and an explanation for the high multiplicity of cdiG metabolism enzymes in various bacteria (Römling et al., 2013). Bioinformatic studies have shown that diguanylate cyclases and phosphodiesterases, which synthesize and degrade cdiG, respectively, are highly abundant in bacteria, for example 29 synthase and/or degradase enzymes have been predicted in *E. coli* alone. However, a clear understanding of the regulation of these enzymes as well as how they regulate the global intracellular pool of cdiG is lacking. A general *in vitro* method for detecting cdiG is advantageous because it can be applied for the study of virtually any organism and ideally could detect changes in cdiG concentration with high sensitivity.

Previously developed methods of detecting cdiG in solution are limited by their sensitivity or the ability to be high-throughput. The commonly used HPLC-MS method has a lower limit of detection (LLOD) of 2 mg/mL or ~2 nM cdiG, but typically requires sample purification and is limited in high-throughput capability (Spangler et al., 2010). Other methods, including circular dichroism or small molecule-based detection

methods, are more accessible but are based on dimerization or G-quadruplex formation of cdiG and thus are only able to detect cdiG at low micromolar concentrations (Nakayama et al., 2011, 2012a; Stelitano et al., 2013). Potential cdiG binding proteins have been identified from whole cell lysates using a sensitive Differential Radial Capillary Action of Ligand Assay (DRaCALA), however this method is aimed at identification of protein-ligand interactions and not for changes of metabolite concentration (Roelofs et al., 2011).

Highly selective *in vivo* cdiG fluorescent biosensors have been developed that take advantage of protein or riboswitch receptors that were naturally evolved to bind cdiG (Christen et al., 2010; Ho et al., 2013; Kellenberger et al., 2013). Protein biosensors that have been developed use PilZ domain-containing proteins, such as natural receptors from pathogenic organisms including YcgR from *Salmonella enterica* and MrkH from *Klebsiella pneumoniae* (Christen et al., 2010; Ho et al., 2013) which give changes in Förster resonance energy transfer (FRET) upon binding cdiG with reported dissociation constants (K_d) of 195 ± 6 nM and 120 nM, respectively. While these protein biosensors are useful for *in vivo* imaging of cdiG, their use *in vitro* requires rigorous purification of the expressed protein from cells to obtain purified protein devoid of any remaining bound cdiG.

In contrast, one distinct advantage of riboswitch-based biosensors is the ability to synthesize RNAs by *in vitro* transcription, which eliminates the possibility of contaminating cdiG from cellular extracts. A GEMM-I class riboswitch aptamer upstream of a Tfox-like gene in *Vibrio cholerae* called Vc2 exhibits remarkably high affinity for cdiG (K_d ~ 11 pM) (Smith et al., 2009; Sudarsan et al., 2008) and has previously been fused to various output domains to create cdiG sensors (Gu et al., 2012; Wood et al., 2012). We and others have created fluorescent sensors by coupling the Vc2 aptamer to the Spinach aptamer, an RNA mimic of GFP (Kellenberger et al., 2013; Nakayama et al., 2012b; Paige et al., 2011, 2012). However, fusion of the Vc2 aptamer to Spinach either through its natural P1 stem (K_d ~ 8 ± 1 nM at 25 °C, 10 mM $MgCl_2$) (Kellenberger et al., 2013) or an unnatural stem (high nanomolar detection of cdiG, K_d not reported) (Nakayama et al., 2012b) results in a loss of affinity for cdiG compared to the WT Vc2 aptamer alone. Breaker and coworkers have fused the Vc2 aptamer to a hammerhead ribozyme sequence through a random transducer stem and selected several sequences that altered ribozyme cleavage upon cdiG binding (affinities range from 70 to 500 nM) (Gu et al., 2012), indicating the potential use of riboswitch aptamers for *in vitro* detection of cdiG. However, a minimalist approach in using the conformational change of the Vc2 aptamer alone has not yet been explored.

We have recently developed a microfluidic mobility shift assay (μMSA) that separates different riboswitch RNA conformational states with high resolution in only 0.3% of the time required for a standard slab gel (Karns et al., 2013). In the original study, we demonstrated that ligand-induced conformational changes could be used to validate computationally predicted SAM-I riboswitch aptamers. Here, we show a different application of μMSA, namely towards *in vitro* quantitation of cdiG using the Vc2 cdiG riboswitch aptamer. The initial EMSA method introduced here is a highly sensitive

assay that detects sub-nanomolar cdiG concentrations, yet requires lengthy equilibration and electrophoretic times to distinguish ligand-bound versus unbound-states. We demonstrate that assay time can be reduced in combination through increasing RNA concentrations as well as conversion to a microfluidic format, which decrease the reaction time while maintaining sensitivity similar to that of HPLC-MS assays. This μMSA format recently been converted to a high-throughput assay, which should enable rapid and sensitive screening of cdiG concentrations in various bacterial strains.

2.3 Results

A tetraloop mutant of the Vc2 aptamer demonstrates an increased electrophoretic mobility shift

While conventional native electrophoretic mobility shift assays (EMSAs) are based upon separation of different molecular weight species, these do not allow the detection of cdiG from unlabeled samples. For example, formation of the riboswitch aptamer-ligand complex using Vc2 RNA and radiolabeled cdiG has been observed by native EMSA, where an electrophoretic mobility difference is easily observed between free and RNA-bound cdiG (Kulshina et al., 2009; Smith et al., 2009; Wood et al., 2012). Smith et al. employed a competition binding experiment in order to analyze binding of unlabeled ligands (Smith et al., 2009), however, these assays have a poorer limit of detection than direct binding assays since low levels of competitor inefficiently compete with the labeled ligand.

We considered that a feasible alternative would be to use native EMSA to separate different radiolabeled RNA conformations induced by ligand binding (Figure 2.1a). This method requires labeled RNA but enables unlabeled ligands to be interrogated by direct binding experiments, which is important for quantifying cdiG from natural sources, evaluating potential ligand candidates (Shanahan et al., 2011), or identifying small molecule inhibitors of riboswitch activity (Blount and Breaker, 2006). Previous studies using small angle x-ray scattering (SAXS) and single molecule FRET (smFRET) experiments have shown that the Vc2 aptamer undergoes a significant structural compaction upon binding cdiG (Kulshina et al., 2009; Wood et al., 2012). Specifically, in an unbound state, the majority of RNAs are in an elongated conformation with distal P2 and P3 stems, but when bound to cdiG, these two stems form close tertiary interactions resulting in a more globular architecture. This structural compaction has been used by Kulshina et al. to determine the specificity of the RNA for cdiG over other nucleotide analogs through native EMSA (Kulshina et al., 2009). In this experiment, RNA (35 μM) was incubated with saturating concentrations of ligand (70 μM) for a short period of time at 37 °C before separating via native PAGE. While this experiment was effective at determining Vc2 selectivity, large amounts of RNA were required to visualize migrated bands by dying with toluidine blue, thus limiting the sensitivity of this experiment.

In contrast to a simple plus/minus assay for binding, we sought to develop an assay that would allow for highly sensitive detection of cdiG. Determination of cdiG

concentrations through EMSA requires good resolution of the bound and unbound bands for accurate quantitation. Thus, initial assays were aimed at increasing the observed mobility shift upon ligand binding. Specifically, we analyzed two strategies for affecting RNA structure: the effects of altering Mg^{2+} concentrations and of weakening a tertiary interaction. Magnesium ions mediate binding of cdiG to the Vc2 aptamer and have been shown to affect mobility shifts of another riboswitch aptamer (Heppell and Lafontaine, 2008; Wood et al., 2012). In addition, one tertiary interaction that stabilizes the globular structure of the bound Vc2 riboswitch is a tetraloop/tetraloop receptor interaction between the P2 and P3 stems (Kulshina et al., 2009; Smith et al., 2009). An A33U mutation to the tetraloop in the P2 stem loop of Vc2 impairs a base-stacking interaction with the tetraloop receptor in the P3 stem, therefore weakening the ability of this tertiary interaction to form (Figure 2.1b) (Smith et al., 2010; Wood et al., 2012).

Radiolabeled WT and A33U Vc2 aptamer RNAs were incubated in buffers with varied $MgCl_2$ concentrations either with or without an excess of cdiG, then were separated on native polyacrylamide gels containing the corresponding concentration of $MgCl_2$ (Figures 2.1c, 2.2). Under all three Mg^{2+} conditions tested, the WT Vc2 aptamer shows a much smaller relative mobility shift upon binding cdiG than the A33U Vc2 aptamer. Interestingly, the main difference in relative mobility shift comes from decreased mobility of the A33U aptamer in the unbound state, an effect that is enhanced with lower magnesium concentrations (Table 2.1). In contrast, the mobility of the cdiG bound WT and A33U Vc2 RNAs is nearly equal within each gel, indicating that the A33U mutation reduces compactness of the unbound aptamer, but that addition of cdiG restores the structure to match the mobility of WT Vc2.

In addition, Mg^{2+} concentration has large effects on overall electrophoretic mobility of the aptamers (Figure 2.1c). First, decreasing the $MgCl_2$ concentration increases the electrophoretic mobility of all RNAs. Second, decreasing the Mg^{2+} concentration also gives larger separations between the bound and unbound RNA conformations for both WT and A33U Vc2 RNAs (Table 2.1), although the effect is more pronounced for the A33U mutant. The combined effect is that lowering the $MgCl_2$ concentration increases both the mobility of the aptamers and the separation of bound and unbound species.

The electrophoretic mobility shift assay allows for high picomolar detection of cdiG

In the original structural study of WT Vc2, an extremely slow off-rate (1.1×10^{-5} min^{-1}) was measured for cdiG dissociation from the riboswitch aptamer under buffer conditions that included 10 mM $MgCl_2$ (Smith et al., 2009). Thus, not only does the WT aptamer have a reduced mobility shift compared to A33U Vc2, but we considered it impractical to utilize WT Vc2 for cdiG quantitation because the time for the binding reaction to reach equilibrium would be on the order of months. In contrast, it was determined that the binding reaction between A33U Vc2 (<100 pM) and non-saturating concentrations of cdiG reaches equilibrium after approximately 75 h of incubation (Figure 2.3a). This equilibration time was observed for reactions whether incubated in buffer with 10 mM $MgCl_2$ and 10 mM KCl or 3 mM $MgCl_2$ and 3 mM KCl, indicating that

the ionic concentrations used here have little effect on kinetics (Figures 2.3a and 2.4). Thus, we used a 75 h incubation time for experiments to determine the optimal buffer conditions for quantifying cdiG binding, as this parameter influences the observed mobility shift and determines the sensitivity of cdiG detection.

While lowering Mg^{2+} levels leads to a larger electrophoretic mobility shift between bound and unbound species, it also results in poorer binding affinity for cdiG (Figure 2.3b,c). At 1 mM $MgCl_2$ the affinity of A33U Vc2 for cdiG is in the nanomolar regime (K_d value of 1.6 ± 0.1 nM), whereas sub-nanomolar affinity is achieved at 3 and 10 mM $MgCl_2$ (K_d values of 520 ± 30 pM and 210 pM, respectively). The LLOD for cdiG is approximately 100 pM with 10 mM $MgCl_2$ (Figure 2.3b), which is an order of magnitude lower than the most sensitive existing methods (Simm et al., 2009; Spangler et al., 2010). However, as a compromise between electrophoretic mobility resolution and binding affinity, further optimization of the assay was performed with 3 mM $MgCl_2$. Under these conditions, the dynamic range of detection between 10-90% of the fraction bound is 55-4400 pM cdiG, providing a method for detecting minute changes in cdiG concentrations with high accuracy.

Optimization of the slab gel EMSA and conversion to μMSA allows for more rapid detection of cdiG

We considered that the long equilibrium incubation time (~75 h) is not only a function of the rate constants but is also dependent on the concentrations of RNA and ligand in the binding reaction. In order to reduce the time to reach equilibrium, the effect of adding excess unlabeled riboswitch aptamer in the radiolabeled binding reactions was analyzed. For example, in a binding reaction containing a total RNA concentration of 1.1 μM A33U Vc2 with 100 nM cdiG, equilibrium was reached within 30 min (Figure 2.5a), which is a 150-fold decrease in incubation time compared to previous experiments using <100 pM of A33U Vc2 with 1 nM cdiG, albeit under slightly varied $MgCl_2$ concentrations (Figure 2.3a).

Under conditions with excess RNA, the amount of the Vc2 aptamer greatly exceeds the dissociation constant, so the signal from bound RNA becomes directly proportional to the amount of cdiG present in the sample. Importantly, the measurement of cdiG concentrations no longer depends on the fraction of RNA bound, but solely on the amount of RNA that is shifted to the bound state (as the high excess of RNA largely remains unbound at low levels of cdiG). This method was used to generate a standard curve for cdiG detection (Figure 2.5b), which has a LLOD of ~5 nM and has a linear response to increased cdiG levels up to 400 nM tested here. The LLOD for cdiG under these conditions is ~5 nM, which matches that of current HPLC-MS methods (Simm et al., 2009; Spangler et al., 2010).

While addition of excess RNA substantially decreased the reaction time, performing the separation on the slab gel still required 12-14 h of gel electrophoresis at 4 °C. To reduce electrophoresis time, we converted to the microfluidic mobility shift assay (μMSA) format (Figure 2.6a). This technique has previously been used for riboswitch characterization and is advantageous over traditional slab-gel assays as it

provides rapid, resource-sparing, and reproducible results using fluorescently-labeled RNA without the precautions required for using radiolabeled materials (Karns et al., 2013). As shown, separation of bound and unbound AlexaFluor488 (AF488)-labeled A33U Vc2 aptamer can be achieved in 30 seconds at room temperature, a ~1,440-fold decrease in the separation time (Figure 2.6b). Meanwhile, the same equilibration time of 30 min was found when monitoring the binding reaction by μMSA (Figure 2.6c).

A standard curve for cdiG detection was generated via μMSA using 1.1 μM AF488-labeled RNA with cdiG concentrations ranging from 1-1000 nM (Figure 2.6d). In the resulting curve, the amount of bound RNA increased linearly with the concentration of cdiG and the LLOD is 3 nM cdiG (S/N ratio ~3) (Figure 2.7). Thus, on the microfluidics platform, we are able to achieve comparable sensitivity and siimilar linearity of response relative to the slab gel format. The aforementioned advantages of the μMSA format long with the ~216,000-fold reduction in experiment time makes this assay advantageous for highly sensitive and rapid detection of unlabeled cdiG.

2.4 Discussion

Here we present the development of a highly rapid and sensitive microfluidic assay for *in vitro* detection of unlabeled cdiG that takes advantage of the natural ligand-induced conformational change of the Vc2 riboswitch aptamer. The μMSA format shown here was previously used to analyze the binding characteristics of several *S*-adenosylmethionine (SAM) riboswitch aptamers and it was found that these RNAs can generally be classified into two groups: those that interconvert between the ligand-bound and unbound states slowly and separate into two distinct electrophoretic bands, and those that interconvert quickly that display a single intermediate band during electrophoresis (Karns et al., 2013). A key characteristic of the Vc2 aptamer is its unusually slow cdiG binding off-rate (Smith et al., 2009), which contributes to the aptamer's high sensitivity for cdiG, but also leads to slow interconversion and two distinct ligand-bound and unbound bands during EMSAs as ligand dissociation is slower than the rate of separation by electrophoresis.

Further increasing the separation of the ligand-bound and unbound aptamer is the use of the A33U Vc2 tetraloop mutant, which enabled greater electrophoretic separation mainly due to an observed slower electrophoretic mobility of the unbound RNA aptamer. Previous affinity studies of the A33U Vc2 aptamer have shown that this mutation results in a 200-fold decrease in affinity (Smith et al., 2010), likely through an increase in the off-rate as this mutation destabilizes an important tertiary interaction and other disruptive mutations mainly facilitate unbinding of the ligand (Smith et al., 2010). Single molecule studies have shown that this tetraloop mutation results in an increase in the amount of statically undocked RNAs, in which the P2 and P3 stems are distal, agreeing with the observation of this RNA in a less compact formation when not bound to cdiG (Wood et al., 2012). The bulk measurement of cdiG levels presented here is aimed at increasing the separation between the electrophoretic mobilities of the ligand bound and unbound states.

The rapid μMSA format can be used to study RNA-ligand binding regardless of whether an RNA aptamer displays rapid or slow ligand-binding interconversions (Karns et al., 2013). In the case of RNAs with a rapid interconversion rate, the ligand concentration can be determined by the distance traveled by the RNA band between unbound and bound RNA species, whereas slowly interconverting RNAs can be measured by the fraction of RNA bound, as shown here. Given that there are numerous riboswitch classes with low nanomolar affinities (Nelson et al., 2013; Sudarsan et al., 2008), and that it is a natural property of riboswitch RNAs to undergo a conformational change upon ligand binding, this technique will likely be applicable to the study of many natural metabolites for which detection methods are underdeveloped. In fact, a SAM-I riboswitch aptamer has been used to verify *S*-adenosylmethionine levels in yeast cell extracts through a standard EMSA (Sadhu et al., 2013). Further, preliminary data shows that mutants of the Vc2 aptamer are capable of binding the recently discovered second messenger 3'-5', 3'-5' c-AMP-GMP, which has been implicated in the regulation of *Vibrio cholerae* virulence (Davies et al., 2012) (Figure 2.8).

In comparison to other cdiG detection methods, the μMSA format presented here is uniquely situated to match the limit of detection of the current most sensitive techniques while offering the possibility for high-throughput screening. A free-standing polyacrylamide gel (*fs*PAG) device has been described that allows for μMSA 96-well multiplexing for sample analysis (Pan et al., 2014). This high capacity format has a throughput of 0.1 min/data point as compared to traditional slab gel EMSAs, which require ~102 min/data point, or individual HPLC-MS runs, which take ~30 min/data point. Given that the assay developed here is aimed at measuring unlabeled amounts of cdiG, it is envisioned that it could be adapted to detect cdiG from various bacterial extracts to learn more about the tight regulation of this key second messenger.

2.5 Figures

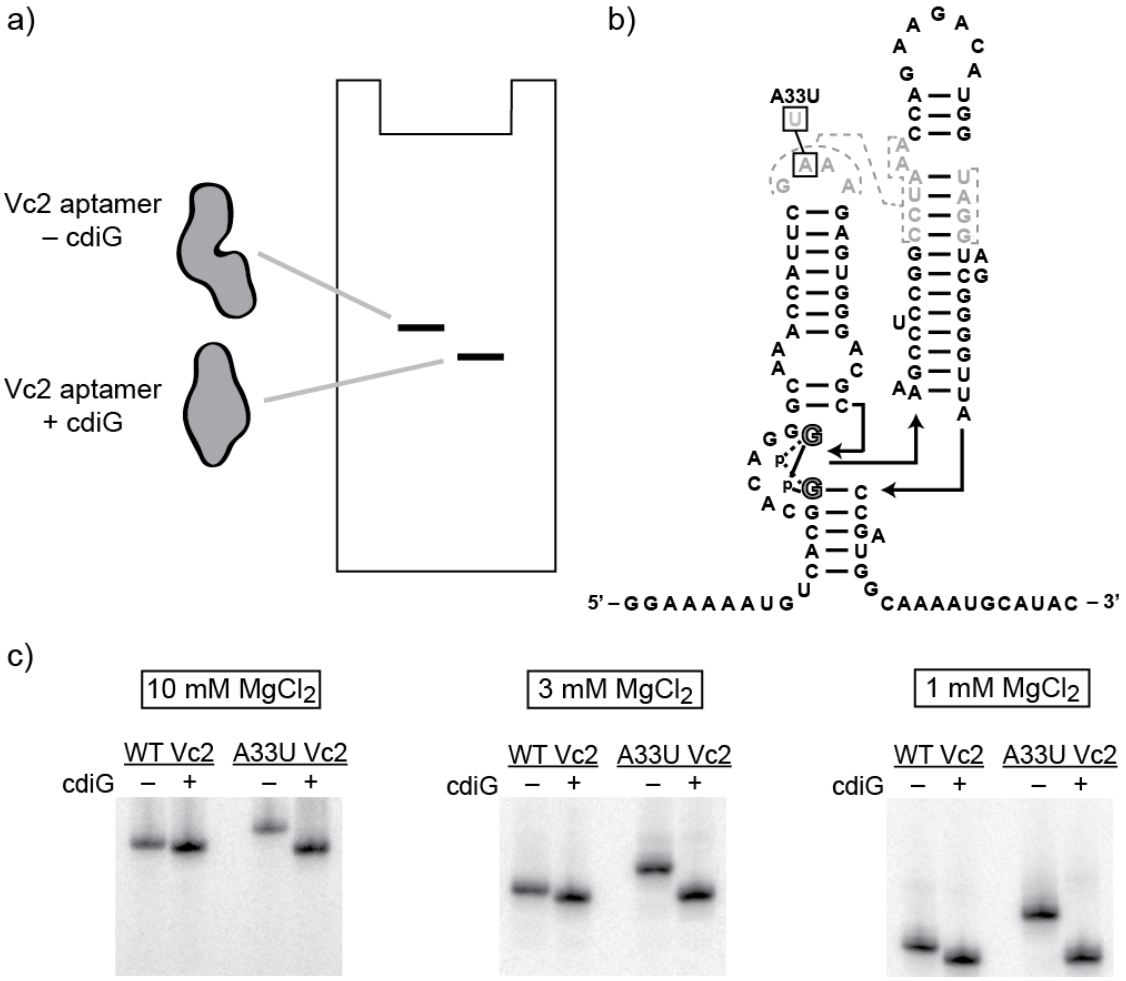

Figure 2.1 An A33U mutation leads to a larger electrophoretic mobility shift of the Vc2 aptamer with dependence on Mg^{2+} concentration. (a) Model of the conformational change resolved by an electrophoretic mobility shift assay. The global RNA conformations are outlines of structures previously solved by SAXS. **(b)** Sequence and secondary structure of the Vc2 aptamer. The A33U mutation is boxed and cdiG is in large letters. The tetraloop-tetraloop receptor interaction is shown in dashed lines and nucleotides involved in this tertiary interaction are in gray. **(c)** EMSA of WT and A33U Vc2 RNAs with or without cdiG run in 10 mM, 3 mM, or 1 mM $MgCl_2$. Approximately 1 nM ^{32}P A33U Vc2 was incubated with 10 μM cdiG for 4 h before loading on 10% polyacrylamide gels run for the same amount of time (14 h) at 4 °C. Images encompass the area 8.5 – 13.5 cm from the top of the gels.

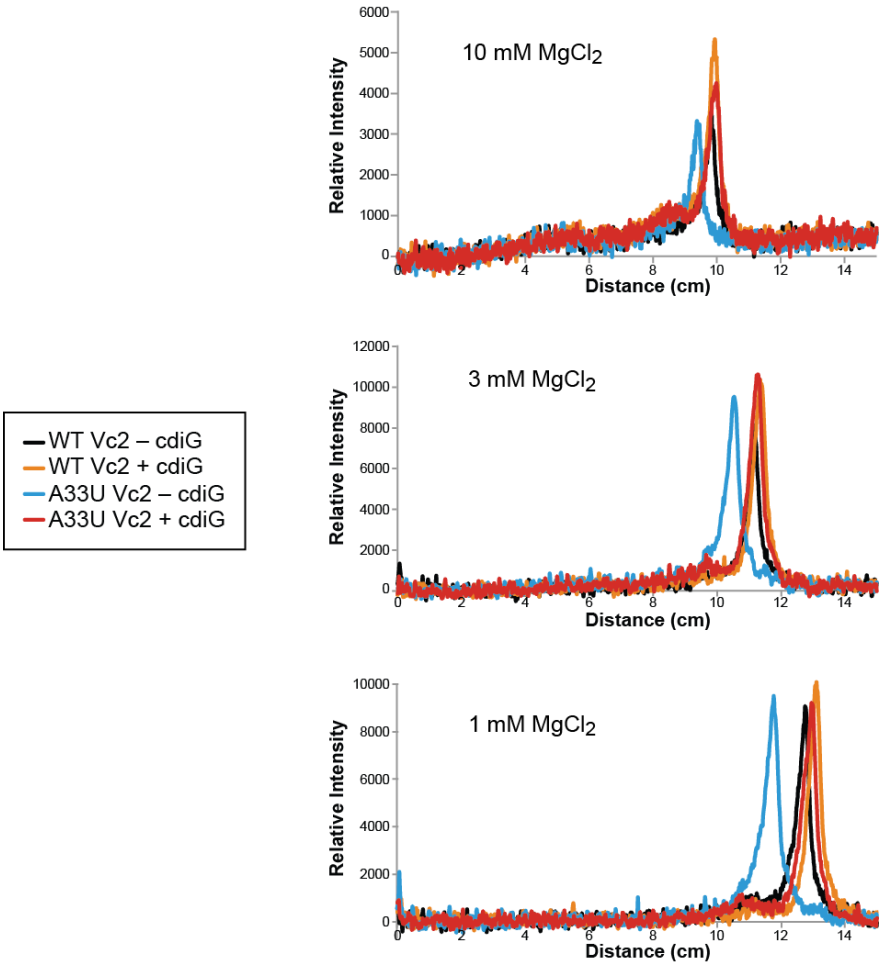

Figure 2.2 Ligand binding and Mg2+ concentration influence the electrophoretic mobility of WT and A33U Vc2 RNAs. Plots represent the distance of the RNA traveled as measured by phosphorimager intensity. The zero point of the plot was measured from the point of loading on the gel.

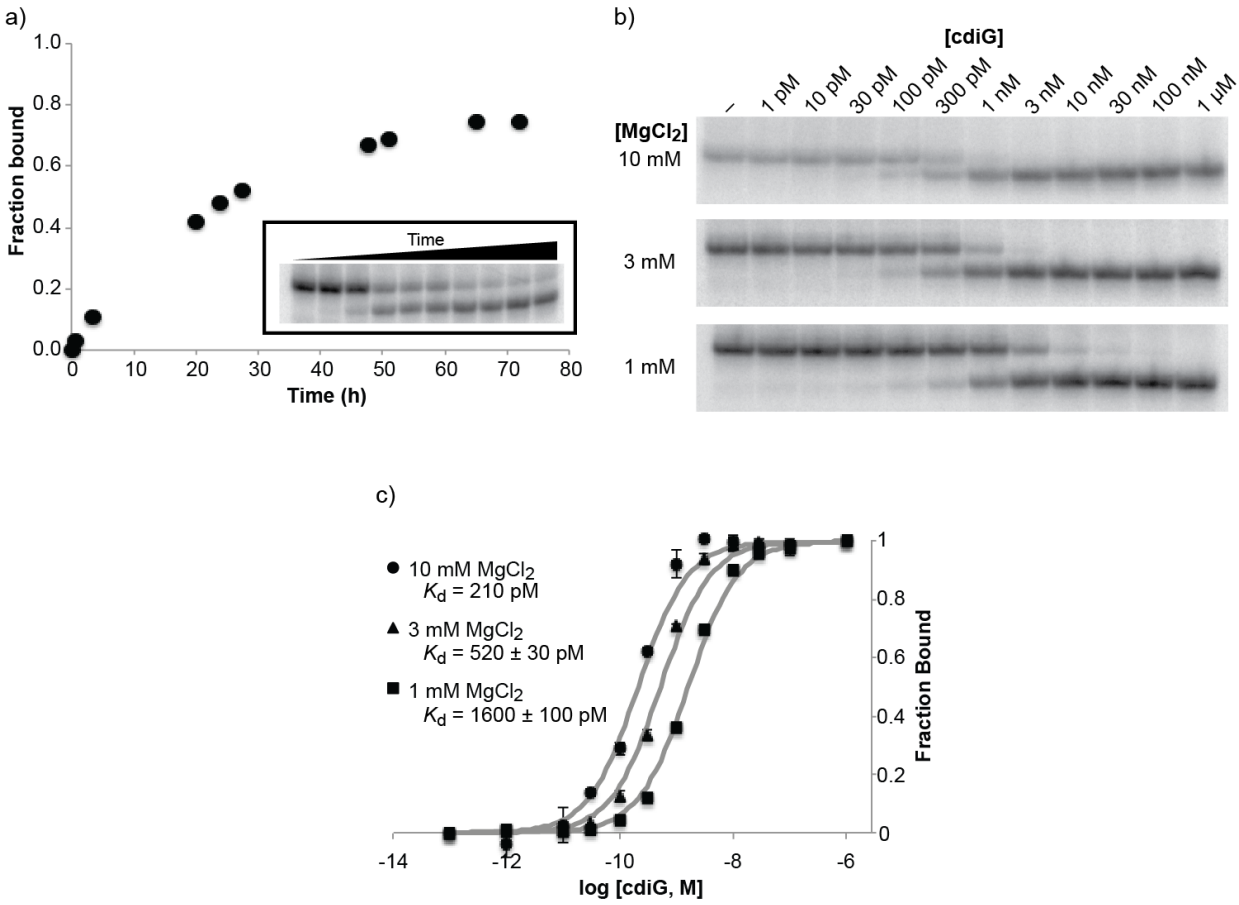

Figure 2.3 The A33U Vc2 aptamer detects high picomolar levels of cdiG. (a) Analysis of A33U Vc2 equilibration time with cdiG. Less than 100 pM ^{32}P A33U Vc2 RNA was incubated with 1 nM cdiG for various times before loading on a 10% polyacrylamide gel run for 14 h at 4 °C. **(b)** EMSAs of A33U Vc2 with cdiG under different $MgCl_2$ concentrations. Less than 100 pM ^{32}P A33U Vc2 was incubated with various concentrations of cdiG for 75 h before separating on a 10% polyacrylamide gel run for 14 h at 4 °C. **(c)** Analysis of A33U Vc2 affinity for cdiG under various $MgCl_2$ concentrations. Data from two or three independent replicates and the best-fit curves are shown.

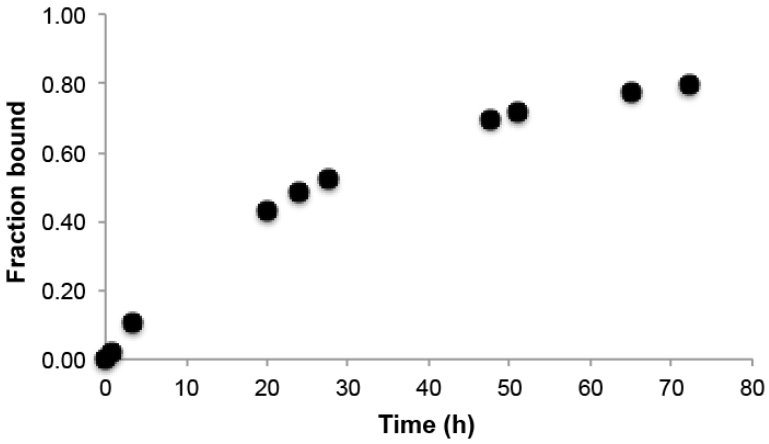

Figure 2.4 Measurement of A33U Vc2:cdiG complex equilibration under 3 mM $MgCl_2$ and 3 mM KCl. The binding reaction between RNA (<100 pM) and cdiG (3 nM) requires ~75 h, which is similar to the same reaction performed in buffer containing 10 mM $MgCl_2$ and 10 mM KCl.

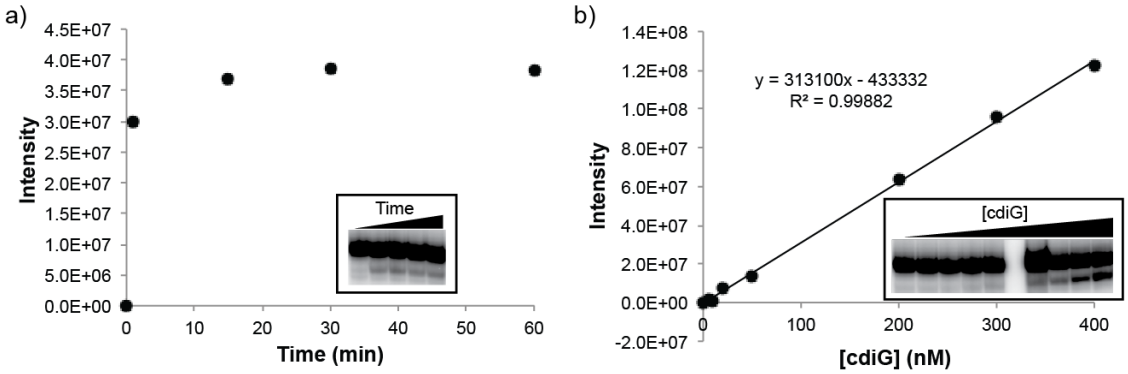

FIGURE 2.5 Addition of excess RNA decreases equilibration time while maintaining low nanomolar sensitivity. (a) Analysis of equilibration time required for an excess of A33U Vc2 to bind cdiG. Approximately 100 pM ^{32}P A33U Vc2 was mixed with 1 µM unlabeled RNA and 100 nM cdiG then was incubated for various times before loading on a 10% native polyacrylamide gel run for 14 h at 4 °C. The gel image insert shows the data points analyzed. **(b)** Standard curve of cdiG binding A33U Vc2. Various concentrations of cdiG were incubated with approximately 100 pM ^{32}P A33U Vc2 and 1 µM unlabeled RNA and 100 nM cdiG for 30 min before loading on a 10% native polyacrylamide gel run for 14 h at 4 °C. The image of the gel analyzes is shown in the insert; the 6th and 7th lanes were excluded from analysis as they were a result of a gel loading error.

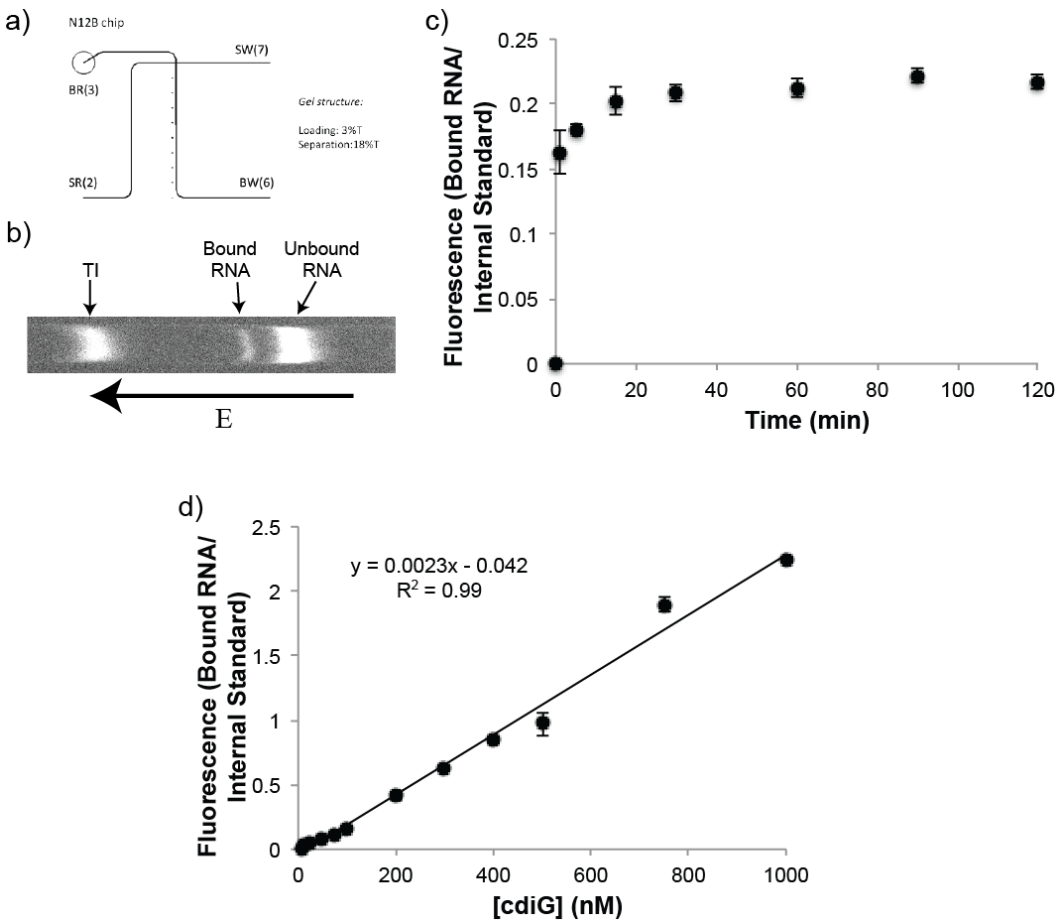

Figure 2.6 Conversion to a μMSA allows for rapid separation of conformational states and low nanomolar cdiG detection. (a) Schematic of microfluidic chip for μMSA. **(b)** Example full-field image of binding experiment. For 60 min, 100 nM cdiG was incubated with 1 μM Alexa Fluor 488-labeled RNA and was then loaded on a polyacrylamide gel run for 30 s at RT. **(c)** Analysis of equilibration time required for an excess of RNA to equilibrate with cdiG. For various amounts of time, 100 nM cdiG was incubated with 1 μM Alexa Fluor 488-labeled RNA and was then loaded on a polyacrylamide gel run for 30 s at RT. **(d)** Standard curve of A33U Vc2 binding cdiG. For 60 min, 1 μM Alexa Fluor 488-labeled RNA was incubated with various cdiG concentrations and was then loaded on a polyacrylamide gel run for 30 s at RT.

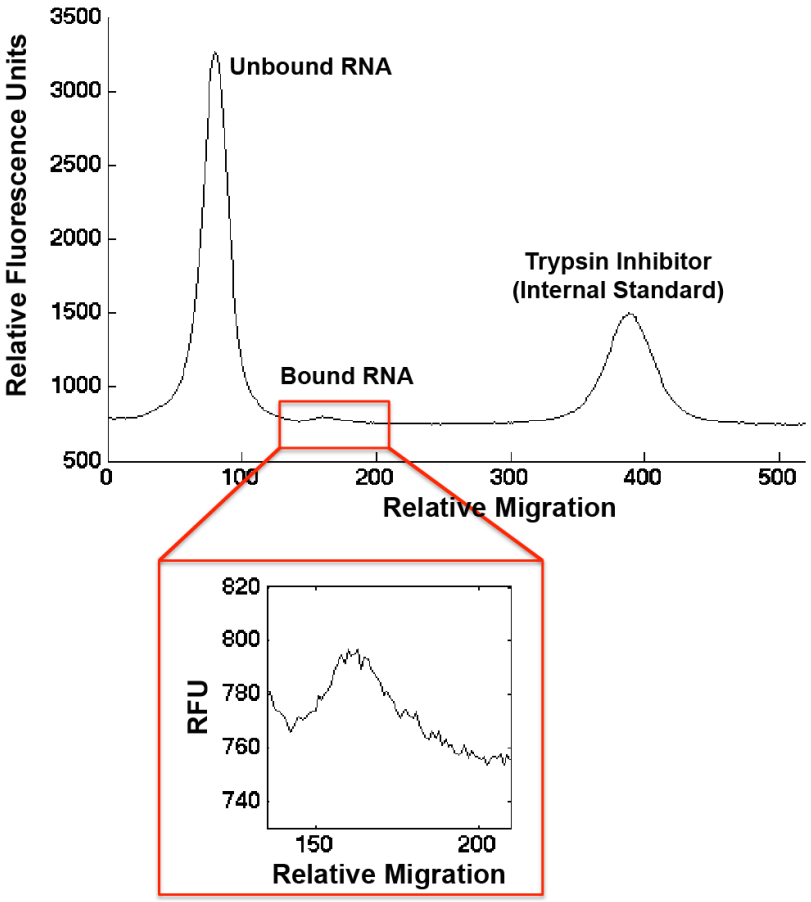

Figure 2.7 Detection limit of μMSA using 1 μM RNA. The electropherogram from a μMSA assay with 1 uM RNA and 1 nM cdiG is shown. The inset highlights the signal to noise ratio (~3) of the bound RNA band under these conditions.

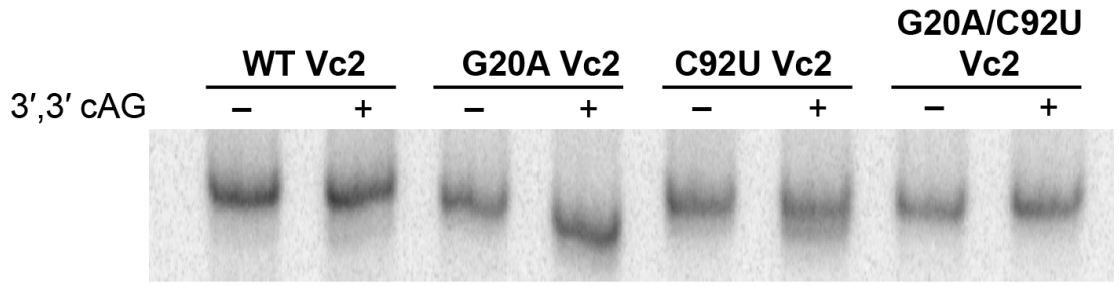

Figure 2.8 Binding pocket mutations to the Vc2 aptamer enable it to bind 3′,3′ cAG. Mutations to the Vc2 riboswitch binding pocket previously shown to change the ligand selectivity were tested for their ability to bind the second messenger 3'-5', 3'-5' cAG. RNA (~1 nM) was incubated with cAG (10 μM) for 4 h and was separated via 12% PAGE for ~24 h at 4 °C.

	10 mM $MgCl_2$	**3 mM $MgCl_2$**	**1 mM $MgCl_2$**
WT Vc2 – cdiG	9.82 cm	11.14 cm	12.75 cm
WT Vc2 + cdiG	9.93 cm	11.35 cm	13.11 cm
A33U Vc2 – cdiG	9.37 cm	10.54 cm	11.77 cm
A33U Vc2 + cdiG	9.98 cm	11.28 cm	12.95 cm

Table 2.1 Distance traveled of WT and A33U Vc2 RNAs under various $MgCl_2$ concentrations. Data were obtained by measuring the distance of the bands shown in Figure 2.1c from the well of the gel using ImageJ software.

2.6 Materials and Methods

Reagents and oligonucleotides
DNA oligonucleotides were purchased from Elim Biopharmaceuticals (Hayward, CA) and IDT (Coralville, IA). Cyclic di-GMP was purchased from Axxora, LLC (Farmingdale, NY). Commercially available reagents were used without further purification.

***In vitro* transcription**
DNA templates were made through PCR amplification using primers that added the T7 polymerase promoter sequence. The templates were transcribed using T7 RNA polymerase (NEB, Ipswich, MA) in 40 mM Tris-HCl, pH 8.0, 6 mM $MgCl_2$, 2 mM spermidine, and 10 mM DTT. RNA was purified by denaturing (7.5 M urea) 6% polyacrylamide gel electrophoresis (PAGE) and was extracted from gel pieces using Crush Soak buffer (10 mM Tris-HCl, pH 7.5, 200 mM NaCl and 1 mM EDTA, pH 8.0). RNAs were precipitated with ethanol, resuspended in TE buffer (10 mM Tris-HCl, pH 8.0, 1 mM EDTA) and accurate RNA concentrations were determined via a thermal hydrolysis assay.

Radiolabeling of RNA
In vitro transcribed RNA was dephosphorylated with alkaline phosphatase (Roche, Basel, Switzerland). The RNA was phenol/chloroform extracted and then ethanol precipitated overnight. RNAs were 5'-end labeled with γ-^{32}P ATP (Perkin Elmer, Waltham, MA) using T4 polynucleotide kinase (NEB) and were purified via PAGE as described previously.

Native Slab Gel EMSAs
Reactions (10 µL) were prepared mixing radiolabeled RNA (<100 pM or 1 µM) with cdiG in buffer containing 89 mM Tris, pH 8.0, 89 mM boric acid, 1-10 mM MgCl2, 100 mM KCl, and 1 mg/mL yeast extract. Reactions were incubated at room temperature for various times, then were mixed with 3 µL 50% glycerol before loading on a 10% native gel containing the same buffer. Gels were run for 14 h at 4 °C, then were dried, exposed on a phosphor cassette and were imaged using a Typhoon laser-scanning system (GE Healthcare).

Fluorescent RNA Labeling
AlexaFluor488-labeled RNA was prepared as described previously (Willkom et al, Handbook of RNA Biochemistry vol1, 2005, pg 86). Briefly, the 3' end of the RNA was oxidized with sodium periodate then AlexaFluor488 hydrazide (Life Technologies, Carlsbad, CA) was coupled to the RNA in sodium acetate buffer. The RNA was precipitated in ethanol and then purified by PAGE as previously described.

Microfluidic Device Fabrication
Glass microfluidic chips were designed in-house and fabricated with standard wet etching process by Caliper Life Sciences (Hopkinton, MA). Prior to gel polymerization in-chip, the microchannel were washed with 1 M NaOH and silanized with a degased mixture solution of 3-(trimethoxysilyl)-propyl methacrylate (Sigma Aldrich), glacial acetic

acid, and water (2:3:5, v/v/v). The solution is introduced to the chip by capillary force. Photopatterning of polyacrylamide sieving matrixes in the glass channels was conducted in-house, and the details can be found in SI. 3-18%T discontinuous polyacrylamide gel was used here to enhance the separation resolution.

μMSA operation

The μMSA device is comprised of two intersecting 80 μm×20 μm microchannels, which are terminated in 4 fluid wells, which are denoted here as sample reservoir (SR), sample waste (SW), buffer reservoir (BR), and buffer waste (BW). Pipet tips (1 cm long) were cut and placed in the wells to expand the reservoirs volume. The riboswitch and ligand pair solution were incubated off-chip and 4 μL sample was pipetted into the sample reservoir well (SR). All other wells were filled with 4 μL of 1× TBMK buffer. Platinum electrodes were inserted into each well, and were connected to a custom built, 8-channel high voltage power supply with current/voltage feedback control. Samples were loaded into the microchannel by applying -12 μA to the SR, -2 μA to BR and BW as pinching voltage and grounding SW for 1 min. After the loading process was stabilized, the voltage plan was switched to sample injection/separation, by applying -32 μA to BR, 10 μA to SR and SW as pulling voltage and grounding BW. A narrow plug of samples were injected into the separation channel, in which individual components in the mixture migrates according to their mobilities and resolves from each other.

μMSA Imaging and Data analysis

Full-field images of sample migration and fluorescence intensity were measured via an IX-70 inverted epi-fluorescence microscope equipped with a Peltier cooled charge-coupled device (CCD) camera (CoolSNAP HQ2, Roper Scientific, Trenton, NJ) and a 10X objective. An X-Cite1 exacte mercury lamp (Lumen Dynamics, Mississauga, Canada) provided the illumination source, which was then filtered by an XF100-3 filter (Omega Optical, Battleboro, VT). In equilibrium time studies, the camera exposure time was 100 ms. For concentration calibration, the electrophoresis process was monitored in real time and stopped when the unshifted RNA band migrated to 1 mm marker, followed by a 500 ms exposure.

Images were analyzed using ImageJ software (NIH, Bethesda, MD). Intensity plots were extracted over the entire microchannel width. Post-processing was performed with OriginPro 8.0 (OriginLab, Northampton, MA). Band peak measurement was extracted with a built-in non-linear Gaussian peak-fitting algorithm. Signal-to-noise ratio (SNR) was calculated by dividing the magnitude of signal peak with the average magnitude value of neighboring noise peaks. A SNR > 5 is typically used to identify a signal by conventional standard.

CHAPTER 3

RNA-Based Fluorescent Biosensors for Live Cell Imaging of Second Messengers Cyclic di-GMP and 3′,3′ Cyclic AMP-GMP

Portions of this work were published in the following scientific journal:

Kellenberger, C. A.; Wilson, S. C.; Sales-Lee, J.; Hammond, M. C. *J. Am. Chem. Soc.* **2013**, *135*, 4906-9.

3.1 Abstract

Cyclic dinucleotides are an important class of signaling molecules that regulate a wide variety of pathogenic responses in bacteria, but tools for monitoring their regulation in vivo are lacking. We have designed RNA-based fluorescent biosensors for cyclic di-GMP and cyclic AMP-GMP by fusing the Spinach aptamer to variants of a natural GEMM-I riboswitch. In live cell imaging experiments, these biosensors demonstrate fluorescence turn-on in response to cyclic dinucleotides, and they were used to confirm *in vivo* production of cyclic AMP-GMP by the enzyme DncV.

3.2 Introduction

Cyclic dinucleotides are a newly expanded class of second messengers that mediate intracellular signaling pathways in bacteria (Gomelsky, 2011). Cyclic di-GMP (cdiG) has been shown to regulate physiological processes such as biofilm formation, motility, and virulence response (Hengge, 2009). More recently, two more cyclic dinucleotides were identified as natural products. Cyclic di-AMP (cdiA) is involved in regulating sporulation, cell size, and cell wall stress tolerance (Corrigan et al., 2011; Oppenheimer-Shaanan et al., 2011), and cyclic AMP-GMP (cAG) has been implicated in affecting intestinal colonization by bacteria (Davies et al., 2012). In addition, there is evidence that these cyclic dinucleotides stimulate the innate immune response in mammalian cells (Burdette et al., 2011; Woodward et al., 2010; Wu et al., 2013). Thus, cyclic dinucleotides are of further interest as potential small molecule adjuvants for vaccine development (Gray et al., 2012).

As with other second messengers, cyclic dinucleotide signaling appears to be tightly temporally and spatially controlled. Thus, there is a critical need for in vivo biosensors that can monitor their dynamics in order to understand how physiological changes are signaled. A Förster resonance energy transfer (FRET)-based biosensor recently has been employed to monitor cdiG in *Caulobacter crescentus* (Christen et al., 2010). It exhibits a modest decrease in net FRET signal upon ligand binding. There are as yet no reported biosensors for cdiA or cAG.

The use of RNA as a tool for in vivo molecular sensing has long been under-developed despite the natural ability of RNAs, such as riboswitches, to selectively recognize small molecules. Paige et al. recently showed that fluorescence turn-on of 3,5- difluoro-4-hydroxybenzylidene (DFHBI) by the Spinach RNA aptamer (Paige et al., 2011) can be activated by ligands binding to aptamers inserted within the Spinach sequence (Paige et al., 2012). Here we show that a selective and sensitive fluorescent biosensor for cdiG can be generated by fusing a natural GEMM-I riboswitch aptamer to Spinach. Furthermore, mutation of the ligand binding pocket of the riboswitch enables recognition of both 3′,3′ cAG and cdiG. Finally, we demonstrate the utility of RNA-based biosensors for detecting the activity of cyclic dinucleotide producing enzymes in live cells and validate the cellular activity of the first discovered 3′,3′ cAG synthase, DncV.

3.3 Results and Discussion

Binding of the conditionally fluorescent molecule DFHBI by the Spinach aptamer is highly dependent on formation of its second stem loop (Paige et al., 2012). We replaced this stem loop with the aptamer domain of the Vc2 GEMM-I class riboswitch that binds cdiG with very high affinity (K_d ~ 0.01 nM) and specificity (Figure 3.1a,b) (Smith et al., 2009; Sudarsan et al., 2008). The natural P1 stem of Vc2 was used directly as the transducer stem, since published structural probing experiments were consistent with P1 stabilization upon ligand binding (Sudarsan et al., 2008). We found that this RNA construct, called wild-type (WT) Vc2-Spinach, exhibits selective fluorescence activation in response to cdiG (Figures 3.1c and 3.2a). As expected, the related RNA construct M1 Vc2-Spinach, which harbors a disruptive mutation in the riboswitch aptamer structure (Sudarsan et al., 2008), exhibits very little fluorescence activation in response to cdiG (Figure 3.1b,c).

We next tested whether specific mutations to the ligand binding pocket would confer responsiveness to the other cyclic dinucleotides of interest. The X-ray crystal structure of the Vc2 aptamer bound to cdiG revealed that nucleobases C92 and G20 (numbered using the riboswitch aptamer sequence, Figure 3.1b) form a Watson−Crick and Hoogsteen base pair, respectively, with each of the guanine nucleotides of the ligand (Kulshina et al., 2009; Smith et al., 2009). It has been shown that the single mutant C92U binds 3′,3′ cAG (K_d = 19 ± 1.7 nM) (Shanahan et al., 2011) and the double mutant G20A/C92U binds cdiA (K_d = 1,200 ± 130 nM) (Smith et al., 2009), albeit in each case nonselectively and with much poorer affinity than the WT aptamer for cdiG. The single mutant G20A also has been shown to bind cdiG (K_d = 0.21 ± 0.07 nM) (Smith et al., 2010), but its affinity for the other cyclic dinucleotides was not determined. These three variants of Vc2-Spinach were assayed for fluorescence activation by cyclic dinucleotides. It was observed that G20A Vc2-Spinach responds robustly to c-di- GMP and 3′,3′ cAG but not to related compounds (Figure 3.2b), while the other variants exhibit little to no fluorescence activation by any of the cyclic dinucleotides (Figure 3.1c). Therefore, we focused the remainder of our analysis on the WT and G20A Vc2-Spinach RNA constructs.

In order to model physiological conditions, in vitro experiments were carried out at 37 °C in buffer containing 3 mM $MgCl_2$, which is in the range of the estimated free Mg^{2+} in the E. coli cytosol (Alatossava et al., 1985; Lusk et al., 1968). Under these conditions, it was found that WT Vc2-Spinach has an apparent K_d of 230 ± 50 nM for c- di-GMP (Figure 3.3a). This binding affinity is much poorer than the previously reported value for the Vc2 aptamer alone and can be attributed to two effects. First, WT Vc2-Spinach exhibits increased sensitivity for cdiG (K_d of 8 ± 1 nM) at 25 °C, 10 mM $MgCl_2$ (Figure 3.4), the conditions used in the previous study (Smith et al., 2009). In parallel, greater fluorescence turn-on is observed (Figure 3.5), consistent with stabilization of the RNA fold under these conditions. The remaining difference in binding affinity appears to be due to placement of the Vc2 aptamer within the context of Spinach, as we observe the same affinity trends for G20A Vc2-Spinach (Figures 3.4 and 3.6). Thus, the apparent insensitivity of C92U and G20A/C92U biosensors is consistent with comparable reductions in binding affinities leading to K_d values much larger than the ligand

concentration (100 μM) used in the assay. Another WT Vc2-Spinach construct with an artificial transducer stem in place of the second stem loop of Spinach has been described that displays weak binding affinity to cdiG even at 25 °C (Nakayama et al., 2012b). In this case, the difference in affinity relative to our WT construct is likely due to alteration of the Vc2 aptamer P1 stem sequence, which reduces ligand binding (Smith et al., 2010).

Since the concentration of cdiG appears to range from <50 nM to a few micromolar in bacteria (Hengge, 2009), WT Vc2-Spinach should be capable of detecting cdiG at biologically relevant concentrations. Furthermore, the dynamic range of the RNA-based biosensor is larger than that of the previously mentioned protein-based biosensor, which binds cdiG cooperatively as a dimer (Christen et al., 2010). The *in vitro* fluorescence signal of WT Vc2-Spinach changes from 10% to 90% between 25 and 2000 nM cdiG (Figure 3.3a). In comparison, the protein-based biosensor exhibits similar affinity as the RNA biosensor, but its FRET signal *in vitro* changes from 90% to 10% between 67 and 560 nM cdiG (Christen et al., 2010). The RNA-based biosensor does display relatively slow activation and deactivation rates (Figure 3.7), so it would need to be improved if it is necessary to monitor rapid dynamics.

We then tested the activity of WT Vc2-Spinach as a fluorescent biosensor to detect cdiG levels in live cells (Figures 3.3b,c and 3.8). All RNA constructs were inserted into a tRNA scaffold to improve stability upon expression in *E. coli* (Ponchon and Dardel, 2007). The tRNA scaffold has a negligible effect on ligand binding affinities (Figure 3.4). Plasmids encoding WT Vc2-Spinach tRNA and variants of the diguanylate cyclase WspR from *Pseudomonas fluorescens* were cotransformed into cells. We verified that the expression levels of RNA constructs were unaffected by expression of different enzymes (Figure 3.9). Besides WT WspR (Malone et al., 2007), we analyzed the D70E mutant, which mimics phosphorylation at that site and is constitutively active, and the G249A mutant, which knocks out the conserved GGDEF domain and is constitutively inactive (Malone et al., 2007). Thus, cells expressing the WT biosensor and G249A WspR represent the fluorescence signal for endogenous levels of cdiG in *E. coli*. As shown, the average fluorescence of these cells is 1.6-fold above the nonspecific background, which is represented by cells expressing Vc2 tRNA, a construct that does not contain the Spinach aptamer (Figure 3.10). In comparison, cells expressing the biosensor and WT or D70E WspR exhibit roughly the same increases in average fluorescence (2.3- and 2.4-fold, respectively) above the signal corresponding to endogenous levels. These data are consistent with production of additional cdiG by the WT and constitutively active enzymes.

In contrast, cells expressing the M1 biosensor do not exhibit average fluorescence above background except in the case where D70E WspR is coexpressed. M1 Vc2-Spinach has very weak binding to cdiG, as we observed *in vitro* (Figure 3.1c), so it appears that levels of cdiG that are endogenous or produced by WT WspR are below the threshold of detection. However, D70E WspR produces cdiG at extremely high concentrations, estimated to be around 3 mM (Nakayama et al., 2011), and so elicits a small fluorescence response from the mutant biosensor. For the WT biosensor, the lack

of a significant difference in fluorescence with overexpression of the active WspR variants suggests that each produces enough cdiG to saturate the biosensor and give maximal fluorescence signal. These data demonstrate that WT Vc2-Spinach is a sensitive biosensor that gives a measurable fluorescence response to endogenous cdiG and increased signal upon elevation of cdiG concentrations.

In order to analyze the G20A Vc2-Spinach aptamer for use *in vivo*, its relative affinities for cdiG and 3′,3′ cAG were determined. The G20A Vc2-Spinach aptamer has an apparent K_d of 1000 ± 150 nM for cdiG and 4200 ± 320 nM for 3′,3′ cAG at 37 °C, 3 mM $MgCl_2$ (Figure 3.6a). The G20A biosensor appears to be not sensitive enough to detect endogenous cdiG but, as expected, gives a fluorescence signal upon expression of WT and D70E WspR (Figure 3.11). In this case, the fluorescence signal with WT WspR is not saturated and is clearly less than the D70E WspR signal. While G20A Vc2-Spinach by itself cannot distinguish between c-di- GMP and 3′,3′ cAG, we considered that comparing the ratio of fluorescence activation between the G20A and WT biosensors may allow us to differentiate between responses to the two cyclic dinucleotides.

The dinucleotide cyclase DncV from *V. cholerae* was recently shown to synthesize cdiG, cdiA, and 3′,3′ cAG *in vitro*, but it preferentially makes 3′,3′ cAG in the presence of all four nucleotide triphosphates (Davies et al., 2012). Also, mass spectrometry analysis of cell lysates supports that 3′,3′ cAG is produced *in vivo* by WT DncV but not by the catalytically inactive D131A/D133A DncV mutant (Davies et al., 2012). However, it was not possible to ascertain whether cdiG also was being produced by this enzyme *in vivo*. We found that cells expressing the WT biosensor and D131A/D133A DncV have an average fluorescence 1.6-fold above background, which is the same as observed with inactive WspR and corresponds to detection of endogenous cdiG (Figure 3.6b,c). Expression of WT DncV does not significantly change the average fluorescence of the WT biosensor, providing direct evidence that this enzyme does not produce cdiG *in vivo* under these conditions.

Cells expressing the G20A biosensor and D131A/D133A DncV exhibit an average fluorescence that is similar to background, represented by M1 Vc2-Spinach (Figures 3.6b,c, 3.12, and 3.13). This result agrees with G20A Vc2-Spinach having a reduced sensitivity for cdiG and E. coli cells not making 3′,3′ cAG. In contrast, cells expressing the G20A biosensor and WT DncV exhibit greater than 4-fold increase in fluorescence above background. Given the results from the WT biosensor, this observation is consistent with fluorescence activation of the G20A biosensor due to production of 3′,3′ cAG by WT DncV. Thus, we have engineered a biosensor that can detect 3′,3′ cAG, a newly discovered second messenger, in live cells.

In summary, we have developed two different fluorescent biosensors for live cell imaging of cyclic dinucleotides. We demonstrate the ability to alter specificity of the RNA-based biosensor by exploiting rational mutations to the ligand binding pocket instead of by inserting distinct aptamers. Ongoing work focuses on improving the binding characteristics of these first generation biosensors and on developing a

fluorescent biosensor for cdiA. We aim to use our biosensors to accurately quantitate changes in the intracellular levels of cyclic dinucleotides upon different physiological stimuli, similar to sensors for cGMP (Nausch et al., 2008). It is envisioned that sensitive and specific biosensors for each cyclic dinucleotide will help elucidate how these different signals are integrated and transduced by bacteria.

3.4 Figures

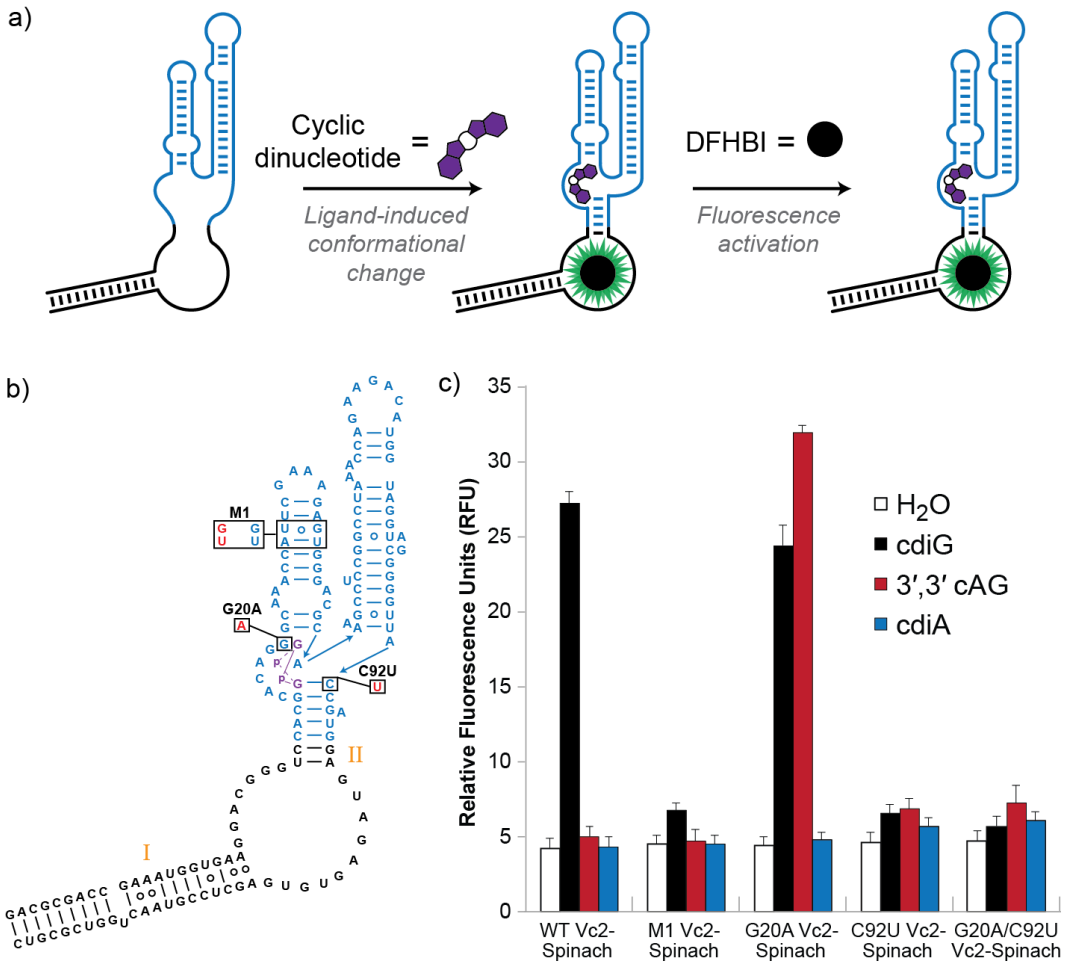

Figure 3.1 RNA-based fluorescent biosensors detect cyclic dinucleotide second messengers. (a) Design scheme for a fluorescent biosensor that detects cyclic dinucleotides. Ligand binding to the Vc2 riboswitch aptamer (blue) enables the Spinach aptamer (black) to bind and activate the conditionally fluorescent molecule DFHBI. **(b)** Sequence and secondary structure model of the Vc2-Spinach construct. Mutants analyzed in the study are boxed, cdiG is shown in purple, and Spinach stems are numbered in orange. **(c)** *In vitro* screen of Vc2-Spinach biosensor variants for fluorescence activation in response to cyclic dinucleotides. Error bars represent the standard deviation of three independent experiments with duplicate samples.

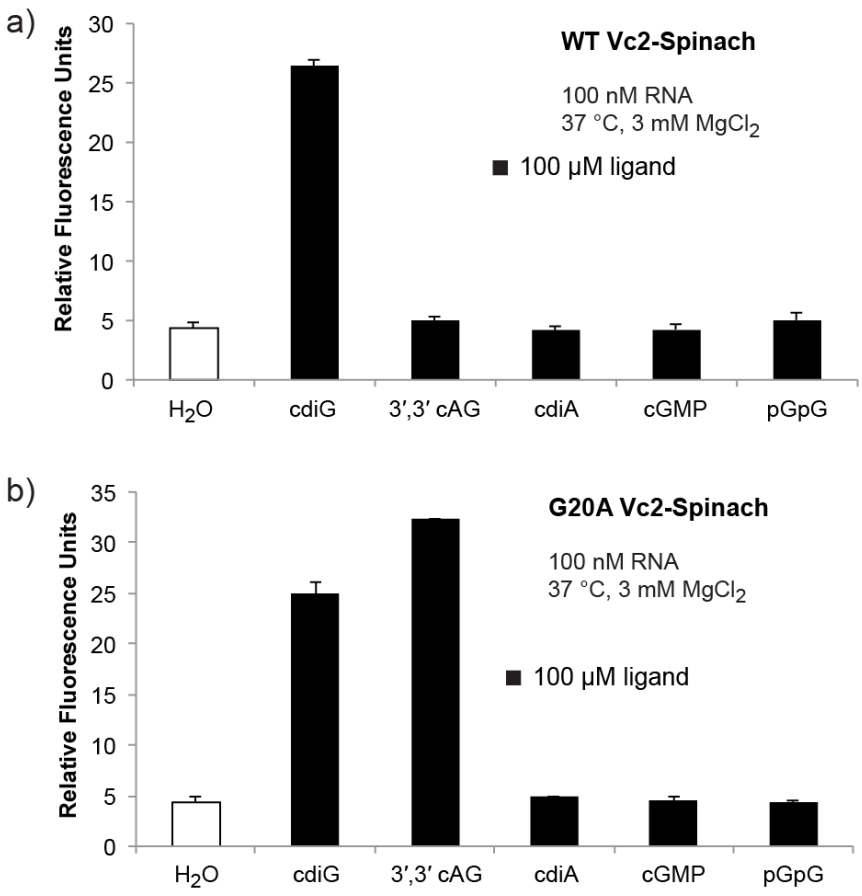

Figure 3.2 Selectivity of WT and G20A Vc2-Spinach sensors. (a) WT Vc2-Spinach is selective for cdiG. WT Vc2-Spinach (100 nM) was incubated with ligand (100 μM) and DFHBI (10 μM) at 37 °C in 40 mM HEPES, pH 7.5, 125 mM KCl, and 3 mM $MgCl_2$. Error bars represent the standard deviation of two independent replicates with duplicate samples. **(b)** G20A Vc2-Spinach responds to cdiG and cyclic AMP-GMP but not to related compounds. G20A Vc2-Spinach RNA (100 nM) was incubated with ligand (100 μM) and DFHBI (10 μM) at 37 °C in 40 mM HEPES, pH 7.5, 125 mM KCl, and 3 mM $MgCl_2$. Error bars represent the standard deviation of two independent experiments with duplicate samples.

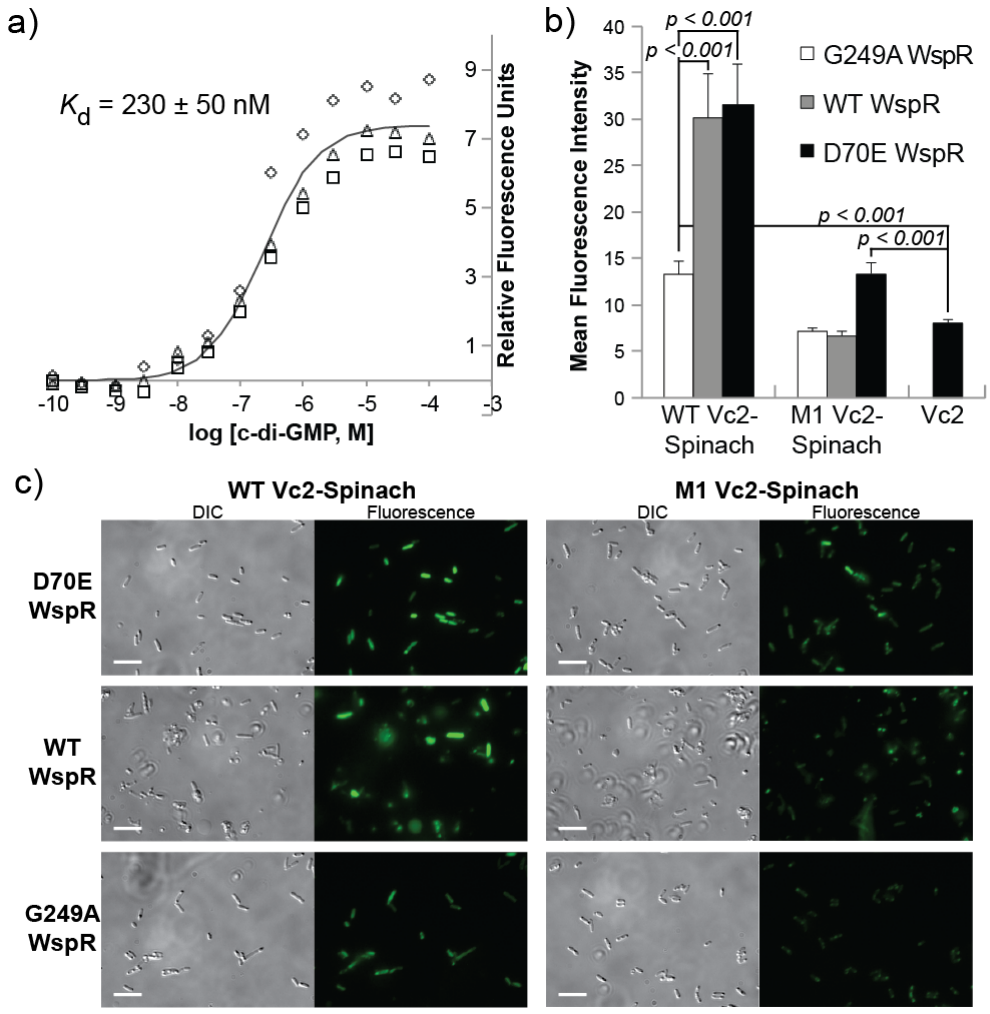

Figure 3.3 WT Vc2-Spinach is a sensitive biosensor for cdiG in live cells. (a) *In vitro* analysis of WT Vc2-Spinach binding affinity for cdiG. Data from three independent replicates and the best-fit curve are shown. Background fluorescence (without cdiG) was subtracted from all data points. **(b)** Quantitation of mean fluorescence intensity of cells. Error bars indicate SEM for at least 50 cells. *P*-values from student's t-test comparisons for fluorescence changes discussed in text are shown. **(c)** Differential interference contrast (DIC) and fluorescence images of E. coli cells expressing Vc2-Spinach tRNAs and WspR enzyme variants after incubation with DFHBI. Cells expressing WT WspR were observed to have more cellular debris compared to other samples. Scale bars represent 10 μm.

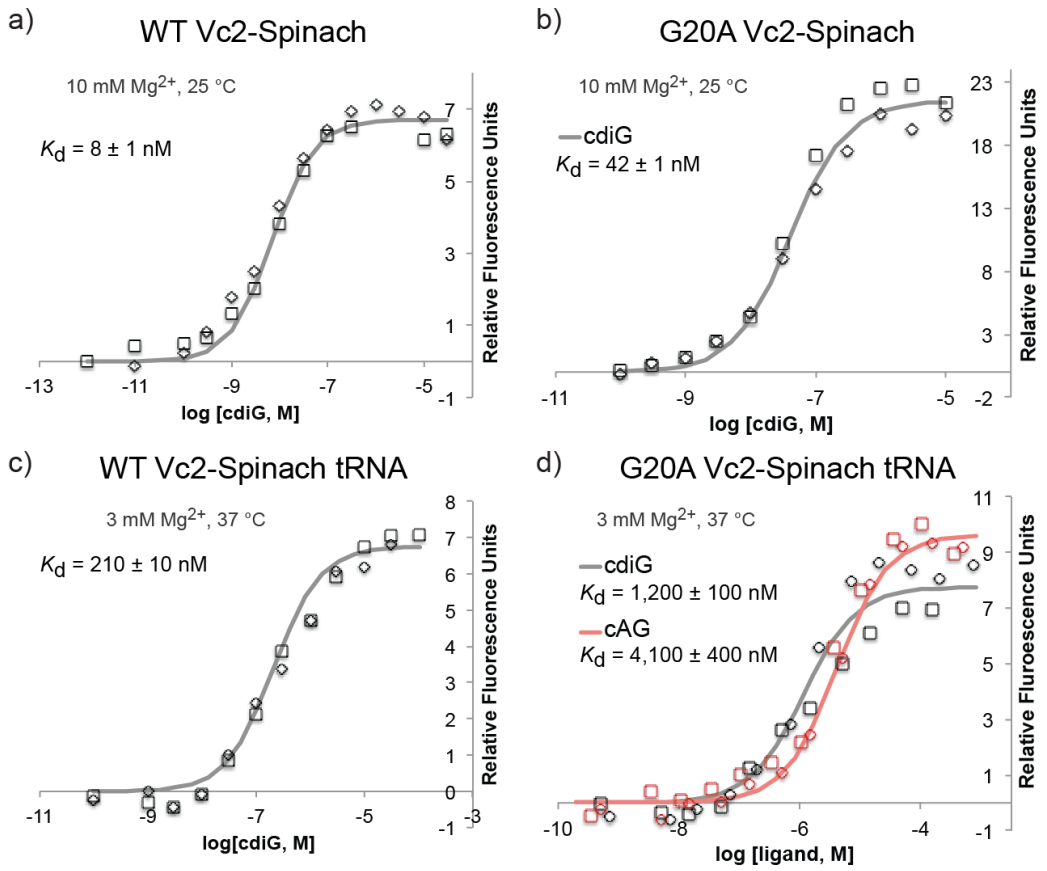

Figure 3.4 Effect of temperature, Mg^{2+} concentration, and the tRNA scaffold on the affinity of WT and G20A Vc2-Spinach. (a) and **(b)** Analysis of WT Vc2-Spinach (a) and G20A Vc2-Spinach (b) binding to cdiG at 25 °C in 40 mM HEPES, pH 7.5, 125 mM KCl, and 10 mM $MgCl_2$. RNA (3 nM for WT, 10 nM for G20A) was incubated with DFHBI (10 μM) and different concentrations of cdiG. **(c)** and **(d)** Analysis of WT Vc2-Spinach tRNA (c) and G20A Vc2-Spinach tRNA (d) binding to cdiG or 3′,3′ cAG at 37 °C in 40 mM HEPES, pH 7.5, 125 mM KCl, and 3 mM $MgCl_2$. RNA (30 nM) was incubated with DFHBI (10 μM) and different concentrations of cdiG. For (a)-(d), data from two independent replicates with duplicate samples and the best-fit curve are shown. Background fluorescence (without cyclic dinucleotide) was subtracted from all points.

By lowering the temperature and increasing the concentration of Mg^{2+}, the apparent K_d value of the WT and G20A Vc2-Spinach aptamers for cdiG decrease. The apparent K_d of WT Vc2-Spinach for cdiG is 8 ± 1 nM at 25 °C in buffer containing 10 mM $MgCl_2$, compared to 230 ± 50 nM at 37 °C in buffer containing 3 mM $MgCl_2$. Similarly, the apparent K_d of G20A Vc2-Spinach for cdiG is 42 ± 1 nM at 25 °C in buffer containing 10 mM $MgCl_2$, compared to 1000 ± 150 nM at 37 °C in buffer containing 3 mM $MgCl_2$. These differences are likely due to increased folding stability of the RNAs at a lower temperature and with higher Mg^{2+}. The addition of the tRNA scaffold to the WT or G20A Vc2-Spinach sequences appears to have no significant effect on the measured K_d.

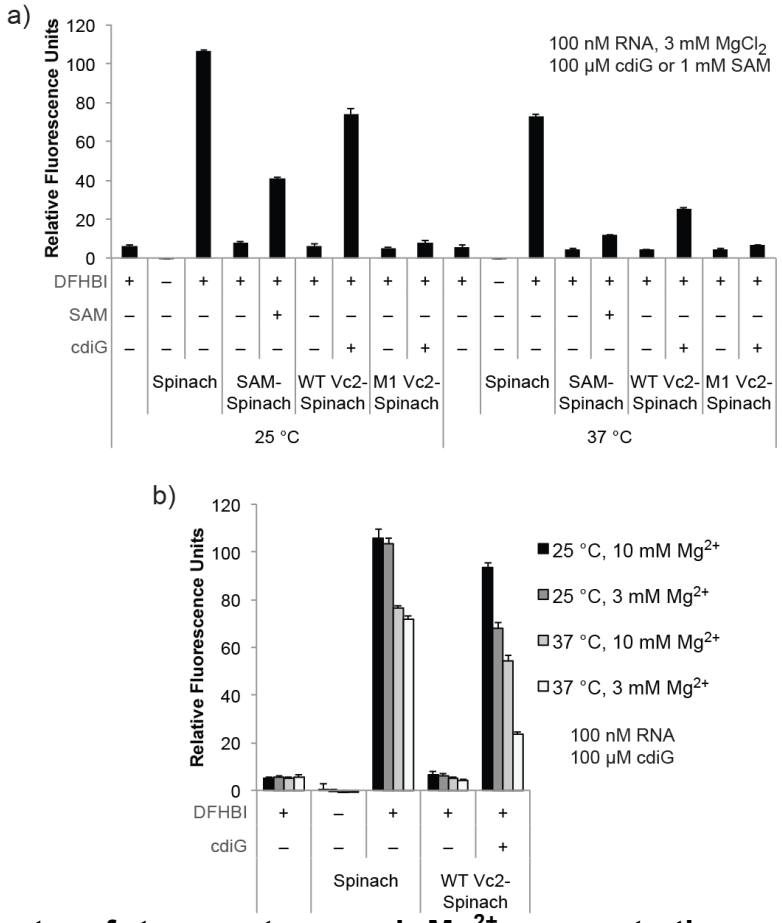

Figure 3.5 Effects of temperature and Mg^{2+} concentration on fluorescence activation of Spinach constructs. (a) Comparison of fluorescence activation between the original Spinach aptamer and several Spinach-derived biosensor constructs at 25 and 37 °C. The *S*-adenosylmethionine (SAM)-Spinach biosensor was published by Paige *et. al.* See main text for description of Vc2-Spinach constructs. RNA (100 nM) was incubated with ligand (100 μM cdiG or 1 mM SAM) and DFHBI (10 μM) in binding buffer. Error bars represent the standard deviation of two independent experiments with duplicate samples. **(b)** Comparison of the effects of temperature and Mg^{2+} concentration between the original Spinach aptamer and WT Vc2-Spinach. Same reaction conditions as described in (a). Error bars represent the standard deviation of two independent experiments with duplicate samples.

Overall, the biosensor constructs (SAM-Spinach and Vc2-Spinach RNAs) have reduced fluorescence compared to Spinach alone. Fluorescence induction of the WT Vc2-Spinach biosensor is higher than that of the published SAM-Spinach biosensor. Fluorescence of all RNAs decreases with higher temperature. The fluorescence of WT Vc2-Spinach is sensitive to changes in Mg^{2+} concentration between 3 and 10 mM, which is consistent with observations for the Vc2 aptamer (Kulshina et al., 2009), whereas the fluorescence of the Spinach aptamer is unchanged in the same conditions. Furthermore, raising the temperature from 25 °C to 37 °C has a slightly larger effect on the fluorescence of WT Vc2-Spinach than decreasing the Mg^{2+} concentration from 10 mM to 3 mM. Thus, we expect both parameters to influence the affinity of the biosensor.

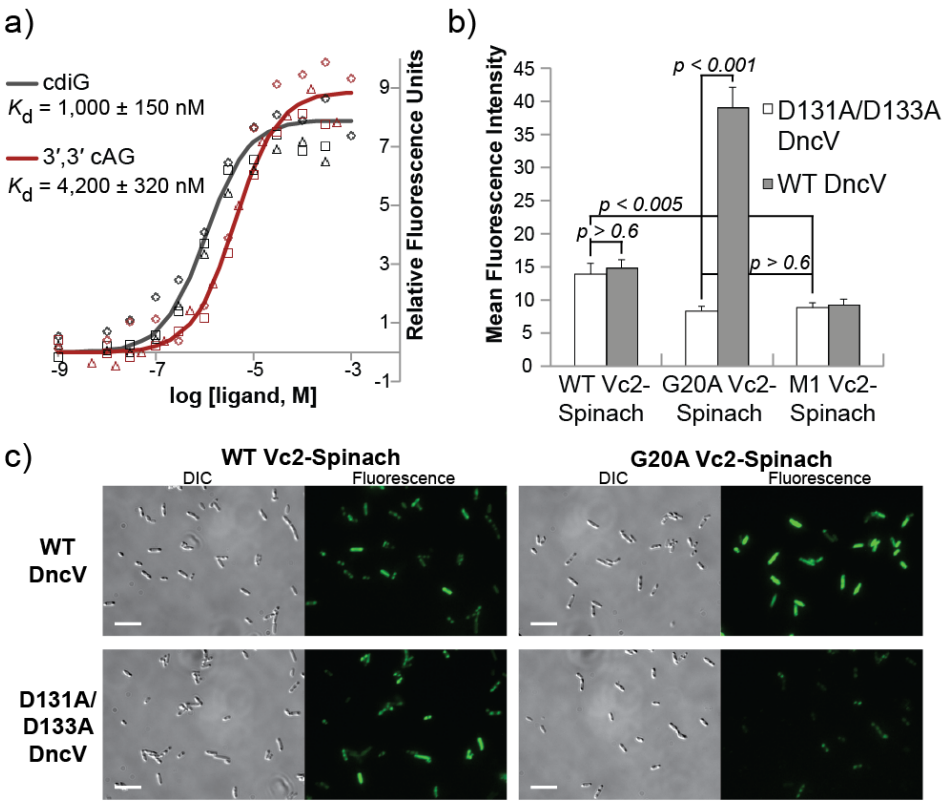

Figure 3.6 Analysis of the enzymatic activity of DncV in live cells using Vc2-Spinach biosensors. **(a)** *In vitro* analysis of G20A Vc2-Spinach binding affinity for cdiG (black) and 3′,3′ cAG (red). Data from three independent replicates each and the best-fit curves are shown. Background fluorescence (without ligand) was subtracted from all data points. b Quantitation of mean fluorescence intensity of cells. Error bars indicate SEM for at least 50 cells. P-values from student's t-test comparisons are shown. **(c)** DIC and fluorescence images of *E. coli* cells expressing Vc2-Spinach tRNAs and DncV enzyme variants after incubation with DFHBI. Scale bars represent 10 μm.

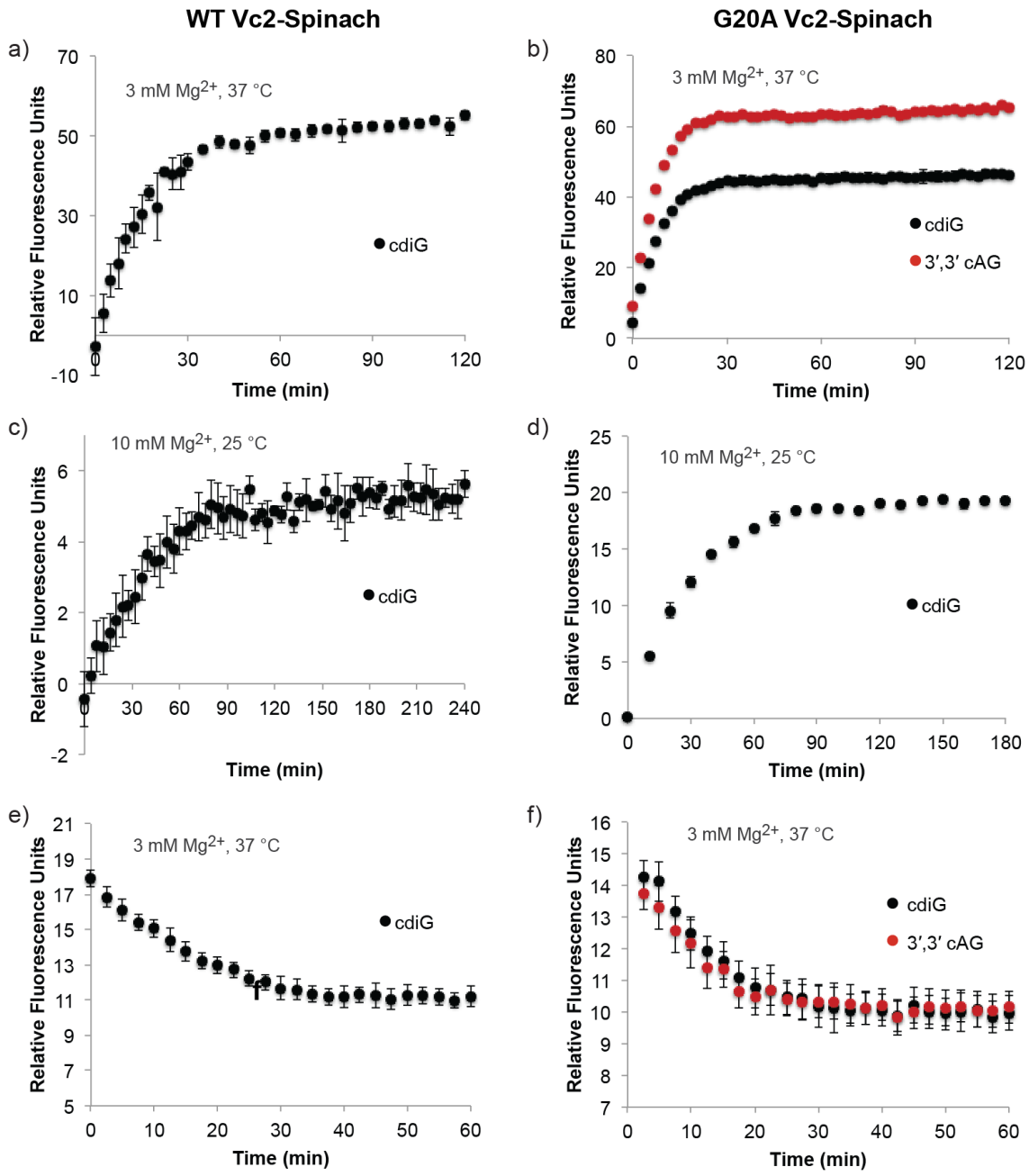

Figure 3.7 Activation and deactivation rates of the WT and G20A Vc2-Spinach aptamers. (a) and **(b)** Fluorescence activation rates of WT Vc2-Spinach (a) and G20A Vc2-Spinach (b) with cdiG or 3′,3′ cAG at 37 °C. RNA (100 nM) was mixed with DFHBI (10 μM) and ligand (100 μM) in 40 mM HEPES, pH 7.5, 125 mM KCl, and 3 mM $MgCl_2$. **(c)** and **(d)** Fluorescence activation rate of WT Vc2-Spinach (c) and G20A Vc2-Spinach (d) with cdiG at 25 °C. RNA (3 nM for WT, 10 nM for G20A) was mixed with DFHBI (10 μM) and cdiG (100 μM) in 40 mM HEPES, pH 7.5, 125 mM KCl, and 10 mM $MgCl_2$. **(e)** and **(f)** Fluorescence deactivation of WT Vc2-Spinach (e) and G20A Vc2-Spinach at 37 °C. RNA (100 nM) was incubated with DFHBI (10 μM) and ligand (10 μM) in 40 mM HEPES, pH 7.5, 125 mM KCl, and 3 mM $MgCl_2$ (data not shown). The fluorescence was

monitored after the RNA was passed through a buffer exchange column equilibrated in buffer without ligand. Control samples where the column was pre-equilibrated with ligand show a decrease of less than 2 RFUs over the course of the experiment. For (a)-(f), error bars represent standard deviation of two replicate samples.

Full activation of WT Vc2-Spinach by ligand binding takes 40 min at 37 °C and 80 min at 25 °C. Conversely, WT Vc2-Spinach is fully deactivated within 40 min at 37 °C. It appears that the current biosensor achieves 75% activation or deactivation in half the time to reach full activation (20 min at 37 °C). The relatively slow response time is due to the slow ligand association and dissociation rates for the Vc2 aptamer.(Smith et al., 2009) While the YcgR protein-based biosensor displays much faster activation kinetics (1-2 min), the redistribution of cdiG during cell division was monitored over the course of 2 h in 15 min intervals.(Christen et al., 2010) Thus, the Vc2-Spinach biosensor already may be suitable for similar purposes.

For G20A Vc2-Spinach, full activation by ligand binding takes approx. 25 min at 37 °C and 80 min at 25 °C. Conversely, G20A Vc2-Spinach is fully deactivated within 30 min at 37 °C. It appears that the current biosensor achieves 75% activation or deactivation in half the time to reach full activation (~12.5 min at 37 °C). In general, the timescale of cyclic dinucleotide signaling processes has not been studied in depth. Current work is aimed at improving the binding kinetics of the RNA-based biosensor.

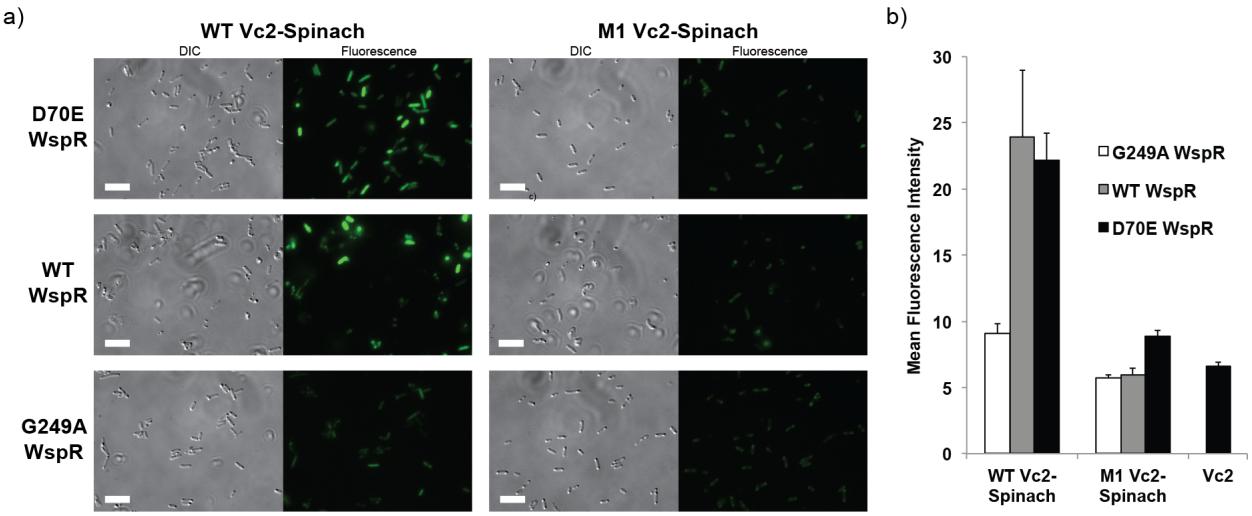

Figure 3.8 Independent replicate of fluorescence microscopy experiments from Figure 3.3. (a) Differential interference contrast and fluorescence images of *E. coli* cells expressing WT (left panels) or M1 (right panels) Vc2-Spinach tRNA and WspR variants after incubation with DFHBI. Scale bars represent 10 μm. **(b)** Mean fluorescence intensity of cells expressing WT or M1 Vc2-Spinach tRNA and various alleles of WspR. Error bars indicate S.E.M. for at least 50 cells.

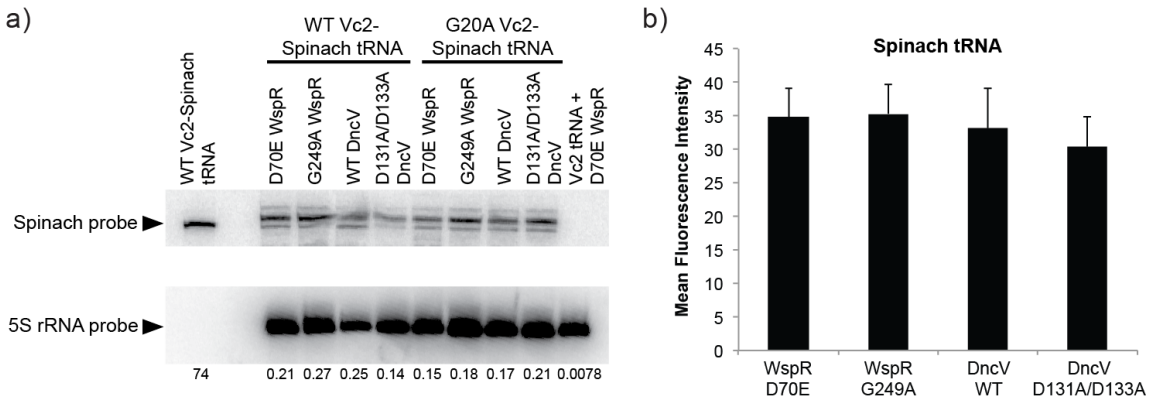

Figure 3.9 Expression levels of the RNA biosensors and Spinach are unchanged by expression of different enzyme variants. (a) Northern blot analysis of total RNA isolated from cells co-expressing Vc2-Spinach tRNAs and WspR or DncV. *In vitro* transcribed WT Vc2-Spinach tRNA served as a positive control for the Spinach probe; it is expected to be shorter than the *in vivo* RNA product, which contains a terminator sequence. Total RNA isolated from cells co-expressing Vc2 tRNA and D70E WspR served as a negative control for the Spinach probe. 5S rRNA served as the loading control. The ratio of signal intensities for the Spinach probe to the 5S rRNA probe is shown for each lane below the Northern blot. **(b)** Quantitation of mean fluorescence intensity of cells expressing Spinach tRNA and different alleles of WspR or DncV. Error bars represent the S.E.M. of at least 70 cells.

The effect of co-expression of different enzyme variants on the levels of the RNA constructs was analyzed by Northern blot and fluorescence microscopy. Northern blot analysis shows that the expression of enzymes D70E WspR, G249A WspR, or WT DncV has negligible effect on RNA biosensor levels, whereas D131A/D133A DncV expression has inconsistent effects that are less than 2-fold. Furthermore, we analyzed the fluorescence of cells co-expressing different enzyme variants and the Spinach tRNA, which should exhibit fluorescence independent of cyclic di-nucleotide levels. As expected, these results show that expression of the enzymes has no significant effect on the mean fluorescence intensity of the cells ($p > 0.4$ for all comparisons). Taken together, these data show that the slight differences in RNA levels are not sufficient to account for the fluorescence changes observed for the biosensors under these conditions.

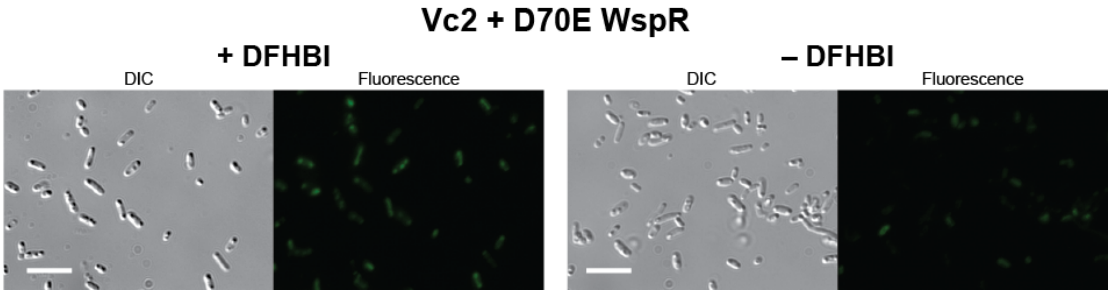

Figure 3.10. Analysis of non-specific background fluorescence. Differential interference contrast and fluorescent images of *E. coli* cells expressing Vc2 tRNA and the constitutively active D70E WspR after incubation with or without DFHBI. Scale bars represent 10 μm.

Non-specific fluorescence from DFHBI is seen in the negative control that consists of *E. coli* expressing RNA not containing the Spinach aptamer sequence. Comparison of cells expressing Vc2 tRNA and D70E WspR with and without DFHBI showed weak, localized fluorescence only with DFHBI that coincide with the location of inclusion bodies, whereas uniform background fluorescence was observed without DFHBI. This difference was observed only in the fluorescence channel monitoring DFHBI emission.

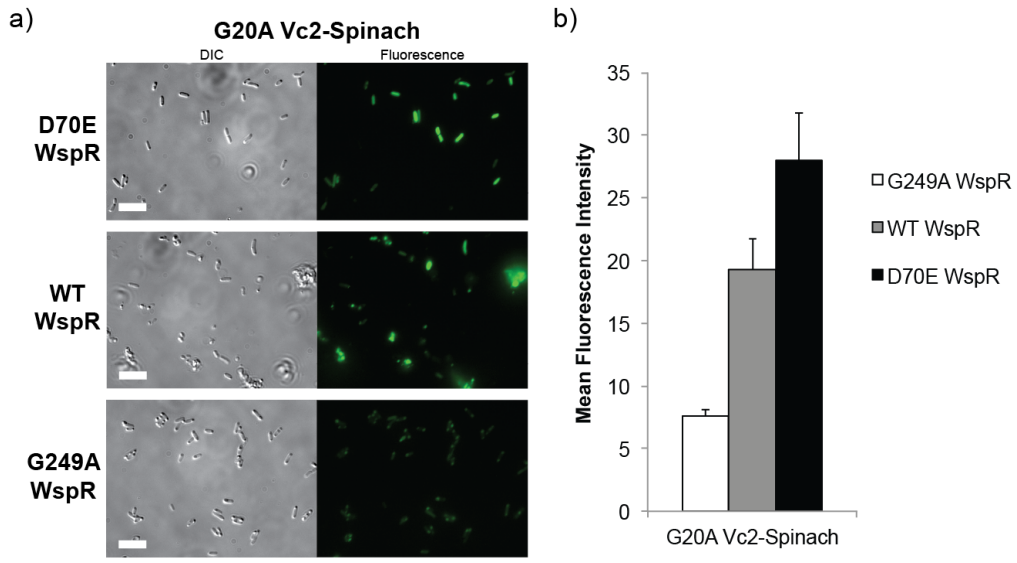

Figure 3.11 G20A Vc2-Spinach biosensor also responds to cdiG. (a) Differential interference contrast (left panels) and fluorescent images (right panels) of *E. coli* cells expressing G20A Vc2-Spinach tRNA and WspR variants after incubation with DFHBI. Scale bars represent 10 μm. **(b)** Mean fluorescence intensity of cells expressing G20A Vc2-Spinach tRNA and various alleles of WspR. Error bars indicate S.E.M. of at least 50 cells per sample.

The G20A biosensor exhibits an intermediate fluorescence signal in response to expression of WT WspR. This suggests that, in contrast to the WT biosensor, it is not saturated by the levels of cdiG produced by WT WspR *in vivo*. The result is consistent with G20A Vc2-Spinach having a poorer affinity for cdiG than WT Vc2-Spinach (K_d of 1000 ± 150 nM versus 230 ± 50 nM). We assume that the G20A biosensor is saturated with cdiG upon expression of D70E WspR, which produces cdiG at concentrations estimated to be around 3 mM.(Nakayama et al., 2011) Background fluorescence is observed for cells expressing the G20A biosensor and G249A WspR (inactive variant), consistent with reduced sensitivity leading to no signal in response to endogenous cdiG levels.

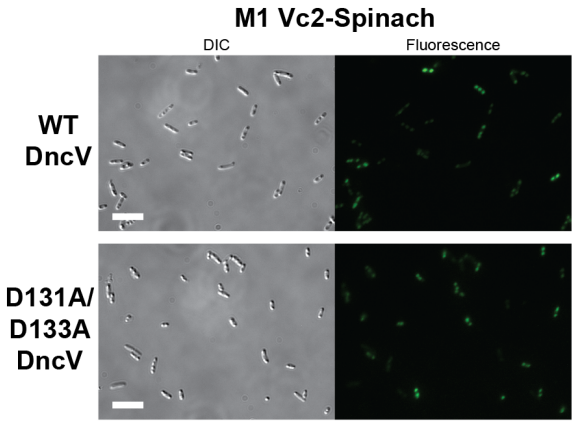

Figure 3.12 M1 Vc2-Spinach tRNA control shows background fluorescence with WT or D131A/D133A DncV. Differential interference contrast (left panels) and fluorescent images (right panels) of *E. coli* cells expressing M1 Vc2-Spinach tRNA and WT or inactive D131A/D133A DncV after incubation with DFHBI. Quantitation of mean fluorescence intensity of this sample is shown in Figure 3.6b. Scale bars represent 10 μm.

Weak, localized spots of fluorescence are observed with the M1 Vc2-Spinach biosensor under these conditions, which resemble the non-specific fluorescence of the negative control (Figure 3.10).

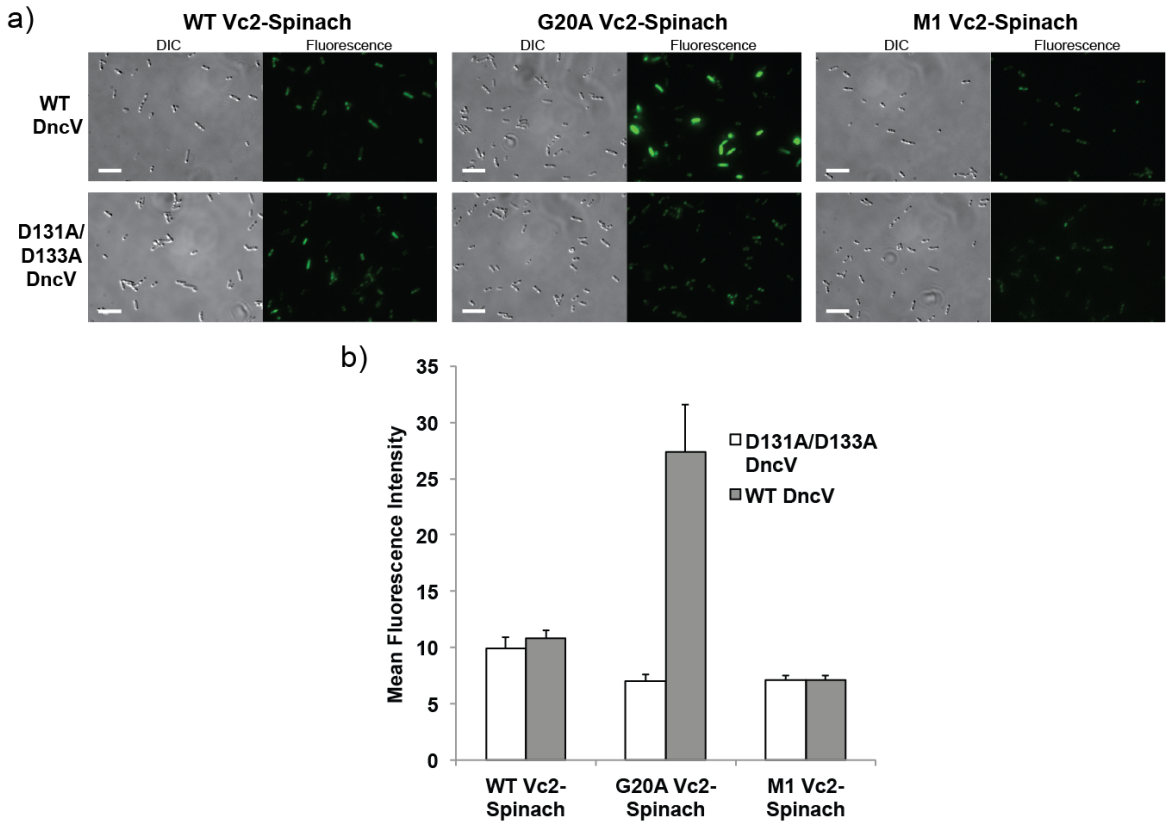

Figure 3.13 Independent replicate of fluorescence microscopy experiments from Figure 3.6. (a) Differential interference contrast and fluorescence images of *E. coli* cells expressing WT (left panels), G20A (center panels), or M1 (right panels) Vc2-Spinach tRNA and DncV variants after incubation with DFHBI. Scale bars represent 10 μm. **(b)** Mean fluorescence intensity of cells expressing WT, G20A, or M1 Vc2-Spinach tRNA and various alleles of DncV. Error bars indicate S.E.M. for at least 50 cells.

3.5 Materials and Methods

Reagents and oligonucleotides

DNA oligonucleotides were purchased from Elim Biopharmaceuticals (Hayward, CA) and IDT (Coralville, IA). Cyclic di-GMP, cyclic di-AMP, cyclic GMP, and pGpG were purchased from Axxora, LLC (Farmingdale, NY). DFHBI was purchased from Lucerna (New York, NY) and was prepared as a 20 mM stock solution in DMSO. Commercially available reagents were used without further purification. Chemically competent BL21 (DE3) Star cells were purchased from Life Technologies (Carlsbad, CA). *Vibrio cholerae* genomic DNA and D70E WspR DNA were gifts from the Marletta lab.

***In vitro* transcription**

DNA templates were made through PCR amplification from the appropriate plasmid DNA using primers that added the T7 polymerase promoter sequence. The templates were transcribed using T7 RNA polymerase in 40 mM Tris-HCl, pH 8.0, 6 mM $MgCl_2$, 2 mM spermidine, and 10 mM DTT. RNA was purified in a denaturing (7.5 M urea) 6% polyacrylamide gel and was extracted from gel pieces using Crush Soak buffer (10 mM Tris-HCl, pH 7.5, 200 mM NaCl and 1 mM EDTA, pH 8.0). RNAs were precipitated with ethanol, resuspended in TE buffer (10 mM Tris-HCl, pH 8.0, 1 mM EDTA) and their concentrations were determined.

Ligand binding assays

To measure the fluorescence of each RNA construct in response to ligand, a solution of ligand (100 μM) and DFHBI (10 μM) was prepared in buffer containing 40 mM HEPES, pH 7.5, 125 mM KCl, and 3 mM $MgCl_2$. The RNA was renatured in buffer at 70 °C for 3 min and cooled to ambient temperature for 5 min prior to addition to the reaction solution at a final concentration of 100 nM. Duplicate 100 μL binding reactions were incubated at 37 °C in a Corning Costar (Tewksbury, MA) 96-well black plate until equilibrium was reached. The fluorescence emission was measured using a Molecular Devices SpectraMax M3 plate reader (Sunnyvale, CA) with the following instrument parameters: 460 nm excitation, 500 nm emission, 495 nm cutoff. The background fluorescence of the buffer without DFHBI was subtracted from each sample to determine the relative fluorescence units. For experiments to measure K_d, the ligand concentration was varied as the concentrations of RNA (30 nM unless otherwise noted) and DFHBI (10 μM) were held constant, and the fluorescence of the sample with no ligand was subtracted to determine relative fluorescence units.

Activation and deactivation assays

The rate of activation of fluorescence was measured as described previously(Paige et al., 2012). Briefly, a solution of ligand (100 μM) and DFHBI (10 μM) was prepared in buffer containing 40 mM HEPES, pH 7.5, 125 mM KCl, and 3 mM $MgCl_2$ and was warmed to 37 °C. The RNA (100 nM) was renatured in buffer at 70 °C for 3 min then cooled to 37 °C prior to addition to the reaction solution. Immediately after the RNA was added, the fluorescence emission was measured every 2.5 min at 37 °C using the same plate reader settings as for the ligand binding assays. The fluorescence of the sample with no ligand was subtracted to determine relative fluorescence units. The same

experiments were carried out with WT Vc2-Spinach (3 nM) or G20A Vc2-Spinach (10 nM) at 25 °C in a buffer containing 10 mM $MgCl_2$ to determine the activation rate at ambient temperature.

Deactivation assays were performed using buffer exchange to remove the cyclic di-nucleotide ligand. RNA (100 nM) was mixed with ligand (10 μM) and DFHBI (10 μM) in a buffer containing 40 mM HEPES, pH 7.5, 125 mM KCl, and 3 mM $MgCl_2$ at 37 °C. Once the reaction had reached maximum fluorescence, half of the reaction was passed through an Illustra NAP-5 column (GE Healthcare) that had been equilibrated with DFHBI (10 μM) in buffer while the other half was passed through the column that had been equilibrated with ligand (10 μM), DFHBI (10 μM), and buffer. Immediately after elution of the RNA, the fluorescence emission was measured every 2.5 min at 37 °C using the same plate reader settings as for the ligand binding assays.

Live cell imaging of *E. coli*

For stable RNA expression *in vivo*, the human $tRNA^{Lys}_3$ scaffold was added to the 5' and 3' ends of WT Vc2-Spinach, as described in Paige *et al.*(Paige et al., 2012; Ponchon and Dardel, 2007). The WT Vc2-Spinach tRNA construct was amplified using primers that added a BglII restriction site and the T7 polymerase promoter sequence to the 5' end and a T7 terminator and XhoI restriction site to the 3' end. The product was then cloned into the pET31b vector for inducible expression in *E. coli*. Vc2-Spinach tRNA mutants were created by PCR amplification of the appropriate Vc2-Spinach sequence using primers that added EagI and SacII restriction sites to the 5' and 3' ends, respectively. Then the WT Vc2-Spinach fragment was removed from pET31b-tRNA by digestion with EagI and SacII and the appropriate Vc2-Spinach variant was cloned in its place. The WspR gene was amplified using primers that added NdeI and XhoI restriction sites to the 5' and 3' ends, respectively, and the product was cloned into pET24a. The DncV gene was amplified using primers that added an NheI restriction site to the 5' end and a 6xHis tag followed by a XhoI restriction site to the 3' end. This product was then cloned into pET24a for inducible expression in *E. coli*. Quikchange (Stratagene, La Jolla, CA) was used according to the manufacturer's protocol to produce the various mutations.

BL21 (DE3) Star *E. coli* cells were co-transformed with 60 ng each of the appropriate plasmids and cells were plated on LB/Carb/Kan plates (Carb: 50 μg/mL, Kan: 50 μg/mL). Single colonies were used to inoculate overnight LB/Carb/Kan cultures grown at 37 °C. Fresh LB/Carb/Kan cultures were inoculated with the overnight culture, and the cells were induced with 1 mM isopropyl β-D-1-thiogalactopyranoside (IPTG) once they reached an OD_{600} ~ 0.5. Induced cells were incubated for another 2.5 h at 37 °C, then were pelleted, washed once with M9 minimal media, pH 6.5, and resuspended in 200 μL M9 minimal media, pH 6.5 to an OD_{600} ~ 1. The cell suspension was pipetted onto poly D-Lysine coated coverslips and incubated at 37 °C for 45 min to allow the cells to adhere. Unattached cells were removed by washing thoroughly with M9 minimal media, and then 200 μL of 200 μM DFHBI in M9 minimal media, pH 6.5 was added to cover the cells. The cells were incubated with DFHBI on the coverslip for 1.5 h at 37 °C before placing them over microscope slides for visualization. Epifluorescence imaging

experiments were performed using a Zeiss 200M AxioVert microscope (Zeiss, Jena, Germany) equipped with a mercury light source X-Cite 120 Series (Exfo Life Science Divisions, Ontario, Canada), a 63x/1.4 Plan-Apochromat oil DIC objective lens and a 1.6x tube lens. For monitoring fluorescence, a GFP filter set with an excitation 470/40 BP, FT 495 beamsplitter, and emission 525/50 BP was used (Filter Set 38 HE).

Fluorescence microscope images were normalized to the brightest sample of the entire set using ImageJ software (NIH, Bethesda, MD). This was done by automatically adjusting the brightness/contrast followed by manually setting the maximum brightness to be the same as the brightest sample.

Image analysis and fluorescence quantitation was carried out using ImageJ software. Cells were manually outlined in the differential interference contrast (DIC) image and saved as individual regions of interest (ROIs). The ROIs were overlaid on the corresponding fluorescence image to measure the mean fluorescence for each cell in the image. The average fluorescence of the black background (e.g. DFHBI solution) was determined for each image and subtracted from the value for each cell to determine the mean fluorescence intensity. At least 50 cells were analyzed to measure the average mean fluorescence intensity. Statistical significance of difference in fluorescence was assessed using a student's t test.

Northern Blot Analysis

Total RNA was isolated using the TRIzol Max Bacterial RNA Isolation Kit (Life Technologies, Carlsbad, CA) from cells grown for 2.5 h after IPTG induction, as described above. Total RNA (~500 ng) was separated on a 9% urea-PAGE gel and the gel was transferred to a Hybond N membrane. After crosslinking, prehybridization was carried out for 4 h at 37 °C in Church's buffer (0.5 M Na_2HPO_4, 0.27 M, NaH_2PO_4, 6% SDS, 2 mM EDTA, and 1% BSA) with 15% formamide. Membranes were incubated with 25 ng ^{32}P-labeled DNA oligo for 6 h before washing with SSC buffer (3 M NaCl, 0.3 M sodium citrate, pH 7) and exposing on a phosphorimager. Quantitative analysis of the blot was performed using ImageQuant (GE Healthcare, Waukesha, WI).

CHAPTER 4

RNA-Based Fluorescent Biosensors for Live Cell Imaging of Second Messenger Cyclic di-AMP

4.1 Abstract

Cyclic di-AMP (cdiA) is a second messenger predicted to be widespread in gram-positive bacteria. In the human pathogen *Listeria monocytogenes*, cdiA regulates cell wall homeostasis and decreased levels of cdiA result in increased antibiotic susceptibility. We now have generated fluorescent biosensors for cdiA through fusion of the Spinach2 aptamer to ligand-binding domains of cdiA riboswitches. Intracellular levels of cdiA were visualized in live *L. monocytogenes* strains by fluorescence microscopy and flow cytometry. Thus, we have expanded the development of RNA-based biosensors as well as their use for *in vivo* metabolite imaging to gram-positive bacteria.

4.2 Introduction

Cyclic dinucleotides are an expanding class of second messengers with key roles in bacterial and eukaryotic immune regulation. A recent addition to this class, cdiA, regulates processes including bacterial sporulation, ion transport, and cell wall homeostasis in many gram-positive and pathogenic bacteria, and is the only cyclic dinucleotide predicted to be in a subset of archaea (Corrigan and Gründling, 2013). In the bacterial pathogens *Staphylococcus aureus* and *Listeria monocytogenes*, decreased levels of cdiA result in smaller cell size and reduced resistance to peptidoglycan-targeting antibiotics (Corrigan et al., 2011; Witte et al., 2013), which makes this pathway interesting from a drug targeting perspective. Additionally, secretion of cdiA by *L. monocytogenes* into the cytosol of infected murine macrophage cells elicits a type I interferon response (Woodward et al., 2010), and further studies have shown the efficacy of cyclic dinucleotides as small molecule adjuvants (Libanova et al., 2012). However, many aspects of cdiA signaling still need to be elucidated, including the mechanism of cell wall regulation, the role of extracellular cdiA, and its function in other microorganisms.

To target this pathway or to identify novel components of cdiA signaling, it is critical to have a robust method for *in vivo* detection of cdiA. Direct methods for detection of cdiA include HPLC-MS (Oppenheimer-Shaanan et al., 2011) and a dye intercalation assay (Zhou et al., 2014), both of which are limited to *in vitro* detection. An interferonbeta-luciferase reporter has been used to indirectly detect secreted cdiA (Witte et al., 2013; Woodward et al., 2010). However, to our knowledge, no sensor for live cell imaging of cdiA has yet been reported.

Recently, we and others have generated novel fluorescent biosensors by combining the ligand-sensing domain of different riboswitches or *in vitro* selected aptamers with the profluorescent dye-binding aptamer Spinach (Figure 4.1a) (Kellenberger et al., 2013; Paige et al., 2012). Here we report the development of two RNA-based biosensors for cdiA that exhibit ligand-induced fluorescence activation *in vitro* and *in vivo*. These fluorescent biosensors were used to examine the levels of cdiA in live *L. monocytogenes* strains by fluorescence microscopy and flow cytometry. To our knowledge, we have generated the first *in vivo* biosensor for cdiA and demonstrated the first application of RNA-based biosensors in a gram-positive bacterium.

4.3 Results and Discussion

The ydaO riboswitch class recently was identified to bind cdiA with high affinity and selectivity (Nelson et al., 2013). Structural probing experiments did not pinpoint the ligand binding site, although it was shown that the pseudoknot outside of the first pairing stem (P1) was not required for ligand binding (Nelson et al., 2013). Thus, several truncations of the riboswitch aptamer from the ydaO gene in *Bacillus subtilis* were fused to the Spinach2 aptamer (Strack et al., 2013) and tested for cdiA-dependent fluorescence activation (Figures 4.1b and 4.2). However, none of these fusion constructs demonstrated fluorescence activation. In contrast, two constructs in which the related riboswitch aptamer from the yuaA gene in *B. subtilis* was fused to Spinach2 through the P1 stem showed 2.4- and 9.0-fold fluorescence activation (P1-6 and P1-4, respectively). Further screening of P1-4 variants of other phylogenetic representatives of this riboswitch class did not identify any with improved fluorescence activation (Figure 4.1c). We instead observed several that exhibit consistent fluorescence deactivation, similar to ydaO P1-4 and P1-5. While turn-off biosensors may be useful to pursue in the future, we initially focused on two candidate biosensors with P1-4 stems, yuaA-Spinach2 and Sc1-Spinach2, because they demonstrated high fold turn-on and ligand sensitivity, respectively.

In contrast to yuaA-Spinach2, the Sc1-Spinach2 biosensor displays some fluorescence activation with 50 nM cdiA, but also exhibits much higher background. Several types of destabilizing mutations to the P1-4 stem of Sc1-Spinach2 were made in order to reduce the fluorescence background (Figure 4.3). It was found that replacement of a C-G base pair with an A-G mismatch via the C3A mutation leads to a biosensor with 2.7-fold fluorescence activation and higher binding affinity relative to yuaA-Spinach2 (Figure 4.1d). Both biosensors respond selectively to cdiA versus other cyclic dinucleotides and related adenosine containing compounds at ligand concentrations up to 100 μM (Figure 4.4).

The x-ray crystal structures of three ydaO class riboswitch aptamers recently revealed that two molecules of cdiA are bound in an RNA fold that exhibits pseudo two-fold symmetry (Gao and Serganov, 2014; Ren and Patel, 2014). This finding was unexpected, and in retrospect, attachment to the P1-4 stem removes the 3’ peripheral end of the pseudoknot that forms part of one cdiA binding site. Fortunately, mutation of this binding site reduced ligand affinity only five-fold (Gao and Serganov, 2014), and our results also corroborate that this binding site is non-essential. However, the importance of this region to the global RNA fold may explain why the biosensor constructs were so sensitive to minor changes in P1 stem truncations, and why most phylogenetic variants were non-functional.

To our advantage, both biosensors harbor a single ligand binding site and display 1:1 stoichiometry of binding to cdiA that gives a good dynamic range of detection (Figure 4.1d). The *in vitro* fluorescence signal changes from 10% to 90% between 3.2 to 260 μM cdiA for yuaA-Spinach2 and between 0.37 to 30 μM for Sc1-Spinach2. Together, these biosensors are able to detect cdiA concentrations spanning roughly three orders of magnitude.

The levels of secreted cdiA have been reported to range from 12-53 nM as isolated from HPLC-purified supernatants of different *L. monocytogenes* strains grown in minimal media (Woodward et al., 2010). For *in vitro* detection of secreted cdiA, Sc1-Spinach2 was utilized due to its lower limit of detection. However, our attempts to directly measure secreted cdiA from supernatants were hindered by high background fluorescence stemming from components of either rich (BHI) or minimal media (Figure 4.5). Apparently, these components are partially consumed or converted by cell growth, as the background is somewhat lower in media that has been used to culture *L. monocytogenes*. Although further optimization of these experiments is required, addition of the C3A Sc1-Spinach2 biosensor to unpurified supernatants generates an increase in observed fluorescence, indicating these samples are likely detecting cdiA excreted from cells. However, further experimentation using a mutant of the biosensor that does not bind cdiA is required to show that this signal is not due to background fluorescence of the biosensor.

For intracellular detection of cdiA, yuaA-Spinach2 is preferred due to its low background fluorescence. While no *in vivo* measurements of cdiA levels have previously been made, HPLC analysis of cell extracts of *Bacillus subtilis* and *S. aureus* cultures indicate low micromolar concentrations of cdiA in cells (Corrigan et al., 2011; Oppenheimer-Shaanan et al., 2011). Thus, this biosensor should be able to detect cdiA at physiologically relevant concentrations.

We were interested in testing the utility of cdiA biosensors in *L. monocytogenes*, a gram-positive bacterium and human pathogen that has served as an important model for cdiA signaling. Control fluorescence microscopy experiments confirmed that DFHBI was able to permeate through the thicker peptidoglycan layer, and expression of Spinach2 in a tRNA scaffold in turn leads to observable cellular fluorescence in *L. monocytogenes* (Figure 4.6). This result also demonstrates that a strong, constitutive promoter provides sufficient expression of Spinach2-based constructs for visualization in bacteria, avoiding the need to engineer an induction system (Figure 4.7).

To test the activity of the yuaA-Spinach2 fluorescent biosensor to detect cdiA in live cells, plasmids encoding the biosensor in a tRNA scaffold were transformed into strains of *L. monocytogenes*. For quantitation by flow cytometry, it was found that the recently described DFHBI-1T dye (Song et al., 2014) dramatically improved the resolution (Figure 4.8). In comparison to wild type, a ΔpdeA mutant carrying a deletion of the *pdeA* gene that encodes the cdiA phosphodiesterase (Witte et al., 2013) exhibits increased cellular fluorescence (Figure 4.9a,b). Alternatively, the ΔdacAΔrelAPQ double deletion strain that rescues lethality of the ΔdacA knockout (Whitely, A., in communication) removes the only known diadenylate cyclase gene and results in decreased cellular fluorescence. In contrast, expression and fluorescent visualization of Spinach2 showed no significant change in these strains (Figure 4.6). Thus, the data are consistent with the yuaA-Spinach2 biosensor giving a fluorescent read-out of differences in endogenous cdiA concentrations for mutant versus wild-type strains of *Listeria*.

Furthermore, we showed that the yuaA-Spinach2 biosensor could be employed in a complementation assay in *Listeria*. The *in vivo* catalytic activity of pdeA gene constructs harboring different domain deletions could be assessed by co-expression with the biosensor in the ΔpdeA mutant background. Whereas the full-length enzyme or truncated versions lacking either the PAS or GGDEF domains could rescue phosphodiesterase activity, constructs without the C-terminal DHH and DHHA1 domains showed no rescue of activity (Figure 4.9c). This result is consistent with the DHH domain being the catalytic domain of the phosphodiesterase, as shown for GdpP phosphodiesterase, a homologue in *B. subtilis* (Rao et al., 2010).

Overall, these biosensors represent the first tools for live cell imaging of cdiA with the potential for many *in vitro* and *in vivo* applications. The development of protein-based biosensors is often hindered without the structural knowledge of a conformational change, yet we demonstrate here the powerful ability of the Spinach system to rapidly screen for active biosensors. The recently solved Spinach crystal structures (Huang et al., 2014; Warner et al., 2014) as well as pioneering studies in new organisms further broaden the potential use of these tools. We envision that the development of these biosensors will not only aid in elucidating cdiA signal transduction, but also in the process of creating new biosensors for many important biological molecules.

4.4 Figures

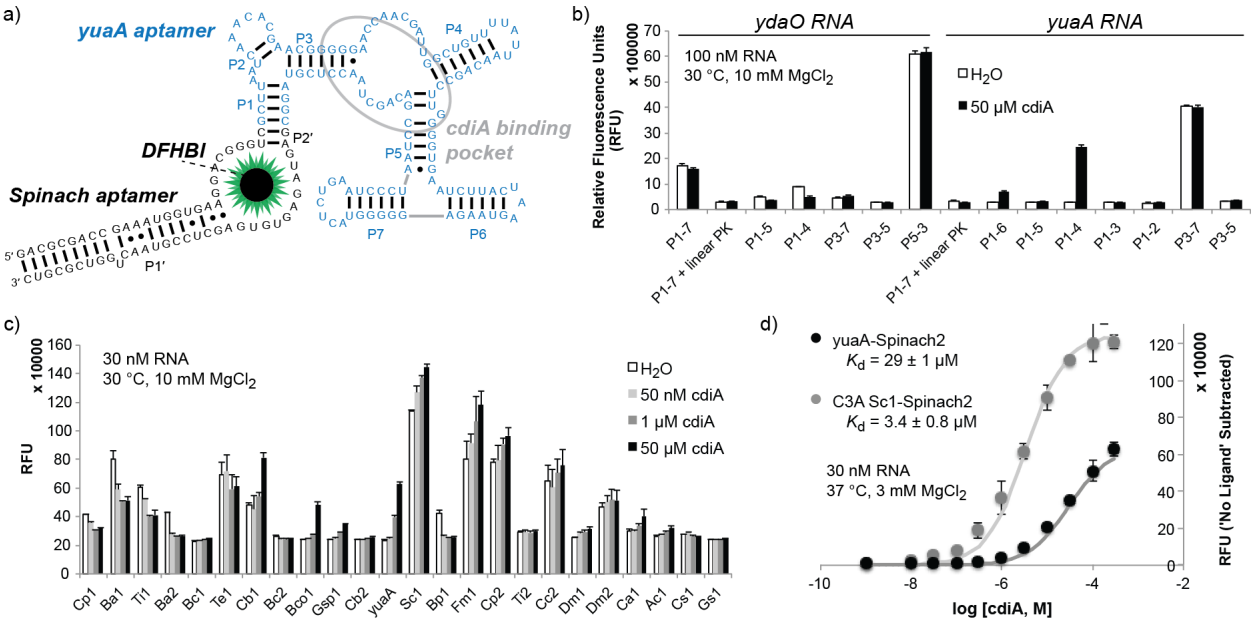

Figure 4.1 Spinach fusion and riboswitch phylogeny screens produce cdiA-activated fluorescent sensors. (a) Sequence and secondary structure of the P1-4 yuaA-Spinach2 aptamer. Binding of cdiA to the yuaA aptamer (blue) renders the Spinach2 aptamer (black) capable of binding DFHBI to elicit fluorescence. **(b)** Spinach2-riboswitch attachment screen. Nomenclature lists the site of Spinach attachment as the riboswitch stem number followed by the number of base pairs included in this stem. Error bars represent the standard deviation between three independent replicates **(c)** Screen of riboswitch phylogenetic variants. Variants of the cdiA aptamer were attached using the P1-4 Spinach2 fusion and were assayed for fluorescence activation. Riboswitch constructs are listed in order of decreasing bit score, from left to right. Error bars represent the standard deviation between two independent replicates. **(d)** *In vitro* affinity measurement of P1-4 yuaA-Spinach2 and C3A Sc1-Spinach2 biosensors for cdiA. The average of three independent replicates along with best-fit curves are shown.

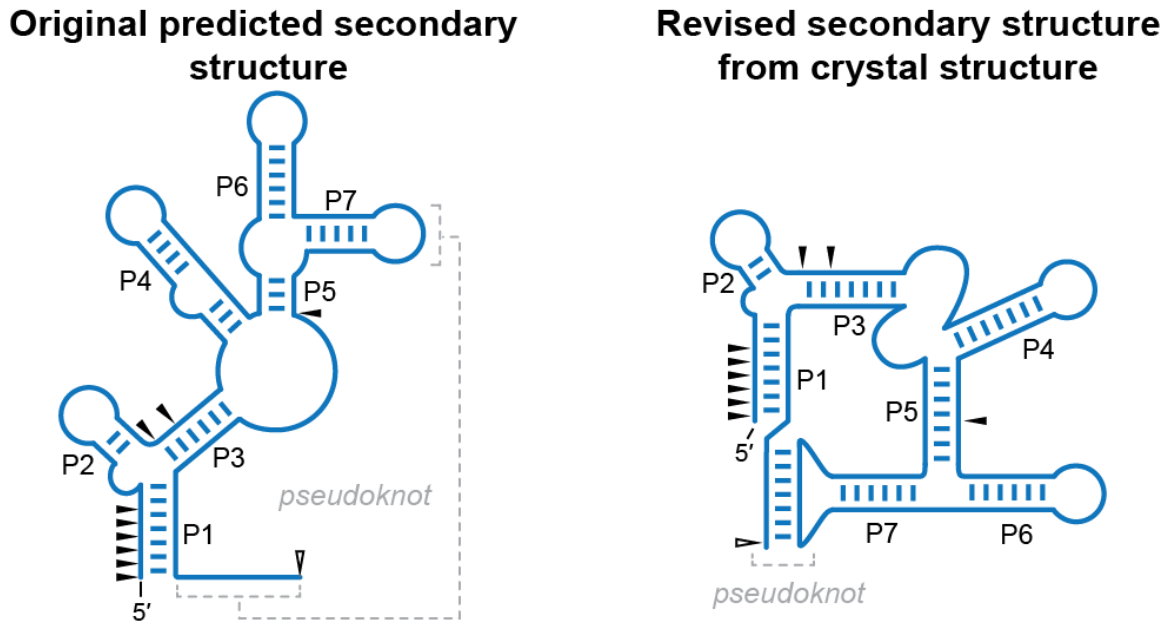

Figure 4.2 Schematic of yuaA fusion sites to Spinach2. A model of the yuaA secondary structure is shown both before and after the crystal structures of three ydaO class aptamers were solved. Black-filled arrowheads indicate base pair positions at which the Spinach2 aptamer was attached in ydaO or yuaA-Spinach2 fusions. The open arrowheads depict constructs that contained the entire aptamer sequence, including the 3′ end of the pseudoknot.

a)

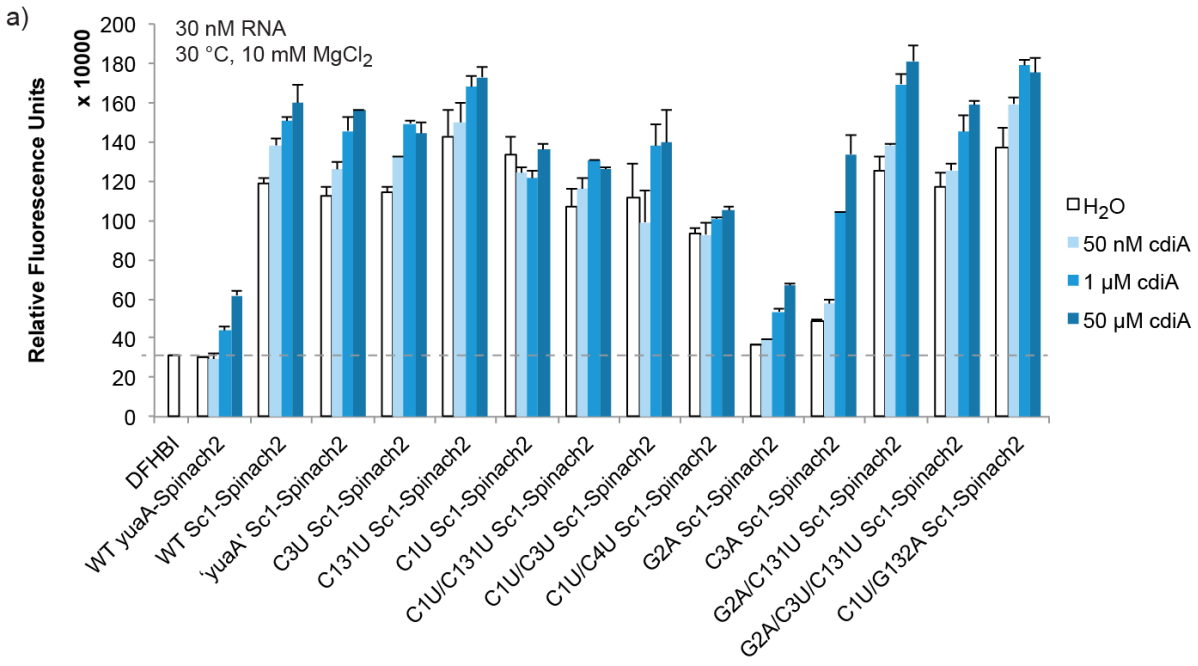

b)

Sequence	P1 stem	Stem Stability (kcal/mol)	NL Fluorescence (RFU)
WT yuaA-Spinach2	gcuu guaa aggc	-1.9	301881
WT Sc1-Spinach2	cgcc guaa ggcg	-7.7	1189934
'yuaA' Sc1-Spinach2	gcuu guaa aggc	-1.9	1121903
C3U Sc1-Spinach2	cguc guaa ggcg	-5	1147130
C131U Sc1-Spinach2	cgcc guaa ggug	-5.8	1429910
C1U Sc1-Spinach2	ugcc guaa ggcg	-6.7	1332865
C1U/C131U Sc1-Spinach2	ugcc guaa ggug	-4.8	1065923
C1U/C3U Sc1-Spinach2	uguc guaa ggcg	-3.5	1118343
C1U/C4U Sc1-Spinach2	ugcu guaa ggcg	-1.6	935145
G2A Sc1-Spinach2	cacc guaa ggcg	-2.8	366104
C3A Sc1-Spinach2	cgac guaa ggcg	0.5	488447
G2A/C131U Sc1-Spinach2	cacc guaa ggug	-6.2	1253840
G2A/C3U/C131U Sc1-Spinach2	cauc guaa ggug	-3.6	1170235
C1U/G132A Sc1-Spinach2	ugcc guaa ggca	-7	1372988

c)

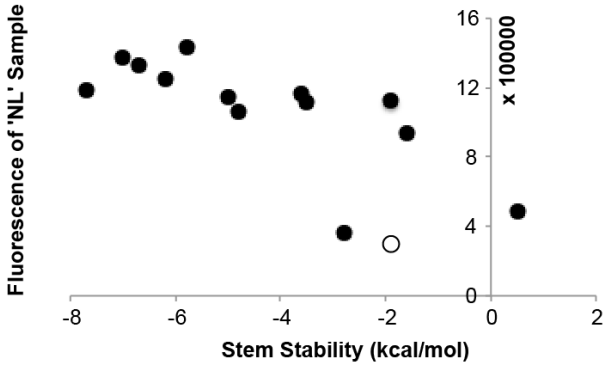

d)

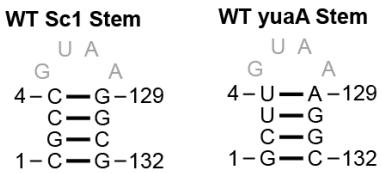

Figure 4.3 Mutation of the Sc1-Spinach2 transducer stem reveals two constructs with lower background fluorescence. (a) *In vitro* fluorescence screen of P1-4 Sc1-Spinach2 mutants. RNA (30 nM) was incubated with DFHBI (10 µM) and varied cdiA

concentrations at 30 °C in buffer containing 10 mM $MgCl_2$. The horizontal dashed line represents the fluorescence background of DFHBI in solution. Error bars represent the standard deviation between two independent replicates. **(b)** Analysis of transducer stem stability via mfold. The stabilities of the four base-pair stems were calculated by measuring the stability of the given stem with a GUAA tetraloop inserted, as in part (d). Default parameters of mfold were used. **(c)** Graphical analysis of the results presented in (b). The open circle represents the WT yuaA-Spinach2 aptamer. **(d)** Sequence of the P1-4 Sc1 and yuaA riboswitch stems used to calculated stem stability.

While the WT Sc1-Spinach2 aptamer, which contains four G-C Watson-Crick base pairs in the transducer stem, displayed 4-fold higher background than WT yuaA-Spinach2 without cdiA, disruption of one of these base pairs with either a G2A or a C3A mutation of the transducer stem reduced the background fluorescence to be within 1.2 or 1.6-fold the background of the yuaA-Spinach2 aptamer, respectively. Grafting of the P1-4 yuaA stem in place of the Sc1 stem ('yuaA' Sc1-Spinach2) and other disruptive mutations of the P1-4 Sc1 stem did not reduce the background fluorescence to within 2-fold of the WT yuaA-Spinach2 aptamer, which has equivalent background fluorescence of DFHBI in solution. Given the significantly greater fluorescence activation of the C3A Sc1-Spinach2 biosensor compared to G2A (2.7 versus 1.8-fold, respectively) under these conditions, the C3A Sc1-Spinach2 sensor was used for further studies.

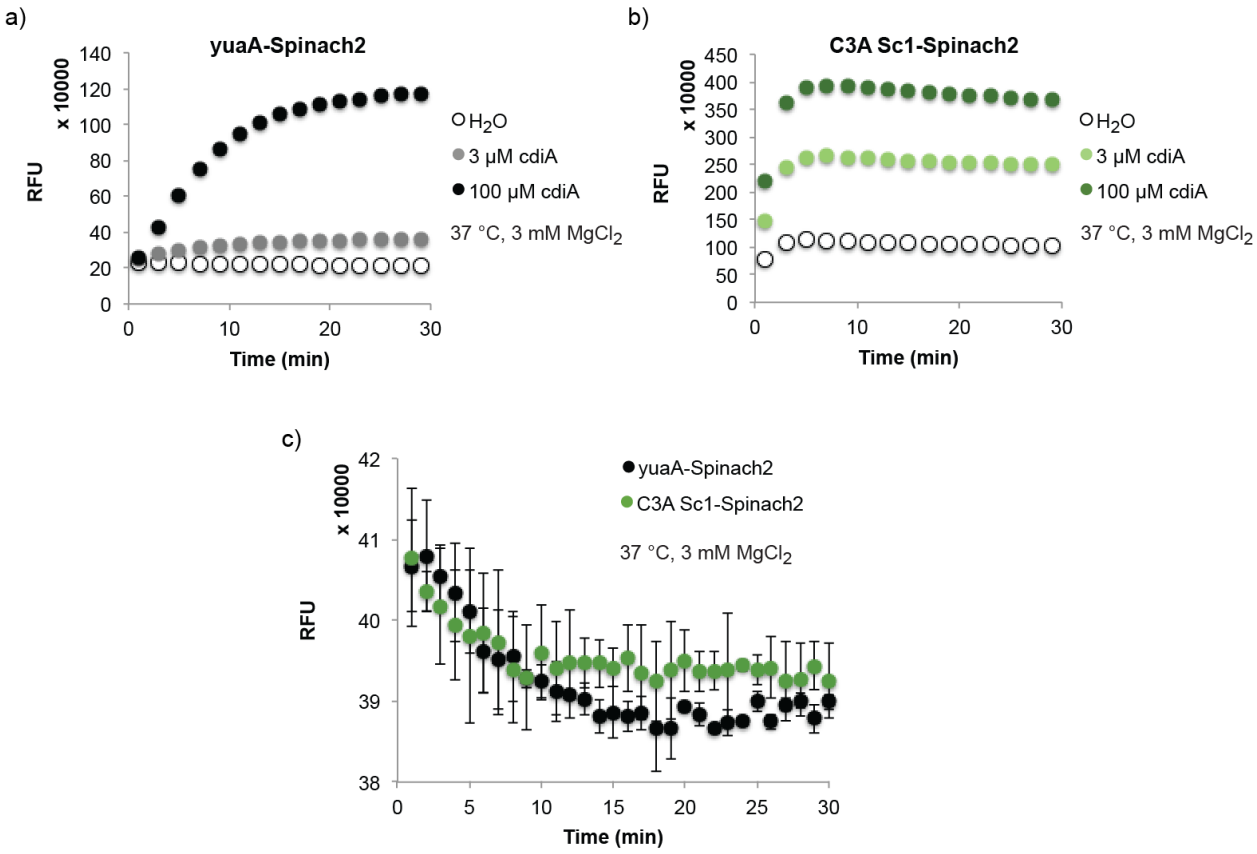

Figure 4.4 Association and dissociation kinetics of the yuaA-Spinach2 and C3A Sc1-Spinach2 biosensors. (a) and **(b)** Activation of the yuaA-Spinach2 (a) and C3A Sc1-Spinach2 (b) sensors. DFHBI (10 µM) and varied cdiA concentrations or H_2O were pre-equilibrated at 37 °C in buffer containing 3 mM $MgCl_2$ before mixing with RNA (100 nM) pre-warmed to 37 °C. Fluorescence measurements were recorded immediately after addition of RNA. Data are representatives of one experiment that has been repeated twice. **(c)** Deactivation of the yuaA-Spinach2 and C3A Sc1-Spinach2 biosensors. RNA (100 nM) that had been pre-equilibrated with DFHBI (10 µM) and cdiA (100 µM for yuaA-Spinach2, 10 µM for C3A Sc1-Spinach2) at 37 °C in buffer containing 3 mM $MgCl_2$ was diluted 100-fold into buffer containing DFHBI (10 µM) without cdiA or RNA. Fluorescence was monitored immediately after dilution. Error bars represent the standard deviation of duplicate samples of this representative experiment.

Full activation of the P1-4 yuaA-Spinach2 and C3A Sc1-Spinach2 biosensors occurs at ~30 min and 7 min, respectively. Deactivation of the sensors occurs within 15 and 9 min for the yuaA-Spinach2 and C3A Sc1-Spinach2 sensors, respectively. As observed previously, 75% activation and deactivation occurs in ~half the time required for full association or dissociation. It seems likely that the binding kinetics of the biosensors are dependent on the properties of the inserted riboswitch aptamer. It was previously observed that the WT Vc2-Spinach biosensor binds relatively slowly to cdiG, similar to the isolated WT Vc2 aptamer.(Kellenberger et al., 2013; Smith et al., 2009) Thus, it seems that the yuaA aptamer has relatively slower binding kinetics than the Sc1 aptamer assayed here. Since the dynamics of cdiA regulation have not previously been

studied, these two biosensors provide two different kinetic regimes for studying different reaction timescales.

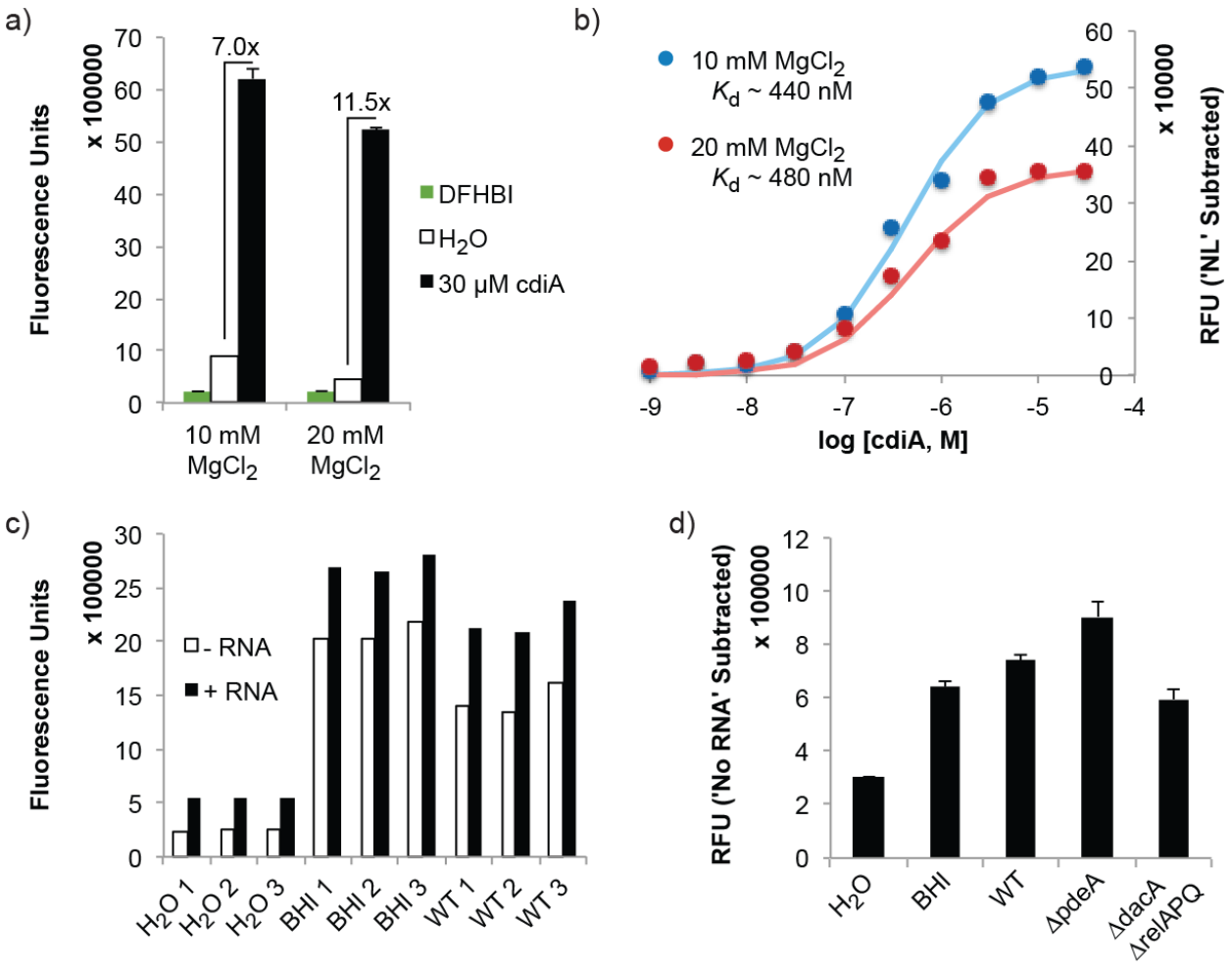

Figure 4.5 Preliminary experiments with C3A Sc1-Spinach2 demonstrate detection of cdiA from *Listeria monocytogenes* supernatants. (a) Increased $MgCl_2$ concentrations decrease background and increase fluorescence activation *in vitro*. RNA (100 nM) was mixed with DFHBI (10 μM) along with H_2O or 30 μM cdiA. The DFHBI sample represents DFHBI alone in buffer. Error bars represent the standard deviation between two replicate samples. **(b)** *In vitro* analysis shows similar affinity of C3A Sc1-Spinach2 biosensor in 10 and 20 mM $MgCl_2$. Best-fit curves are shown for one independent sample. **(c)** *In vitro* fluorescence analysis of *L. monocytogenes* culture supernatants. Each pair of bars represents the reading for an individual biological replicate. **(d)** Average 'No RNA'-subtracted fluorescence of *L. monocytogenes* culture supernatants. Error bars represent the error between three independent, 'No RNA'-subtracted biological replicates.

In order to increase the resolution between small differences in cdiA concentrations, the fluorescence background of the C3A Sc1-Spinach2 biosensor was first decreased, leading to an increase in fluorescence activation, by further increasing the Mg^{2+} concentration to 20 mM, which is known to be important for RNA stabilizing the RNA fold.(Ren and Patel, 2014) While increased $MgCl_2$ concentration decreases the background fluorescence, it has no significant effect on affinity of the biosensor for cdiA.

When applying these conditions to study *L. monocytogenes* culture supernatants, it was found that the BHI media alone had significantly higher fluorescence over the normal background (H_2O samples). Further investigation revealed that this each sample demonstrated variability in background fluorescence, as demonstrated by the difference in fluorescence of biological replicates without RNA added to the sample. Thus, to take account for differences in background BHI fluorescence, fluorescence of the sample without RNA was subtracted from the same reaction with RNA added. Average fluorescence of these background-subtracted samples shows the expected trend for cdiA levels between these strains, where ΔpdeA *L. monocytogenes* secretes the highest levels of cdiA, followed by WT and ΔdacAΔrelAPQ strains. Further experiments would be required to eliminate the background fluorescence of the BHI media and to use this assay for cdiA quantitation.

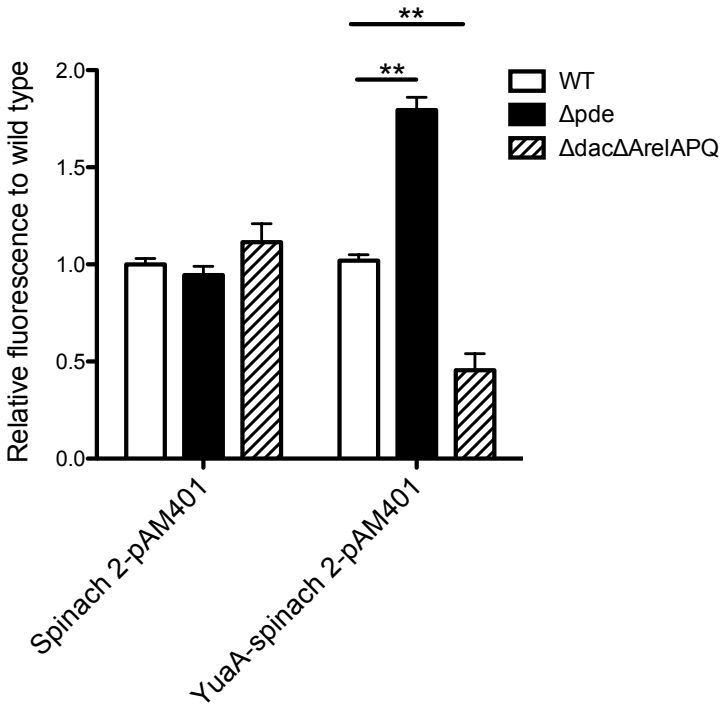

Figure 4.6 The Spinach2 sensor levels are consistent between tested strains of *L. monocytogenes*. Flow cytometry analysis of *L. monocytogenes* strains expressing the Spinach2 or yuaA-Spinach2 biosensor using DFHBI-1T as substrate. ** $p<0.01$ N=3.

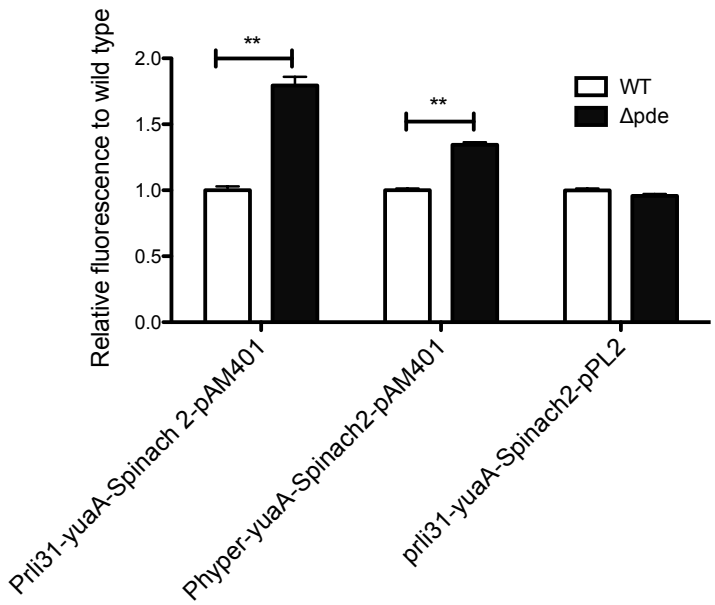

Figure 4.7 Promoter and plasmid copy number affects yuaA-spinach2 sensor sensitivity in live *L. monocytogenes*. Different promoters (Pli31 and Phyper) and *L. monocytogenes* vectors (High copy-pAM401 and integration vector pPL2) were compared for yuaA-Spinach2 sensor expression in *L. monocytogenes*. Sensitivity of each construct was evaluated by flow cytometry analysis in WT and Δpde *L. monocytogenes* strains. ** $p<0.01$, N=3.

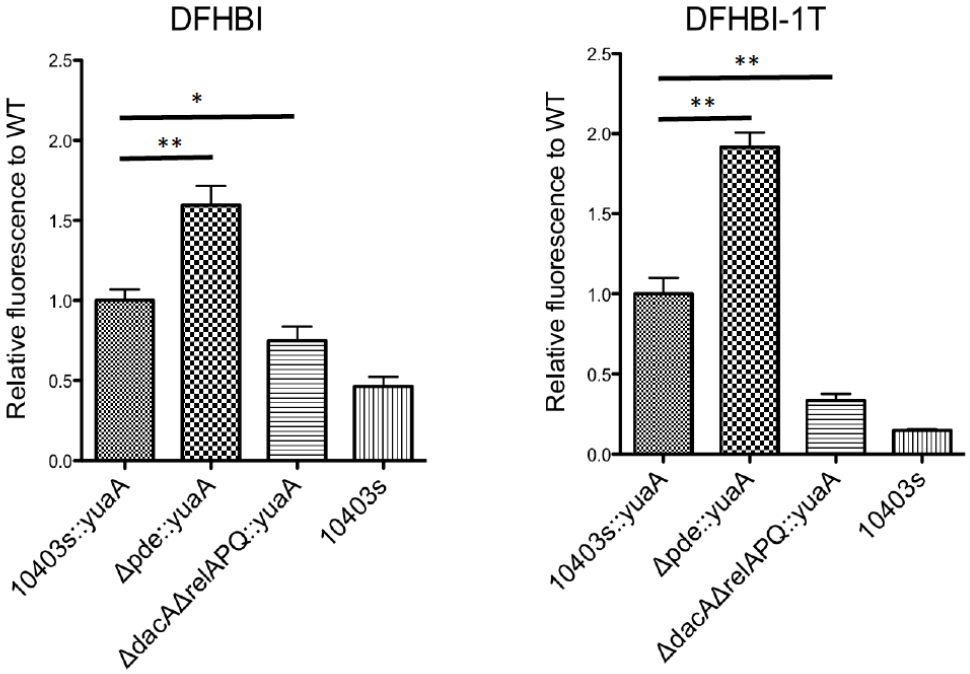

Figure 4.8 DFHBI-1T resolves difference in yuaA-Spinach2 signal better than DFHBI. The DFHBI and DFBHI-1T fluorophores were used as substrates for yuaA-Spinach2 to compare the sensitivity and resolution between different strains. Use of the DFHBI-1T increased overall signal and obtained higher resolution between different strains. * $p<0.05$, ** $p<0.01$, N=4.

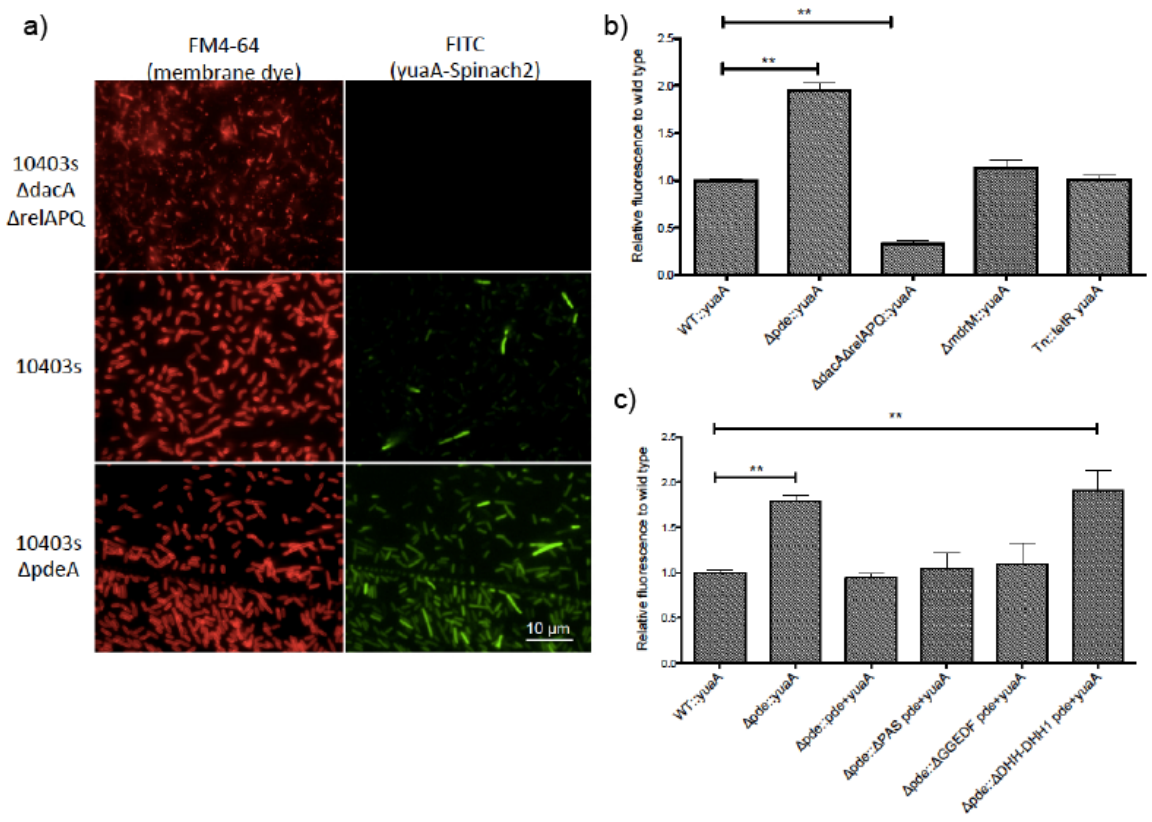

Figure 4.9 The yuaA-Spinach2 biosensor detects cdiA production in live *L. monocytogenes*. (a) Representative fluorescence microscope images of *L. monocytogenes* strains ΔdacAΔrelAPQ, WT, and ΔpdeA expressing the yuaA-Spinach2 biosensor using DFHBI as substrate. **(b)** Flow cytometry analysis of *L. monocytogenes* strains shown in (a) ** $p<0.01$ N=4. **(c)** Flow cytometry analysis of the catalytic domain of pdeA. ** $p<0.01$ N=3.

4.5 Materials and Methods

General reagents and equipment
DNA oligonucleotides were purchased as Ultramer oligos from IDT (Coraleville, IA). Cyclic and linear dinucleotides were purchased from Axxora (Farmingdale, NY) and were used without further purification. DFHBI and DFHBI-1T fluorophores were either purchased from Lucerna (New York, NY) or were synthesized following previously described protocols(Paige et al., 2011; Song et al., 2014) and were stored as 20-40 mM stocks in DMSO at -20 °C. *In vitro* fluorescent measurements were made using a Molecular Devices SpectraMax Paradigm plate reader.

***In vitro* transcription**
RNA was transcribed following previously reported protocols.(Kellenberger and Hammond; Kellenberger et al., 2013) Briefly, a DNA template was prepared by PCR amplification of the desired sequences using primers that added a T7 promoter directly upstream of the Spinach construct. DNA templates were purified by PCR purification, then were used in a transcription reaction with T7 RNA polymerase (NEB, Ipswich, MA). RNAs were purified by denaturing polyacrylamide gel electrophoresis (PAGE), then were eluted from gel pieces and ethanol precipitated. Accurate RNA concentrations were determined using a hydrolysis assay to eliminate the hypochromic effect from these structured RNAs.(Wilson et al., 2014)

***In vitro* Ligand binding assays**
Fluorescent ligand binding assays were performed as previously described.(Kellenberger and Hammond; Kellenberger et al., 2013) In brief, reactions were prepared in a 96-well Corning Costar (Tewksbury, MA) 3915 black plate with final buffer concentrations of 40 mM HEPES, pH 7.5, 125 mM KCl, either 3 or 10 mM $MgCl_2$ with 10 μM DFHBI and the appropriate ligand concentration. RNAs were renatured by mixing with an equal volume of binding buffer (800 mM HEPES, pH 7.5, 2500 mM KCl, and either 60 or 200 mM $MgCl_2$), heating it to 70 °C for 3 min, and then cooling at ambient temperature for 5 min before adding to the reactions at a 10-fold dilution (30 nM or 100 nM final concentration). Fluorescence was monitored at 5 min intervals using an excitation of 460 nm and emission of 500 nm. Data was collected and analyzed after samples had reached equilibrium (within 0.5-2 h).

In general, assays to screen for ligand binding were carried out at 30 °C in buffer with 10 mM $MgCl_2$, which increases the sensitivity of these experiments.(Kellenberger et al., 2013) Assays aimed at understanding *in vivo* properties were carried out under the more physiologically relevant conditions of 37 °C in buffer with 3 mM $MgCl_2$.

***In vitro* association and dissociation experiments**
Association of the biosensors with ligand was measured following a similar protocol as described previously.(Kellenberger and Hammond; Kellenberger et al., 2013) Briefly, buffer containing 40 mM HEPES, pH 7.5, 125 mM KCl, 3 mM MgCl2, 10 μM DFHBI, and the appropriate ligand was pre-warmed to 37 °C. The RNA (final concentration 100 nM) was renatured as described above and pre-warmed to 37 °C before mixing with

buffer solution. Fluorescence was monitored immediately after RNA addition at 2 min intervals with an excitation of 460 nm and emission of 500 nm.

Ligand dissociation experiments were prepared by first equilibrating RNA (100 nM) and ligand (100 µM for P1-4 yuaA-Spinach2 and 10 µM for C3A Sc1-Spinach2) at 37 °C in the buffer described for association experiments. A deactivation buffer (200 µL) containing just 40 mM HEPES, pH 7.5, 125 mM KCl, 3 mM $MgCl_2$, and 10 µM DFHBI was pre-warmed in the same plate to 37 °C. Once the RNA binding reaction had equilibrated, it was diluted 100-fold into the pre-warmed deactivation buffer. Fluorescence was monitored immediately after dilution at 1 min intervals with an excitation of 460 nm and emission of 500 nm.

Bacteria and plasmids

The yuaA-Spinach2 sensor was cloned into the *L. monocytogenes* high-copy-number shuttle plasmid pAM401 or the integration plasmid pPL2 to generate *in vivo* cdiA biosensors. Briefly, Splicing by Overlap Extension (SOEing) PCR was used to fuse a *L. monocytogenes* small RNA promoter (Prli31) or a constitutive promoter (Phyper) with the yuaA-Spinach2 construct flanked on either side by a tRNA scaffold and a final 3′ T7 terminator.(Kellenberger et al., 2013; Ponchon and Dardel, 2007) SOE PCR products were gel purified, digested with EagI and SalI and then ligated with either pAM401 or pPL2-Cm digested with the same restriction enzymes. For the phosphodiesterase (PDE) gene complementation study, the *L. monocytogenes* PDE gene was truncated by PCR and cloned into KpnI/XhoI sites of the pPL2-Erm integration plasmid under the native PDE promoter.

The resulting plasmids were confirmed by sequencing and transformed into different *L. monocytogenes* strains as previously described.(Lauer et al., 2002) Briefly, pAM401 or pPL2-Erm was transformed into SM10, and the resulting strains were mated into different *L. monocytogenes strains* carrying a streptomycin resistance mutation.

Fluorescence Microscopy

Fluorescence microscopy experiments of bacterial cultures were carried out following previous protocoles.(Paige et al., 2011) Briefly, ~1 OD_{600} of *L. monocytogenes* overnight culture grown in BHI was spun down at 5000rpm for 5 min, and resuspended in 2 mL of PBS. A 50 µL aliquot of resuspended culture was then plated on poly-L-lysine coated 96 well glass-bottom dishes (MatTek) to adhere the cells for one hour at 37 °C. Adherent bacteria were washed three times with PBS to remove unbound cells and then incubated with 200 µM DFHBI-1T for 30 min at 37 °C. Fluorescent images were taken through a 60x oil objective mounted on a Olympus IX71 microscope. All images were taken with same exposure settings and analyzed with Image J.

Flow Cytometry

Flow cytometry experiments were carried out by pelleting ~1 OD_{600} of overnight *L. monocytogenes* culture, which were then washed twice with 1x PBS and resuspended in 1 mL PBS. Then, 10 µL bacterial culture was mixed with 100 µL 100 µM DFHBI in 1x PBS or DFHBI-1T in polystyrene FACS tube. Samples were protected from light and

incubated at 37 °C for 30 min before Flow cytometry analysis. Data was collected using a LSR Fortessa (BD Biosciences) and analyzed using FlowJo software. For each sample at least 50,000 bacteria were gated by size and singlet gate (FSC-H/FSC-A). Then, mean fluorescent intensity from the FITC channel was calculated for each sample.

CHAPTER 5

GEMM-I Riboswitches from *Geobacter* Sense the Bacterial Second Messenger 3′,3′ c-AMP-GMP

5.1 Abstract

Cyclic dinucleotides are an expanding class of signaling molecules that control many aspects of bacterial physiology, including cell growth, virulence, biofilm formation, and surface colonization. These soluble second messengers act by binding and modulating the activity of biomolecule effectors. A synthase for 3',3' c-AMP-GMP (cAG) has been identified, but other components of the signal transduction pathway are unknown. We now have discovered that a subset of GEMM-I class riboswitches (GEMM-Ib) from *Geobacter* are specific effectors for cAG and demonstrate that *G. sulfurreducens* produces cAG. GEMM-Ib riboswitches regulate genes functionally associated with extracellular electron transfer, thus revealing a role for cAG in the control of *Geobacter* electrophysiology and furthermore implicating many genes of unknown function in this process. Finally, we have developed an RNA-based fluorescent biosensor for live cell imaging of cAG. This selective, genetically-encodable biosensor will be useful to probe the biochemistry and cell biology of cAG signaling in diverse bacteria.

5.2 Introduction

Cyclic dinucleotides are a structurally related class of second messengers that are produced as key intracellular signals triggering physiological changes in response to environmental stimuli (Figure 1.1). Cyclic di-GMP (cdiG) was first identified to be widespread in bacteria through the prevalence of GGDEF domain-containing proteins encoded in sequenced genomes and studied for its regulation of the critical transition from motile to sessile, biofilm-forming lifestyle (Römling et al., 2013; Ross et al., 1987). Recently, two other cyclic dinucleotides, cyclic di-AMP (cdiA) and cyclic AMP-GMP (cAG, or 3',3'-cGAMP, Figure 5.1a) have been discovered in bacteria (Davies et al., 2012; Witte et al., 2008). Furthermore, an isomer of cAG containing a non-canonical 2'-5' phosphodiester linkage (2',3'-cGAMP) has been found to be produced in response to cytosolic DNA in mammalian cells (Ablasser et al., 2013; Diner et al., 2013; Gao et al., 2013a; Wu et al., 2013). The mammalian sensor STING is stimulated by both bacterial cyclic dinucleotides and 2',3'-cGAMP to activate the innate immune response (Danilchanka and Mekalanos, 2013). In bacteria, however, specific recognition of each second messenger is presumably necessary to deconvolute the signaling pathways.

Of the three bacterial cyclic dinucleotides, the least is known about the signal transduction pathways for cAG (Figure 5.1a). So far, the only component that has been identified is the *V. cholerae* cAG synthase, DncV, which has limited homology to genes in other bacteria, but has homology to the mammalian cGAS enzyme through its 2',5'-oligoadenylate synthase (OAS1) domain (Davies et al., 2012). To our knowledge, no sensors or effectors that respond selectively to cAG have yet been reported, although the second messenger has been shown to affect chemotaxis and intestinal colonization of *V. cholerae* (Davies et al., 2012). In addition, it remains an open question how prevalent cAG signaling is in bacteria.

5.3 Results and Discussion

Previously, we developed an RNA-based fluorescent biosensor that could be used as a tool to visualize cdiG signaling *in vivo* (Kellenberger et al., 2013). This

biosensor was created by fusing a natural cdiG-sensing GEMM-I class riboswitch aptamer (Vc2) to the Spinach aptamer (Figure 5.1b) (Paige et al., 2011, 2012; Sudarsan et al., 2008). Although the WT Vc2 aptamer is highly selective for cdiG (Sudarsan et al., 2008), we showed that engineering the binding pocket through a G20A mutation altered ligand selectivity to render the aptamer capable of binding cAG and cdiG with similar affinities (Kellenberger et al., 2013). Intriguingly, prior phylogenetic analysis revealed that while 76% of sequences in the GEMM-I riboswitch class have a G at this position (referenced hereafter as G20, following the Vc2 numbering) that was shown to form a Hoogsteen base-pair with cdiG, 23% instead had an A20 that presumably allows for recognition of cAG (Smith et al., 2010). We thus surveyed several of these A20 phylogenetic variants through the fluorescent biosensor screen to determine if any GEMM-I sequences are naturally selective for cAG.

A modest screen of natural A20 GEMM-I sequences revealed that the majority display promiscuous binding to cAG and cdiG, similar to G20A Vc2-Spinach (Figure 5.2a, performed with Stephen Wilson, Thomas Brewer, and Yichi Su). A few sequences retain cdiG-selectivity or have undetermined selectivities. However, one initial candidate, Gm0970, demonstrated a marked selectivity for cAG (Figure 5.2, performed with Stephen Wilson, Thomas Brewer, Yichi Su and Yu-Fang Hsieh). This sequence is from the bacteria *Geobacter metallireducens* GS-15, which has 17 predicted GEMM-I riboswitches annotated in its genome (Genbank accession NC_007517.1). Analysis of all GEMM-I sequences from this species revealed that 15/17 contain an A20 and are selective for cAG or have undetermined selectivities (Figure 5.3a and Table 5.1, performed with Stephen Wilson and Yichi Su). The remaining 2/17 contain a G20, and one binds both cAG and cdiG, whereas the other has undetermined selectivity. A similar screen of all GEMM-I sequences in *Geobacter sulfurreducens* PCA and select sequences in other *Geobacter* confirmed that the majority of GEMM-I sequences from *Geobacter* species preferentially bind cAG (Figures 5.3b-d, performed with Stephen Wilson and Yichi Su).

In order to validate that these riboswitch aptamers are naturally selective for cAG and that selectivity is not altered through the context of the Spinach aptamer, we performed in-line probing analysis on the isolated Gm0970 and Gs1761 aptamers (data not shown, performed by Scott Hickey). Ligand-induced changes in the RNA fold are revealed by alteration of the in-line probing pattern, which corresponds to the extent of RNA self-cleavage at each nucleotide position. The Gm0970 aptamer has a dissociation constant (K_d) of ~16 nM for cAG and ~26 μM for cdiG, which means it is ~1,600-fold selective for cAG over cdiG. Similarly, the Gs1761 aptamer has a K_d of ~530 pM for cAG and ~660 nM for cdiG and thus is ~1,200-fold selective. Furthermore, high concentrations of up to 0.5 mM of cdiA or 2',3' cGAMP induced very little conformational change in either aptamer, indicating that the two riboswitch aptamers do not recognize these other cyclic dinucleotides. These data also demonstrate that natural GEMM-I riboswitches from *Geobacter* bind cAG selectively. To our knowledge, these RNAs are the first specific effectors for cAG that have been identified. These sequences constitute a novel subclass of GEMM-I riboswitches, herein termed GEMM-Ib, that respond selectively to cAG (Figures 5.1b,c).

The cyclic dinucleotide content of *Geobacter* bacteria has not been analyzed previously, although bioinformatics analyses have predicted the presence of enzymes related to cdiG and cdiA signaling (Bai et al., 2012; Seshasayee et al., 2010) and corresponding GEMM-I and ydaO class riboswitches (Nelson et al., 2013; Sudarsan et al., 2008). Our current results strongly suggest that these organisms also produce cAG as an endogenous signaling molecule, even though their genomes do not harbor any homologues of DncV. Thus, we performed organic-aqueous extraction of cyclic dinucleotides from *G. sulfurreducens* PCA cells. LC-MS, MS/MS, and HRMS analysis revealed that all three bacterial cyclic dinucleotides are present in *G. sulfurreducens* cell extracts (Figures 5.4, 5.5, and data not shown performed with Scott Hickey, Stephen Wilson, and Anthony Iavarone). Only cdiG is observed when cells are grown to a similar density in media without supplemented yeast extract, and corresponding analysis of yeast extract alone did not yield any signal for cyclic dinucleotides (Figure 5.6, performed with Scott Hickey). Thus, these experiments demonstrate the presence of cAG as a native signaling molecule in *G. sulfurreducens*, and based on the ligand selectivity of their riboswitches, we expect cAG to be present in other *Geobacter* species as well. These results are significant, because they provide the first evidence that cAG signaling extends to delta proteobacteria and furthermore, beyond bacteria that harbor homologues of DncV.

We predict that the signaling molecule cAG turns on the expression of genes or operons associated with GEMM-Ib riboswitches via regulating the formation of rho-independent transcription terminators (Table 5.1). For example, the Gs1761 riboswitch upstream of the *pgcA* gene is expected to form a terminator stem with portions of the aptamer domain, but the terminator would be disrupted in the cAG bound structure, as the P1 and P3 stems act as anti-terminator sequences (Figure 5.7a). In-line probing analysis of an extended riboswitch sequence in the presence of cAG reveals pattern changes consistent both with P1 and P3 stem formation and with disruption of the terminator stem (Figure 5.7b). These structural changes are observed at low concentrations of cAG (starting at 10 nM), but are not observed with cdiG until concentrations ~1,000-fold greater (10-50 μM), which agrees with our previous results on selectivity for ligand binding. Thus, we demonstrate that cAG binding to the Gs1761 riboswitch aptamer disrupts terminator stem formation. Consistent with these results, an increase in full-length transcription with cAG was observed for another GEMM-Ib riboswitch (Nelson et al., 2014).

A key metabolic feature of the *Geobacter* genus is the ability to perform extracellular electron transfer. In addition to playing an important role in natural geochemistry through the reduction of environmental metals (Lovley and Coates, 1997), *Geobacter* have been described as “living batteries” that have the capacity to generate electricity from organic waste (Lovley, 2008). Significantly, the genes regulated by GEMM-Ib class riboswitches and thus activated by cAG signaling include many that are functionally linked to this process (Table 5.1). For example, the gene regulated by the Gs1761 riboswitch, *pgcA*, encodes a periplasmic cytochrome c protein that is conserved in *Geobacter* species and is more highly expressed during growth on insoluble Fe(III) oxide versus Fe(III) citrate (Ding et al., 2006, 2008).

Interestingly, a C to T transition that maps to the Gs1761 riboswitch in the *pgcA* transcript was shown to double the rate of Fe(III) oxide reduction by *G. sulfurreducens* (Tremblay et al., 2011). We analyzed the extended C78U Gs1761 riboswitch sequence by in-line probing and found that the point mutation indeed destabilizes the terminator stem, as the observed pattern is similar to that of WT Gs1761 bound to cAG (Figure 5.7b). However, unlike the WT riboswitch, the C78U mutant is insensitive to the presence of cAG or cdiG (Figure 5.8, performed with Scott Hickey). This result shows that the C78U mutation to the riboswitch would constitutively turn on gene expression, which corroborates the ~15-fold increase of *pgcA* transcripts observed in the mutant strain (Tremblay et al., 2011). Taken together, our data provide functional evidence for cAG regulation via a GEMM-Ib riboswitch *in vitro* and explain the results of a prior study that implicated riboswitch-based regulation of the *pgcA* gene *in vivo*.

Several other cytochrome c-containing and biogenesis proteins appear to be regulated by cAG, including OmcS, which has been shown to be essential for metal oxide reduction and more highly expressed upon growth on insoluble Fe(III) or Mn(IV) oxides (Aklujkar et al., 2013; Mehta et al., 2005). Though cytochrome genes are remarkably abundant in *Geobacter* species, they are not well conserved, making it difficult to base functional assignments of electron conduits on phylogenetic arguments (Butler et al., 2010). The identification of a subset of cytochromes co-regulated by cAG suggests that they are part of a specific pathway and distinguishes them from others encoded in the genome.

In addition to extracellular cytochromes, *Geobacter* produce specialized type IV pili that are intimately involved in contacting insoluble metal sources, including electrodes, and there is evidence for direct electron shuttling by the pili (Vargas et al., 2013), although this mechanism is still under active debate (Bonanni et al., 2013). The Gm0970 and Gs0745 riboswitches reside within an operon conserved in *Geobacter* that contains genes encoding minor pilins and pilus assembly proteins (data not shown, performed by Tania Gonzalez). Thus, the genes of known function associated with GEMM-Ib appear to be involved in extracellular electron transfer, and allow us to propose a role for cAG signaling in the regulation of *Geobacter* electrophysiology (Figure 5.7c). More significantly, the majority of genes associated with GEMM-Ib are of unknown or uncharacterized function, including two (Gsu2033 and Gsu2885) that are co-transcribed with PilMNOPQ and OmcAHG, respectively. An intriguing hypothesis is that these genes play a previously unrecognized role in extracellular electron transfer.

In order to further elucidate and study cAG signaling pathways in *Geobacter* and other bacteria, we envisioned developing a genetically-encodable fluorescent biosensor for live cell imaging of cAG. The original Gm0970-Spinach construct, which harbors a 3-nt base paired transducer stem (P1-3), displays modest (~2-fold) fluorescence activation (Figure 5.9a). Through optimization studies of the transducer stem, two selective biosensors were developed that display much higher fluorescence activation (14.1-fold for P1-4 and 7.8-fold for P1-4delA) in response to cAG (Figures 5.9a and 5.10, performed with Yu-Fang Hsieh). Both biosensors exhibit similar apparent binding

affinities in the low micromolar regime and reasonable binding kinetics for cAG at 3 mM Mg^{2+} and 37 ºC (Figures 5.9b and 5.11). Importantly, fluorescence microscopy and flow cytometry experiments demonstrate that biosensors based on the Gm0970 riboswitch aptamer function *in vivo* (Figures 5.9c-e, 5.12, and 5.13). Furthermore, these new fluorescent biosensors are able to clearly distinguish between enzymatic production of cAG versus cdiG.

To identify sequence determinants of cAG selectivity, sequence alignment was performed on all GEMM-I sequences screened. All sequences that displayed >50-fold selectivity for cAG were compared for sequence conservation and it was found that cAG-selective sequences that contain an A20 also contained two mutations directly overlaying the A20 compared to Vc2. Specifically, cAG-selective sequences tested here harbor a conserved C-G and U-G base pairs overlaying the A20, compared to a G-C and C-G base pair found in Vc2 (Figure 5.14a,b). The two overlaying base pairs make some H-bonding interactions with cdiG in the Vc2 aptamer crystal structure (Kulshina et al., 2009; Smith et al., 2009), yet it is not clear how these nucleotide changes govern ligand selectivity.

To analyze the role of these nucleotides in determining selectivity, site directed mutagenesis was performed on both the P1-4 Gm0970-Spinach and WT-Vc2 Spinach biosensors (Figure 5.14c,d). An A20G mutation in Gm0970-Spinach altered the biosensor to be ~50-fold selective for cdiG, similar to the effect of the G20A Vc2-Spinach on cdiG selectivity. Flipping the C-G (C21G/G46C) base pair in Gm0970 had no significant effect on selectivity of the Gm0970. Surprisingly, the U22C Gm0970-Spinach biosensor displayed similar promiscuity as the G20A Vc2-Spinach biosensor, indicating a significant role for the U22 nucleobase in ligand recognition. Combination of the A20G and C22U mutations in Gm0970-Spinach completely switched selectivity to cdiG, and conversion of this entire region to the motif found in Vc2 (A20G/C21G/U22C/G46C) resulted in a Gm0970-Spinach biosensor with similar affinity for cdiG and improved brightness compared to the WT Vc2-Spinach sensor. Analogous mutational analysis to convert the WT Vc2-Spinach biosensor to be cAG-selective revealed that while these mutations are necessary for cAG-selectivity of the Gm0970-Spinach biosensor, they are not sufficient to alter selectivity (Figure 5.14d). Regardless, a bioinformatics search of GEMM-I sequences that contained the cAG selectivity motif found here isolated only four sequences from *Pelobacter propionicus*, a very close relative of *Geobacter* spp. (Lonergan et al., 1996). Interestingly, the three sequences that showed fluorescence signal all were >50-fold selective for cAG (Figure 5.15), indicating another organism that possibly uses this second messenger for signaling. Since the sequence motif found in Gm0970 is not sufficient for cAG selectivity, it remains to be determined what other sequence or structure requirements govern specificity for cAG.

It is clear that much remains to be discovered about cAG signaling. For example, whereas the cAG synthase DncV is found in *V. cholerae*, both GEMM-I riboswitches in this bacterium appear to be selective for cdiG, and so far no phosphodiesterases or effectors for cAG have been identified (Sudarsan et al., 2008). In contrast, we now have

revealed that cAG is produced by *G. sulfurreducens* and that this bacterium harbors riboswitches as effectors that are selective for cAG, but homology searches to DncV did not identify any candidate cAG synthase in the genome (Davies et al., 2012). The identification of novel enzymes and other signaling components that regulate the levels of cAG will be greatly assisted by the availability of cAG-selective fluorescent biosensors. These experiments are ongoing in our lab, and we expect will provide further insight into how widespread cAG signaling is in the eubacterial kingdom.

One final intriguing aspect of cAG as a second messenger is its structural similarity to cdiG and cdiA. While most *Geobacter* GEMM-I riboswitches we tested are selective for cAG, a few are conspicuously promiscuous for cAG and cdiG (Figure 5.2, performed with Yichi Su). This may exemplify a mechanism for constructing a Boolean OR logic gate with just one riboswitch aptamer, instead of two as previously observed (Sudarsan et al., 2006). Tandem GEMM-I riboswitches are also prevalent in *Geobacter*, but the representatives we have tested appear to recognize the same ligand and so likely function to provide more “digital” regulatory outputs in response to the second messenger (Welz and Breaker, 2007). Our analysis of the ligand selectivities of GEMM-I riboswitches in *Geobacter* suggests that cAG and cdiG can be selectively recognized to produce different gene expression outcomes, or in specific cases, these cyclic dinucleotide signals are integrated at the riboswitch level.

5.4 Figures

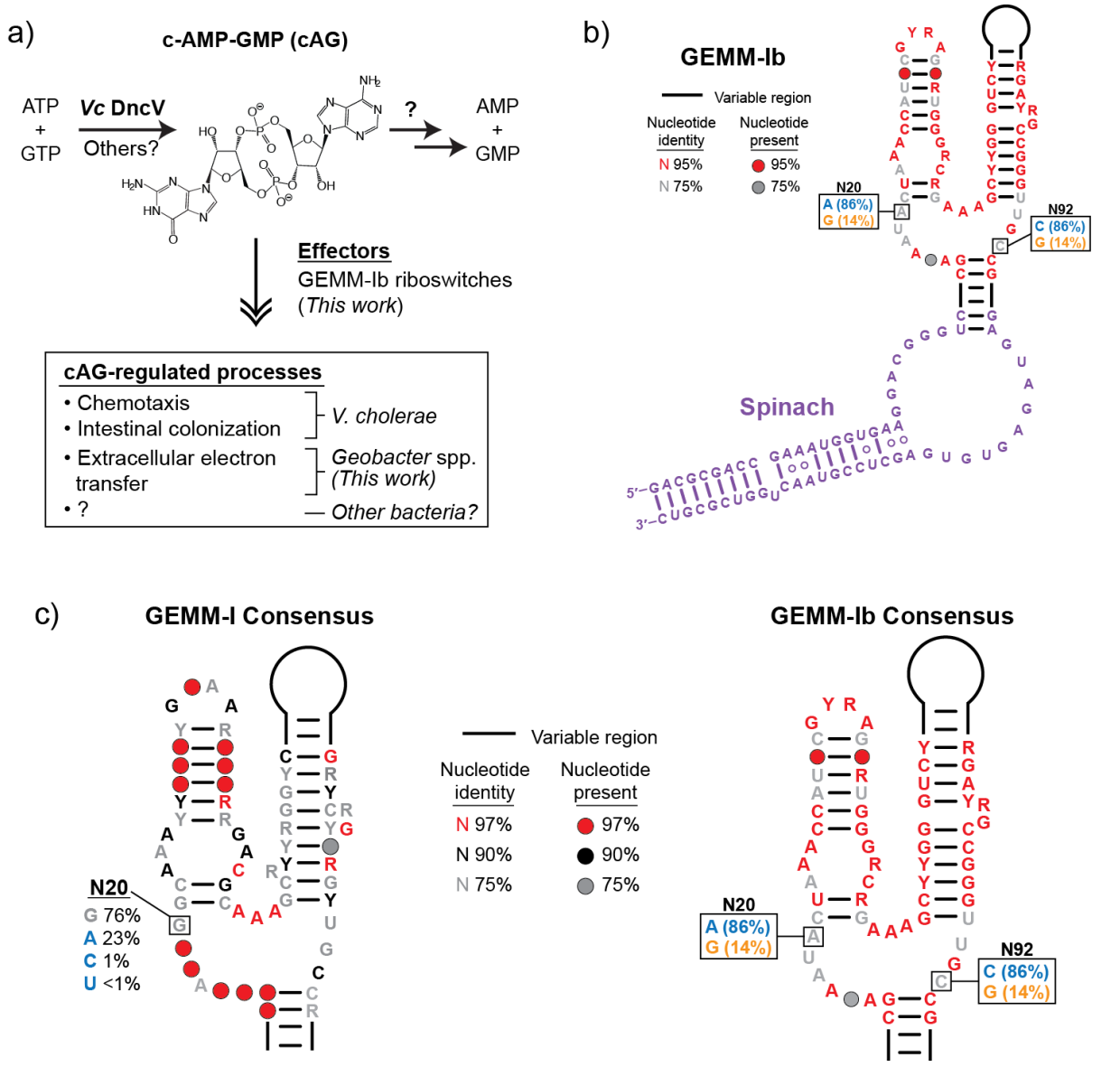

Figure 5.1 GEMM-I riboswitches from Geobacter bacteria are selective for cAG. (a) Cyclic AMP-GMP signaling. **(b)** Sequence and secondary structure model of GEMM-I-Spinach fusion constructs. The consensus for cAG-selective riboswitches in the GEMM-Ib subclass is shown. **(c)** Comparison of full GEMM-I and GEMM-Ib subclass consensus sequences and secondary structures. The latter is based on experimentally confirmed cAG-selective sequences (also see Table 5.1). Covariation of the N20 and N92 positions (following the Vc2 numbering convention) in GEMM-Ib sequences is highlighted in blue and orange.

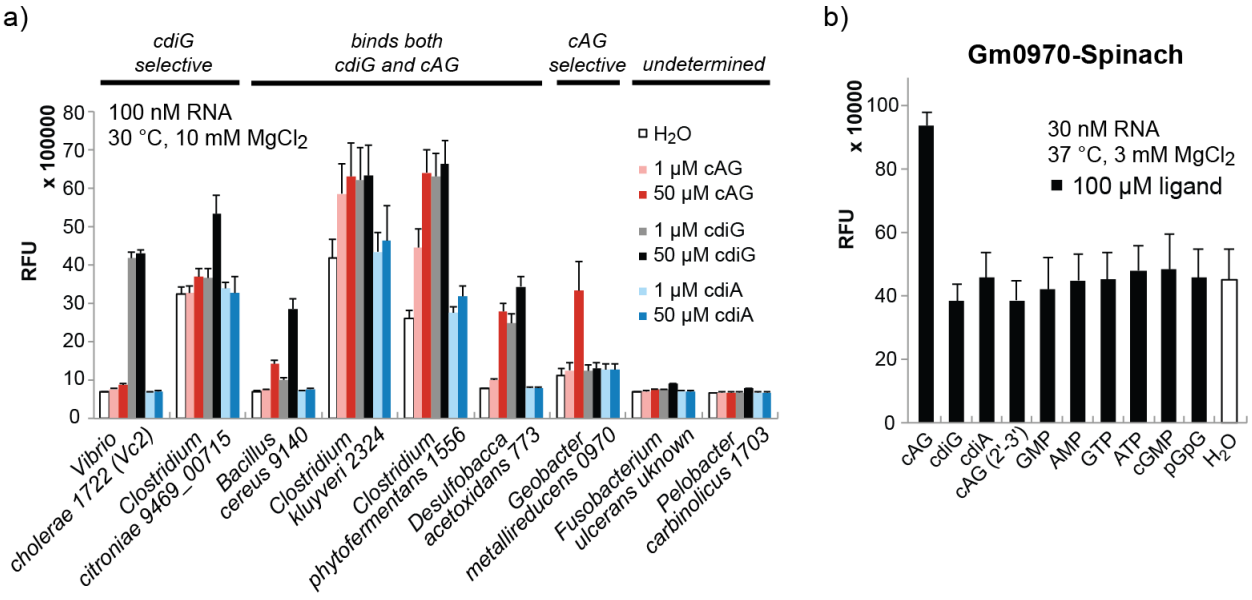

Figure 5.2 Screen of natural A20 GEMM-I variants reveals a sequence with natural cAG selectivity. (a) Spinach-based selectivity screen of GEMM-I riboswitch aptamers from diverse bacteria. All sequences have an A20 except for Vc2-Spinach, which has G20. **(b)** Full selectivity profile of initial candidate Gm0970-Spinach.

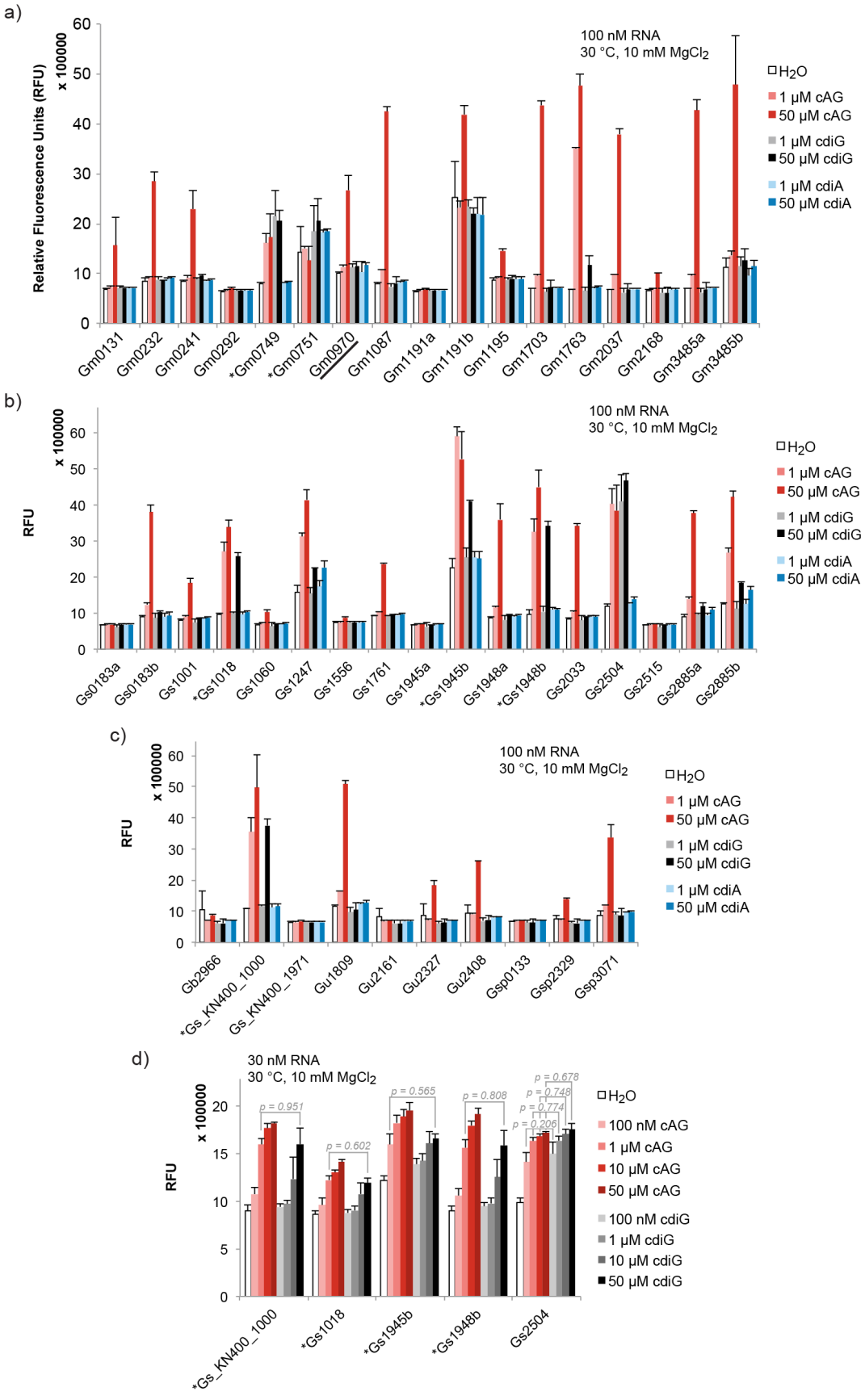
a)
Relative Fluorescence Units (RFU)
x 100000
100 nM RNA
30 °C, 10 mM MgCl2
H2O
1 µM cAG
50 µM cAG
1 µM cdiG
50 µM cdiG
1 µM cdiA
50 µM cdiA
Gm0131
Gm0232
Gm0241
Gm0292
*Gm0749
*Gm0751
Gm0970
Gm1087
Gm1191a
Gm1191b
Gm1195
Gm1703
Gm1763
Gm2037
Gm2168
Gm3485a
Gm3485b
b)
RFU
x 100000
100 nM RNA
30 °C, 10 mM MgCl2
H2O
1 µM cAG
50 µM cAG
1 µM cdiG
50 µM cdiG
1 µM cdiA
50 µM cdiA
Gs0183a
Gs0183b
Gs1001
*Gs1018
Gs1060
Gs1247
Gs1556
Gs1761
Gs1945a
*Gs1945b
Gs1948a
*Gs1948b
Gs2033
Gs2504
Gs2515
Gs2885a
Gs2885b
c)
RFU
x 100000
100 nM RNA
30 °C, 10 mM MgCl2
H2O
1 µM cAG
50 µM cAG
1 µM cdiG
50 µM cdiG
1 µM cdiA
50 µM cdiA
Gb2966
*Gs_KN400_1000
Gs_KN400_1971
Gu1809
Gu2161
Gu2327
Gu2408
Gsp0133
Gsp2329
Gsp3071
d)
RFU
x 100000
30 nM RNA
30 °C, 10 mM MgCl2
p = 0.951
p = 0.602
p = 0.565
p = 0.808
p = 0.678
p = 0.748
p = 0.774
p = 0.206
H2O
100 nM cAG
1 µM cAG
10 µM cAG
50 µM cAG
100 nM cdiG
1 µM cdiG
10 µM cdiG
50 µM cdiG
*Gs_KN400_1000
*Gs1018
*Gs1945b
*Gs1948b
Gs2504

Figure 5.3 Screen of all annotated *G. sulfurreducens* GEMM-I sequences and select other *Geobacter* GEMM-I sequences highlights cAG selectivity. (a) and **(b)** Spinach-based selectivity screen of GEMM-I riboswitch aptamers from *G. metallireducens* GS-15 (a) and *G. sulfurreducens* strain PCA (b). All sequences have an A20 except for those marked with an asterisk, which have G20. **(c)** Spinach-based selectivity screen of other GEMM-I riboswitch aptamers from *G. bemidjiensis* (Gb), *G. sulfurreducens strain KN400* (Gs_KN400), *G. uraniireducens* (Gu), and *Geobacter sp.* (Gsp). **(d)** Additional analysis of *G. sulfurreducens* riboswitch aptamers to probe relative affinities to cAG and cdiG.

G. sulfurreducens PCA has 17 predicted GEMM-I riboswitches annotated in its genome (Genbank accession NC_002939.5), of which 11/17 are selective for cAG, whereas 1/17 binds both cAG and cdiG. Interestingly, four sequences in *G. sulfurreducens* (three in the PCA strain, one in the KN400 strain) that display cAG selectivity harbor a G20. These sequences also contain a G at the position that recognizes a ligand nucleobase through a Watson-Crick base pair, which corresponds to C92 in the Vc2 riboswitch (*14*). Furthermore, one sequence containing an A20 displays promiscuous binding to cdiG and cAG (Gs2504). Taken together, these data suggest that additional sequence and structural requirements beyond the N20 and N92 positions of the riboswitch aptamer are necessary to confer selectivity between cAG and cdiG.

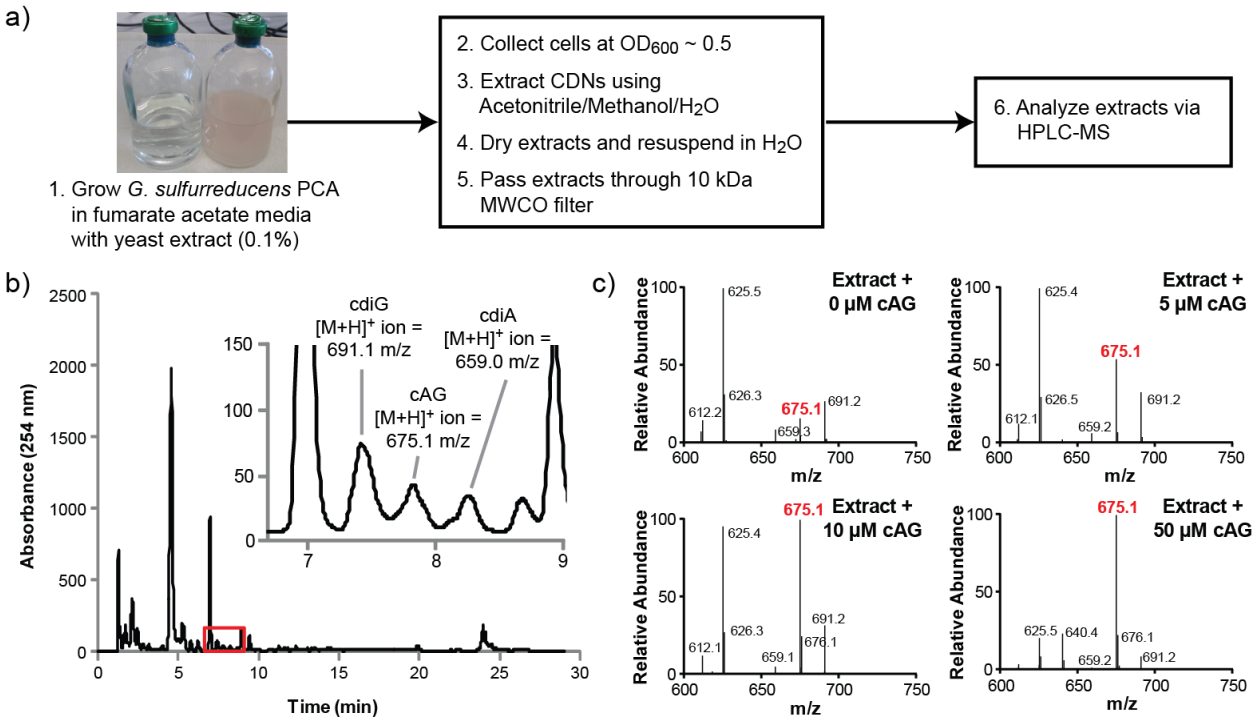

Figure 5.4 *G. sulfurreducens* strain PCA produces cAG as well as cdiG and cdiA. **(a)** HPLC-MS analysis of *G. sulfurreducens* PCA cell extracts. Shown is the MS spectrum integrating the retention time region containing all three cyclic dinucleotides. **(b)** Full HPLC chromatogram of the cell extract. Inset shows the region containing peaks assigned to the cyclic dinucleotides (Figure 5.5). **(c)** Similar analysis as shown in (a) for samples doped with 5 or 10 μM cAG.

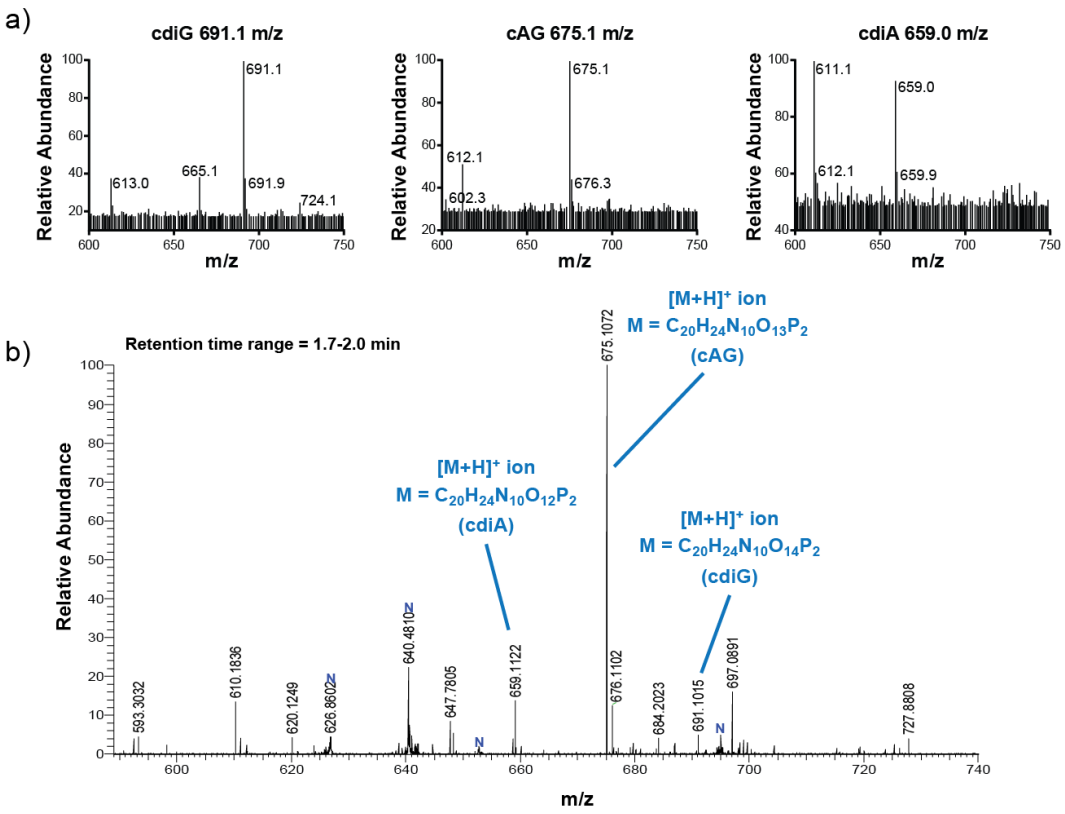

Figure 5.5 ***G. sulfurreducens*** **PCA produces cdiG, cAG, and cdiA. (a)** MS traces for peaks labeled as cdiG, cAG, and cdiA in Figure 5.4b. **(b)** High resolution mass spectrometry of of *G. sulfurreducens* PCA extract (HPLC trace not shown, performed by Stephen Wilson).

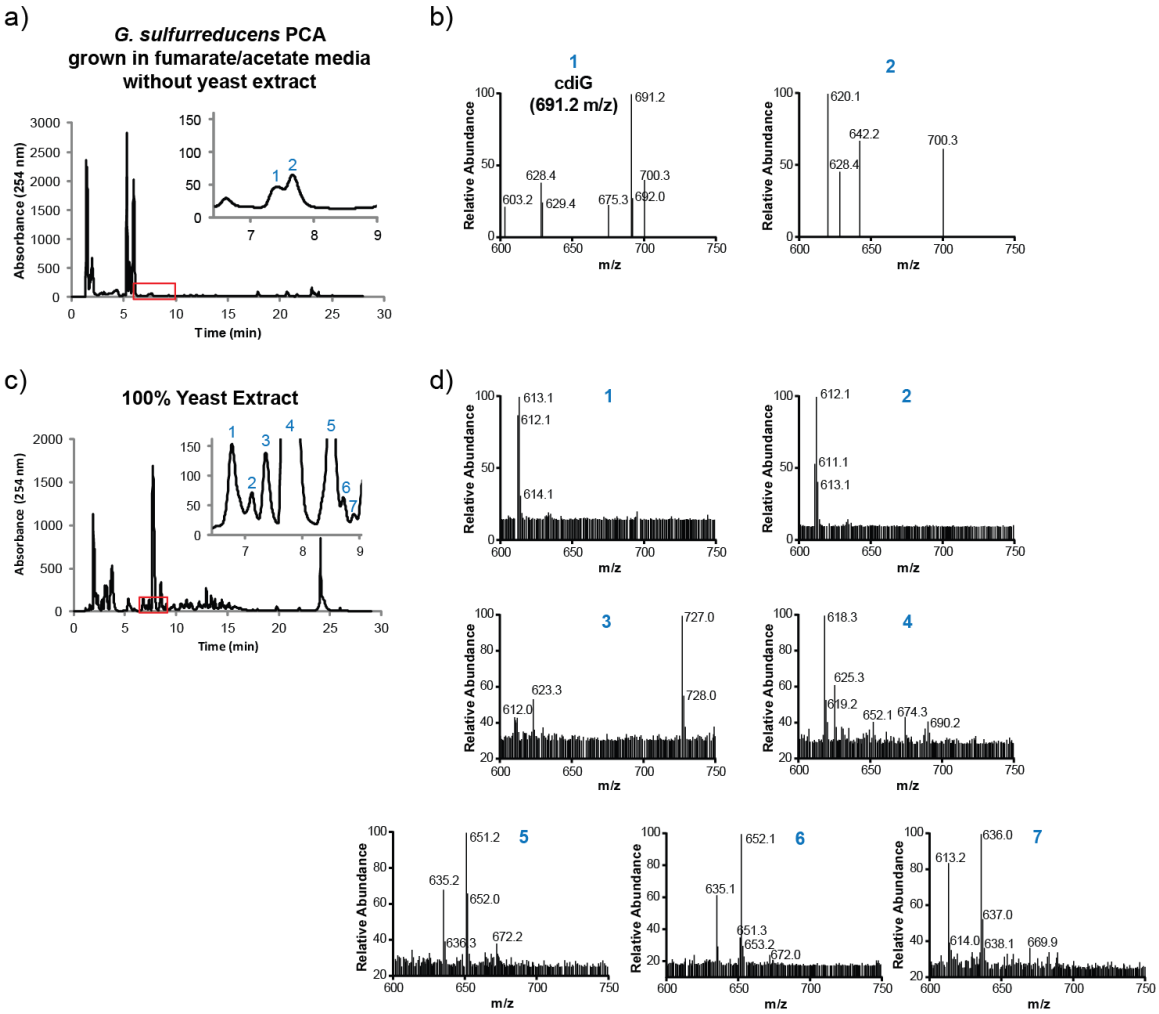

Figure 5.6 No cAG or cdiA is detected in extracts of *G. sulfurreducens* PCA grown without added yeast extract; no cAG is detected in yeast extract. (a) and **(b)** HPLC and MS traces for *G. sulfurreducens* PCA extracts from cells grown in fumarate-acetate without yeast extract supplementation. The inset shows the expected region for elution of cyclic dinucleotides, and the MS traces of the labeled peaks are shown in B. **(c)** and **(d)** HPLC and MS traces for 100% yeast extract processed in same manner as the cell extracts. The inset shows the expected region for elution of cyclic dinucleotides and the MS traces of the labeled peaks are shown in (d).

Only cdiG is detected in the cell extract of *G. sulfurreducens* grown without yeast extract supplementation. The second peak does not correspond to any known cyclic dinucleotides. No cAG or cdiA was observed with larger injection volumes or upon concentration of the extract.

The analysis of yeast extract alone shows that cyclic dinucleotides are not present in the media itself. While many compounds appear to elute in the retention time range of cyclic dinucleotides, none of the MS traces show the presence of cyclic dinucleotides. Taken together, this supports that cyclic dinucleotides are produced by *G. sulfurreducens* PCA cells grown with supplemented yeast extract.

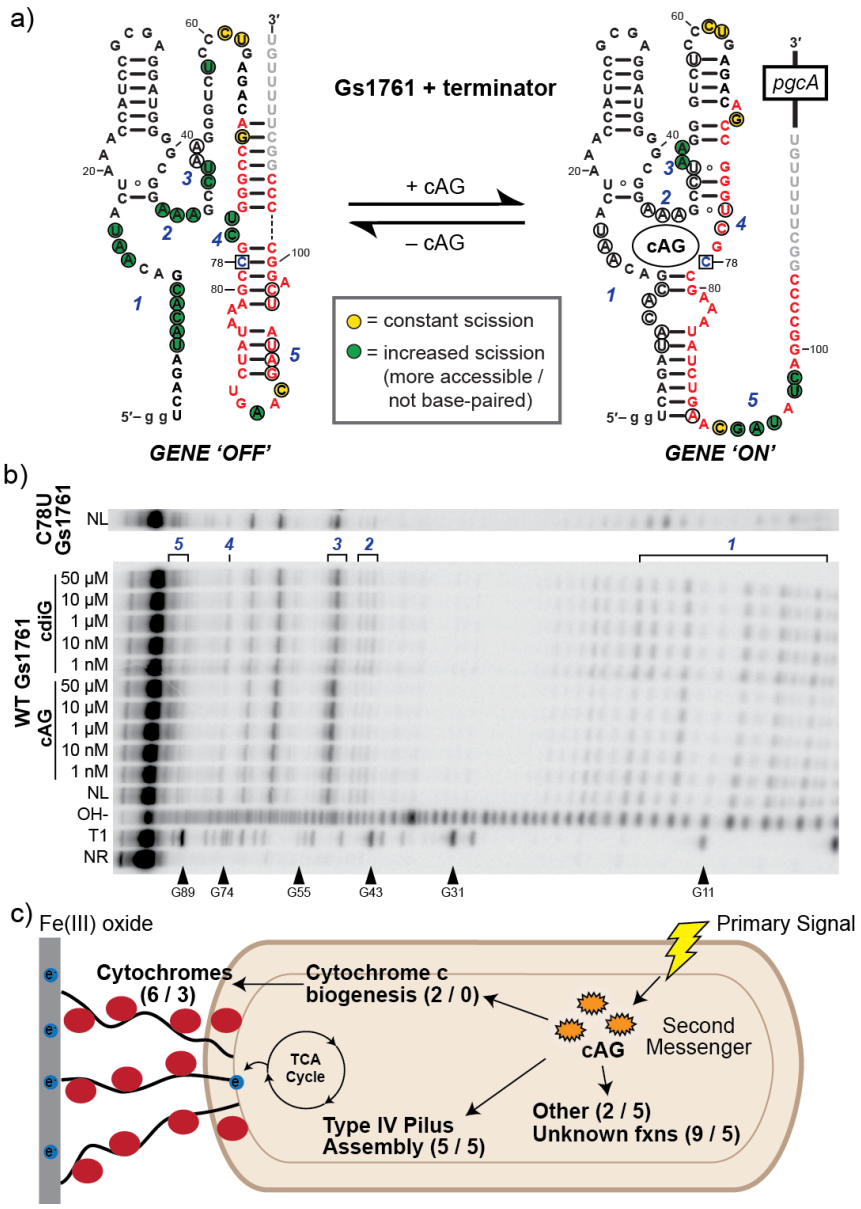

Figure 5.7 GEMM-Ib riboswitches activate genes involved in extracellular electron transport in response to cAG. (a) and **(b)** In-line probing analysis of the full Gs1761 riboswitch (aptamer and transcription terminator) mapped onto the secondary structure models with and without cAG. Default transcription termination turns off gene expression, whereas cAG binding favors full-length transcription to the pgcA coding sequence (Gene 'ON'). Red nucleotides form the terminator stem. Grey nucleotides were excluded from the RNA construct tested. Blue numbers correspond to regions on the gel shown in (b). The full gel for the C78U mutant is shown in Figure 5.8. **(c)** Schematic of extracellular electron transport that highlights the roles of genes turned on by cAG signaling. The number of genes is indicated for *G. sulfurreducens* and *G. metallireducens*, respectively (Table 5.1). Depicted are cytochromes (red circles), pili (black lines), and electrons (blue circles).

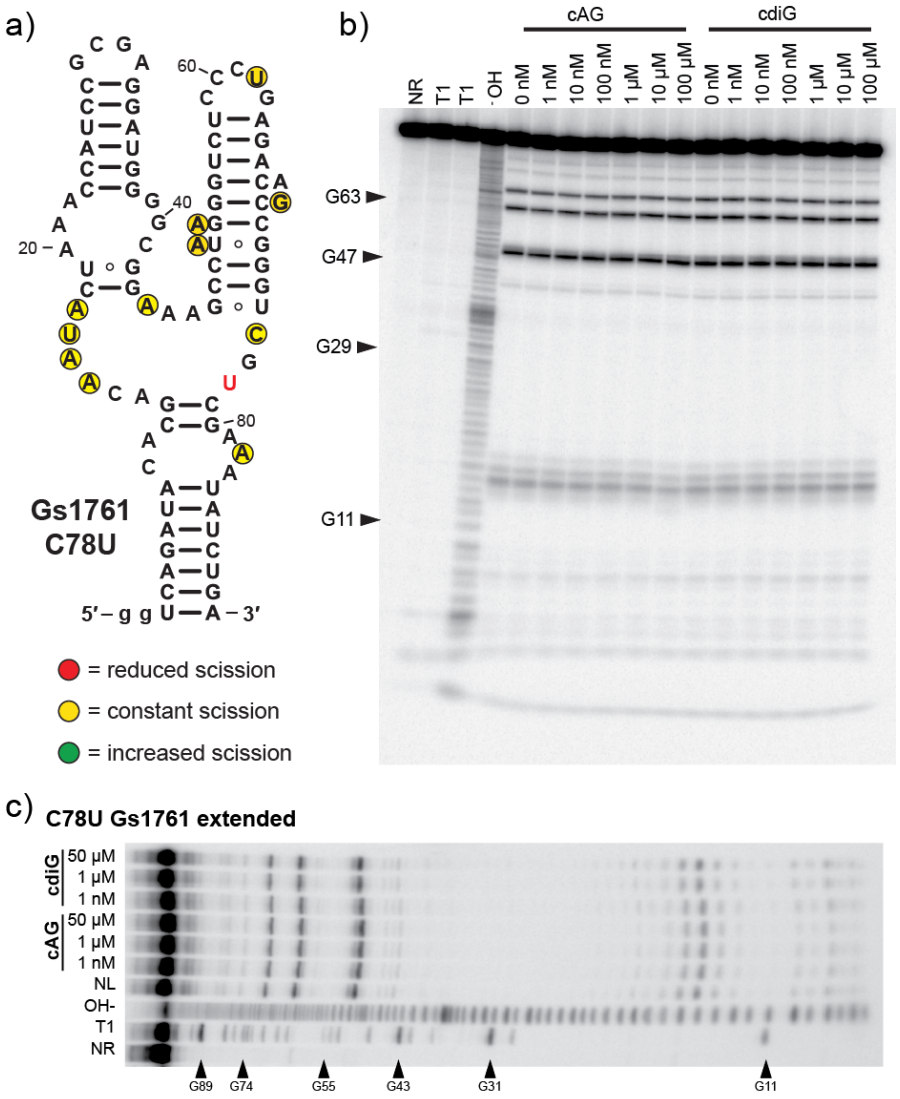

Figure 5.8 In-line probing analysis of C78U Gs1761 riboswitch aptamer and extended riboswitch including terminator. (a) Sequence and secondary structure of the C78U Gs1761 aptamer with mapped nucleotides that exhibit high in-line cleavage signal. **(b)** In-line probing gel for C78U Gs1761. No reaction (NR), treatment with RNase T1 (T1), which cleaves after G nucleotides, and partial base hydrolysis ($^{-}$OH) serve as control and ladders. **(c)** In-line probing gel for the full C78U Gs1761 riboswitch (aptamer and transcription terminator) with no ligand versus different concentrations of cAG or cdiG.

The in-line probing pattern for the C78U Gs1761 riboswitch aptamer does not change in response to cAG or cdiG (Figure 5.8b), and closely resembles that of WT in the absence of ligand (Figure 5.7b). This shows that the mutation disrupts the ability of the Gs1761 riboswitch aptamer to bind ligand, and is consistent with observations that the corresponding C92U mutation to Vc2 perturbs ligand binding.

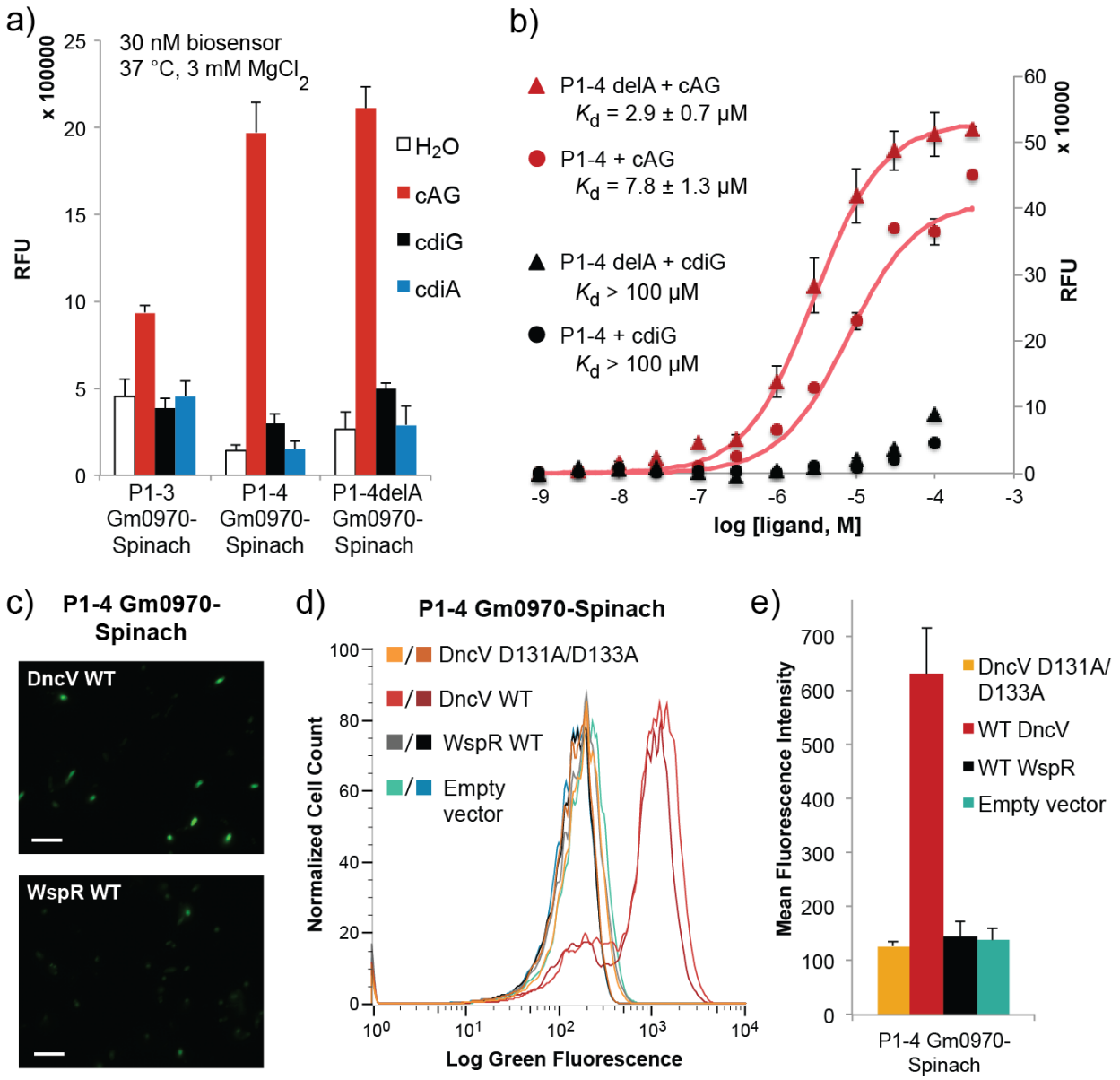

Figure 5.9 Riboswitch-based fluorescent biosensors selectively respond to cAG *in vitro* and in live cells. (a) Fluorescence activation and selectivity of optimized Gm0970-Spinach constructs with 100 μM ligands (also see Figure 5.13). **(b)** *In vitro* binding curves of biosensors for cAG and cdiG for determination of apparent dissociation constants. Error bars for (a) and (b) represent the standard deviation of three independent replicates. **(c)** Fluorescence microscopy of *E. coli* coexpressing the P1-4 Gm0970-Spinach biosensor with a cAG (DncV) or cdiG (WspR) synthase. Scale bars represent 10 μm. **(d)** Flow cytometry analysis of *E. coli* cells co-expressing the P1-4 biosensor and cyclic dinucleotide synthases or empty vector by a Guava flow cytometer. **(e)** Quantitation of flow cytometry data for *E. coli* co-expressing a biosensor and synthase enzyme or empty vector shown in Figure 5.9d. Error bars represent the standard deviation in mean fluorescence of independent biological replicates of <10,000 analyzed cells

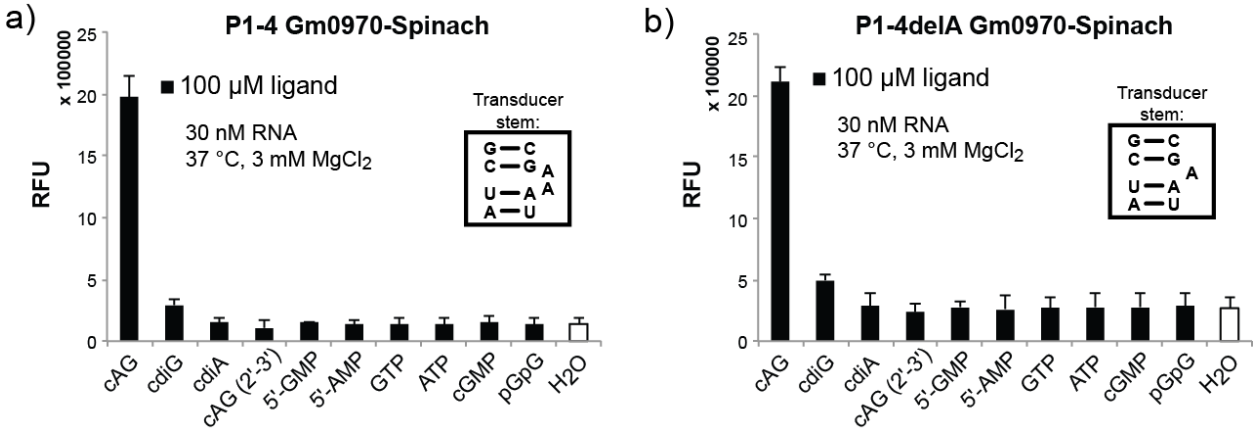

Figure 5.10 Gm0970-Spinach biosensors are selective for cAG. (a, b) Full selectivity profiles for P1-4 (a) and P1-4delA (**b)** Gm0970-Spinach biosensors. Inset shows the sequence of the transducer stem, which corresponds to the P1 stem of the riboswitch aptamer. Error bars represent the standard deviation of three independent replicates with duplicate samples.

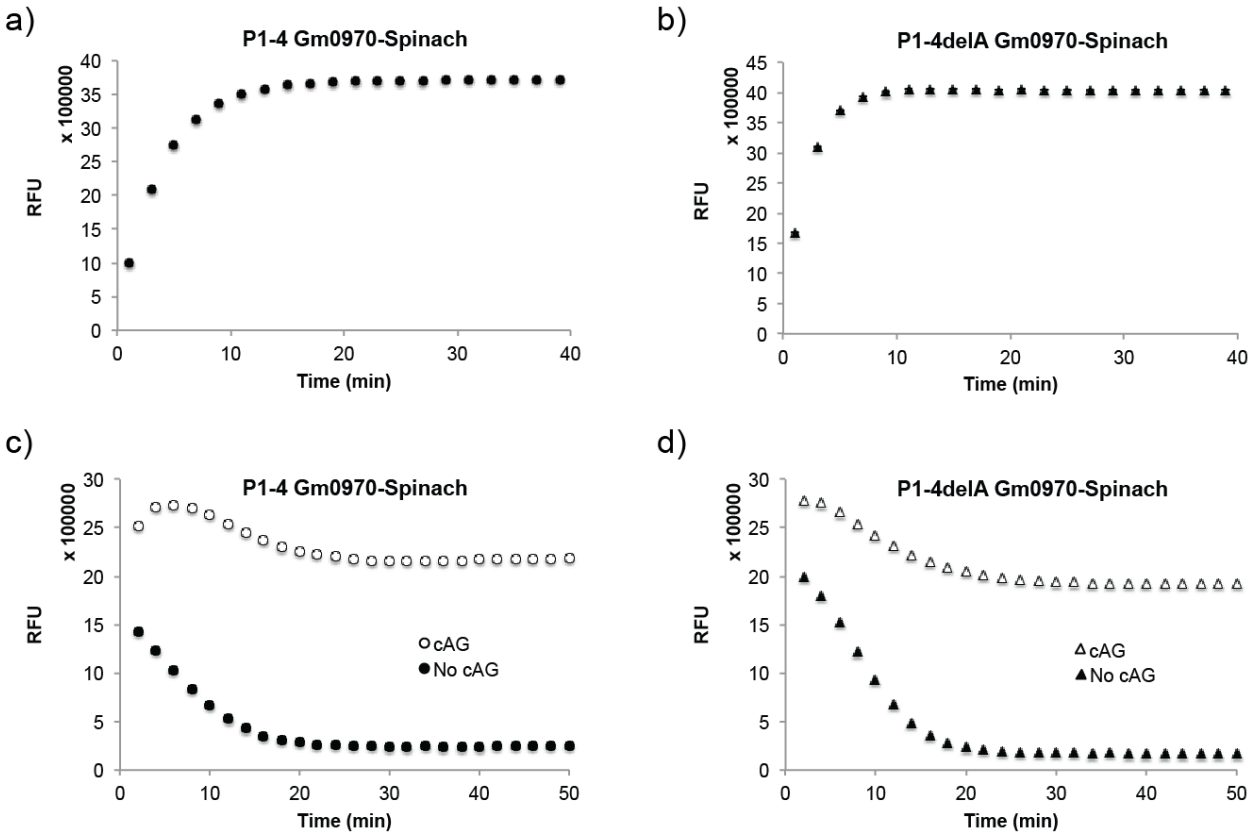

Figure 5.11 Activation and deactivation of Gm0970-Spinach biosensors. Fluorescence activation rate of P1-4 **(a)** and P1-4delA **(b)** Gm0970-Spinach biosensors with cAG at 37 °C. RNA (100 nM) was mixed with DFHBI (10 μM) and cAG (100 μM) in 40 mM HEPES, pH 7.5, 125 mM KCl, and 3 mM $MgCl_2$. Fluorescence deactivation of P1-4 **(c)** and P1-4delA **(d)** Gm0970-Spinach at 37 °C. RNA (100 nM) was incubated with DFHBI (10 μM) and cAG (30 μM) in 40 mM HEPES, pH 7.5, 125 mM KCl, and 3 mM $MgCl_2$. The fluorescence was monitored after the RNA was passed through a buffer exchange column pre-equilibrated in buffer without cAG. Control samples in which the RNA was passed through a buffer exchange column pre-equilibrated in buffer with cAG shows some capture of ligand.

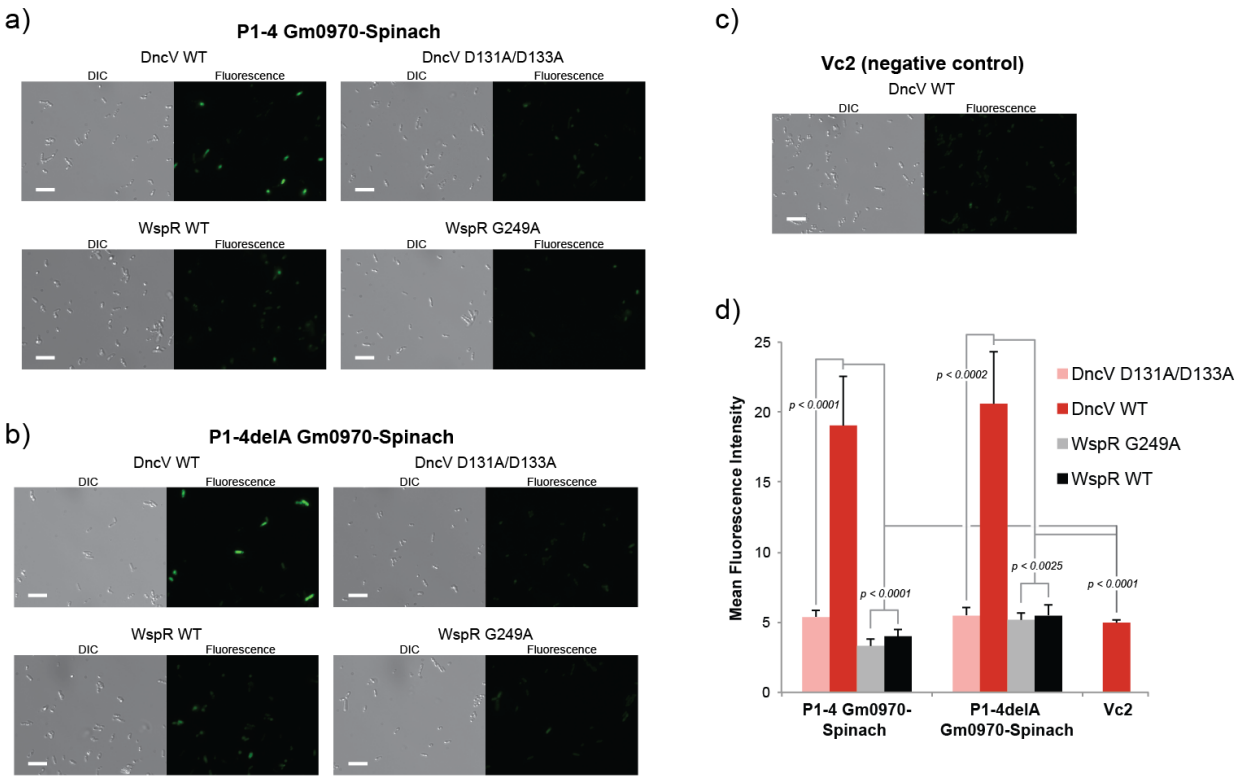

Figure 5.12 Live cell fluorescence microscopy of Gm0970-Spinach biosensors in *E. coli*. Differential interference contrast (left panels) and fluorescent images (right panels) of *E. coli* cells expressing P1-4 Gm0970-Spinach **(a)**, P1-4delA Gm0970-Spinach **(b)**, or Vc2 RNA **(c)** and dinucleotide cyclase variants after incubation with DFHBI. Scale bars represent 10 μm. **(d)** Mean fluorescence intensity of cells expressing Gm0970-Spinach biosensors or Vc2 and various dinucleotide cyclases. Error bars indicate S.E.M. of at least 50 cells per sample.

To show the specificity of the biosensors *in vivo*, both Gm0970 biosensors were coexpressed with either DncV WT, a cAG synthase from *V. cholerae*, or WspR WT, a cdiG synthase from *Pseudomonas fluorescens* (Davies et al., 2012; Malone et al., 2007). Besides the wild-type versions of these enzymes, inactive alleles of DncV and WspR were also co-expressed in *E. coli* to serve as controls for the biosensors. The DncV D131A/D133A allele contains two aspartate to alanine mutations in the catalytic Dx[D/E] domain, which have previously been shown to eliminate DncV cAG synthase activity both *in vitro* and *in vivo* (Davies et al., 2012; Kellenberger et al., 2013). Similarly, a guanine to alanine mutation in the conserved GGDEF domain of WspR G249A results in a loss of cdiG synthase activity (Kellenberger et al., 2013; Malone et al., 2007)

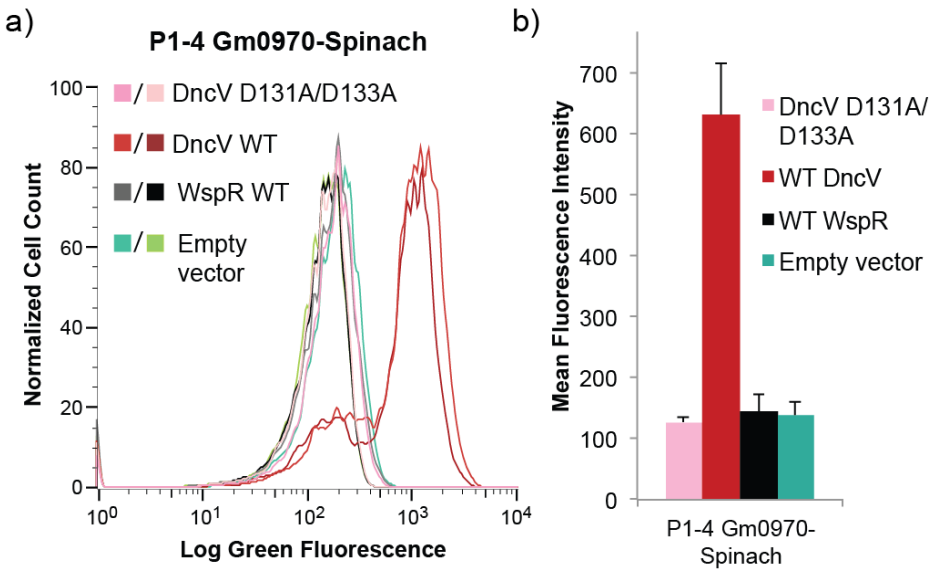

Figure 5.13 Flow cytometry analysis of *E. coli* expressing a cAG fluorescent biosensor to detect enzyme activity. (a) Flow cytometry trace of *E. coli* cells co-expressing the P1-4 Gm0970-Spinach biosensor and synthase enzymes or empty vector. For each independent biological sample shown, ~50,000 cells were analyzed by a Guava easyCyte 8HT flow cytometer. **(b)** Quantitation of data shown in part (a). Error bars indicate the standard deviation between mean fluorescence intensities of the two independent biological replicates shown.

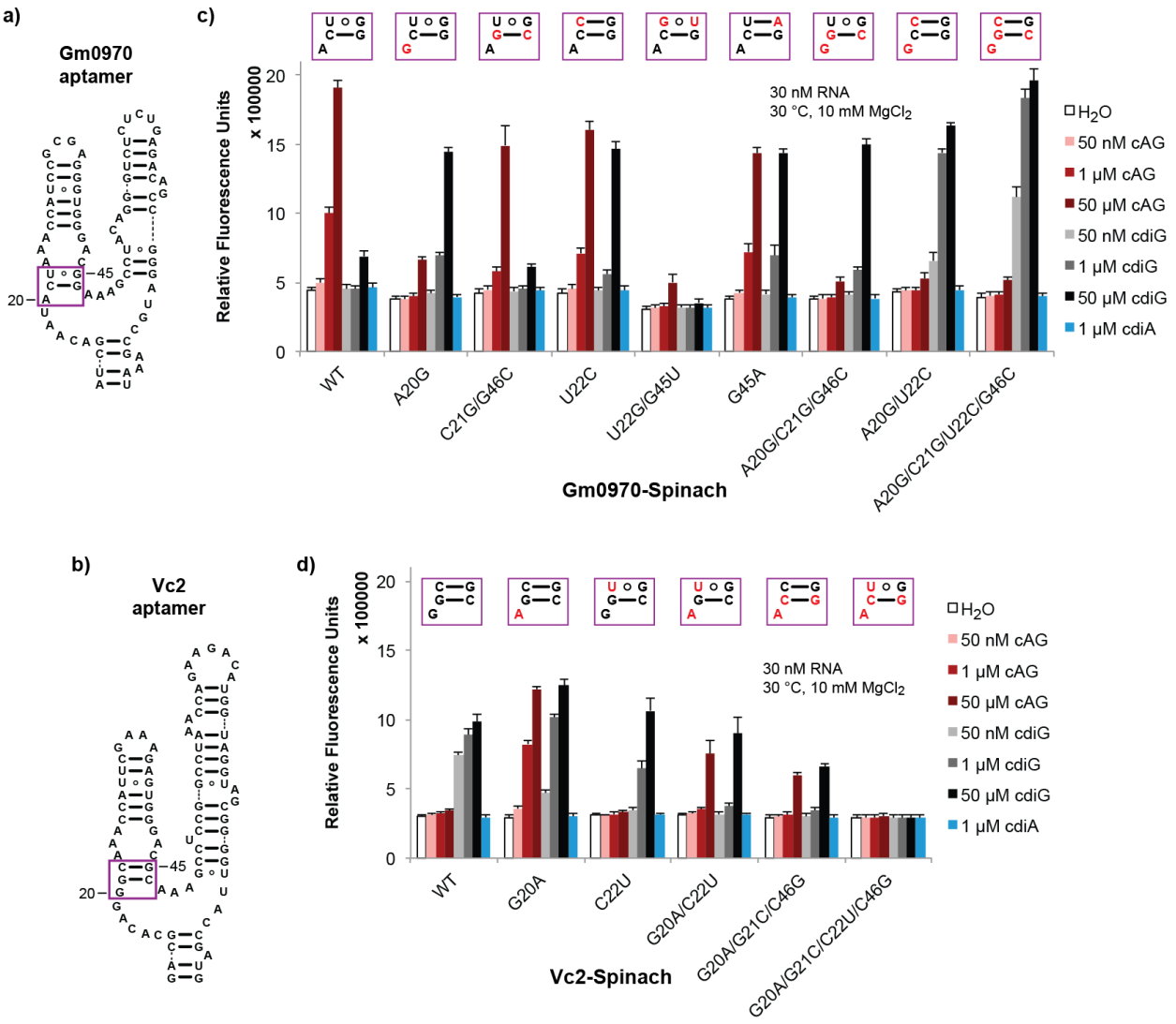

Figure 5.14 Site-directed mutagenesis of Spinach biosensors to identify cAG-selectivity determinant. (a) and **(b)** Sequence and secondary structures of the WT Gm0970 (a) and Vc2 (b) aptamers. Nucleotides in the purple boxes are mutated in (c) and (d). **(c)** and **(d)** Site-directed mutagenesis of the Gm0970-Spinach and Vc2-Spinach sensors. Boxed nucleotides above each mutant depict in red the mutated nucleotide from the purple boxes in (a) and (b).

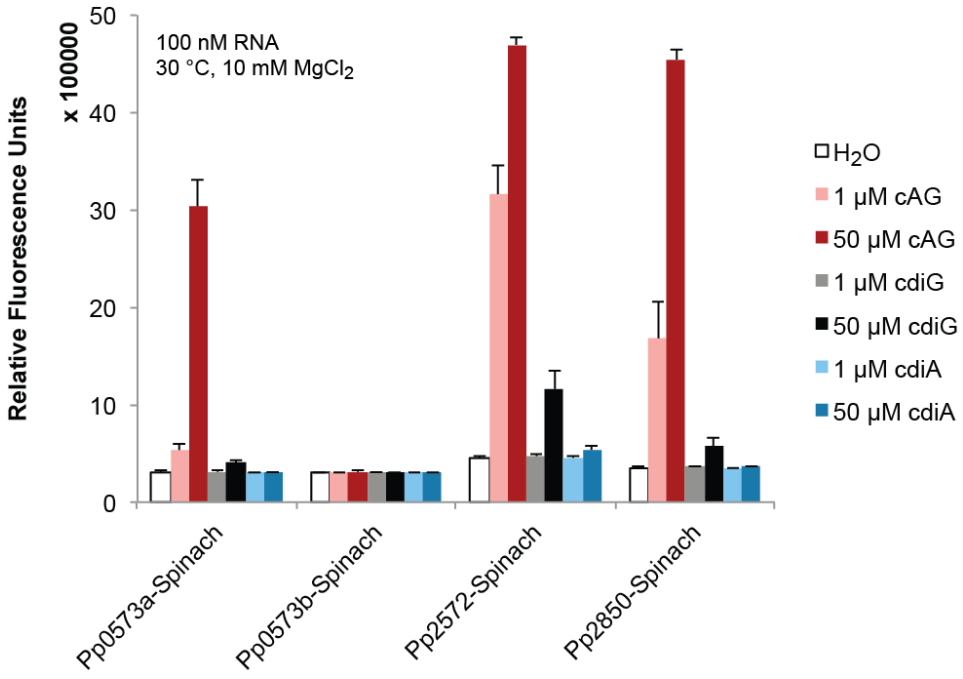

Figure 5.15 Select GEMM-I riboswitches from *Pelobacter propionicus* are selective for cAG. Three GEMM-I sequences from *P. propionicus* (14 total) containing the cAG-selectivity motif found in Gm0970 display cAG selectivity.

Table 5.1 Gene contexts for *G. metallireducens* and *G. sulfurreducens* GEMM-Ib riboswitches.

LEGEND: GEMM-I riboswitch aptamers are considered cAG-selective if they meet the following screening criteria: at least 50-fold selective for cAG and greater than 1.5-fold fluorescence activation with cAG. If fluorescence activation was less than 1.5-fold, it is considered to have undetermined selectivity (N/A, row greyed out). Entries with undetermined selectivities were not included in Figure 5.11c. * = putative operon, not experimentally confirmed. ** = Not tested because putative GEMM-I overlaps with coding sequence and manual inspection showed it to be a poor candidate.

Geobacter sulfurreducens					
Ribo-switch	**N20**	**Select-ivity**	**Gene ON/OFF**	**# Genes**	**Gene Categories**
Gs183a	A	N/A	On	3*	Peptidoglycan L,D-transpeptidase (2), Lipoprotein (1)
Gs183b	A	cAG	On	"	"
Gs1001	G	cAG	On	1	Hypothetical (1)
Gs1018	G	cAG	On	1	Hypothetical (1)
Gs1060	A	N/A	On	1	Hypothetical (1)
Gs1247	A	cAG	On	1	Hypothetical, YXWGXW motif (1)
Gs1556	A	N/A	On	1	Lipoprotein (1)
Gs1761	A	cAG	On	1	PgcA (cytochrome c, 1)
Gs1945a	A	N/A	On	1	Hypothetical, bacterial Ig domains (1)
Gs1945b	G	cAG	On (weak)	"	"
Gs1948a	A	cAG	On	2*	Hypothetical (2)
Gs1948b	G	cAG	On	"	"
Gs2033	A	cAG	On	6	XRE-family TF (Uncharacterized, 1), PilM-N-O-P-Q (Pilus, 5)
Gs2504	A	**cAG+cdiG**	Unknown	2	OmcS-T (cytochrome c, 2)
Gs2515	A	N/A	On	1	Cytochrome c oxidase subunit III (cytochrome c, 1)
Gs2885a	A	cAG	On	6	Hypothetical, bacterial Ig domains, NHL repeat (1), OmcA-H-G-ResB-C (cytochrome c, 5)
Gs2885b	A	cAG	On	"	"

TOTAL cAG-Related: Hypothetical/Lipoprotein/Uncharacterized (9); Cytochrome containing/biogenesis (8);
Pilus (5); Peptidoglycan L,D-transpeptidase (2)

Geobacter metallireducens					
Ribo-switch	**N 20**	**Select-ivity**	**Gene ON/OFF**	**# Genes**	**Gene Categories**
Gm0131	A	N/A	On	1	Hypothetical (1)
Gm0232	A	cAG	On	1	Hypothetical (1)
Gm0241	A	cAG	On	1	Lipoprotein (1)
Gm0292	A	N/A	On	1	Cytochrome c (1)
Gm0749	G	**cAG+cdiG**	On	1	Subtilase family serine protease, bacterial Ig domains (1)
Gm0751	G	N/A	Unknown	1	Subtilase family serine protease, bacterial Ig domains (1)
Gm0970	A	cAG	On	6*	XRE-family TF (Uncharacterized, 1), PilM-N-O-P-Q (Pilus, 5)
Gm1087	A	cAG	On	1	Cytochrome c oxidase subunit III (cytochrome c, 1)
Gm1191 a	A	N/A	On	1	Cytochrome c oxidase subunit III (cytochrome c, 1)
Gm1191 b	A	cAG	On	"	"
Gm1195	A	cAG	On	1	Subtilase family serine protease (1)
Gm1452		NOT TESTED**			
Gm1703	A	cAG	On	1	Cytochrome c (1)
Gm1763	A	cAG	On	1	Hypothetical, YXWGXW motif (1)
Gm2037	A	cAG	On	1	N-acylhomoserine lactone synthetase-related (1)
Gm2168	A	N/A	On	1	Cytochrome c, VCBS repeats (1)
Gm3485 a	A	cAG	On	3*	Peptidoglycan L,D-transpeptidase (2), Lipoprotein (1)
Gm3485 b	A	cAG	On	"	"

TOTAL cAG-Related: Hypothetical/Lipoprotein/Uncharacterized (5); Cytochrome containing/biogenesis (3); Pilus (5);
Peptidoglycan L,D-transpeptidase (2), Serine protease (2), AHL synthetase (1)

5.5 Materials and Methods

General Reagents and Oligonucleotides

GEMM-I-Spinach DNA oligonucleotides were purchased as Ultramers from Integrated DNA Technologies (IDT, Coralville, IA) and other oligonucleotides were purchase from Elim Biopharmaceuticals (Hayward, CA). Cyclic dinucleotides were purchased from Axxorra, LLC (Farmingdale NY). DFHBI was either purchased from Lucerna (New York, NY) or was synthesized following previously described protocols (Paige et al., 2011) and was stored as a ~20 mM stock in DMSO. *Geobacter sulfurreducens* PCA was obtained from the Coates lab at UC Berkeley. Genomic DNA from *G. sulfurreducens* was isolated using the Purelink Genomic DNA mini kit (Invitrogen).

In Vitro Transcription

Preparation of RNAs was carried out as previously described in section 3.5. Briefly, DNA templates for *in vitro* transcription were prepared via a PCR that added the T7 polymerase promoter sequences. Templates were then transcribed using T7 RNA polymerase and were purified either by 96-well spin column (ZR 96 Clean & Concentrator, Zymo Research) for screening experiments or by denaturing (7.5 M urea) 6% PAGE for characterization experiments. RNAs purified by PAGE were subsequently eluted from gel pieces in Crush Soak buffer (10 mM Tris-HCl, pH 7.5, 200 mM NaCl and 1 mM EDTA, pH 8.0), precipitated with ethanol, and resuspended in 1 x TE buffer (10 mM Tris-HCl, pH 8.0, 1 mM EDTA). RNAs purified by 96-well spin column were purified according to the manufacturer's protocol and were resuspended in 0.5 x TE buffer. Accurate measurement of RNA concentration was determined after performing a hydrolysis assay to eliminate the hypochromic effect due to secondary structure in these RNAs (Wilson et al., 2014).

In Vitro Fluorescence Assays of GEMM-I-Spinach Variants

To screen GEMM-I riboswitch aptamer selectivity, a solution of ligand (0, 1, 50, or 100 μM) and DFHBI (33 μM) was prepared in buffer containing 40 mM HEPES, 125 mM KCl, and 10 mM $MgCl_2$ at pH 7.5 Each RNA was renatured in buffer at 70 °C for 3 min and cooled to ambient temperature for 5 min prior to addition to the reaction solution at a final concentration of 100 nM. Binding reactions were incubated at 30 °C in a Corning Costar 3915 96-well black plate until equilibrium was reached. The fluorescence emission was measured using a Molecular Devices SpectraMax Paradigm plate-reader with the following instrument parameters: 460 nm excitation, 500 nm emission. The background fluorescence of the buffer alone (without DFHBI) was subtracted from each sample to determine the relative fluorescence units.

To analyze selectivity or binding affinity of RNA biosensor constructs, assays were run as described above, except at 37 °C with 3 mM $MgCl_2$ to mimic physiological conditions. Selectivity experiments were performed using 100 nM RNA and 100 μM ligand. Experiments to measure K_d were performed with 30 nM RNA and various ligand concentrations, and the fluorescence of the sample with DFHBI and RNA in buffer without ligand was subtracted to determine relative fluorescence units.

Biosensor Activation and Deactivation Assays

Activation and deactivation assays were performed as previously described in section 3.5. Briefly, to determine activation rate, the ligand (30 μM) and DFHBI (33 μM) in buffer were prepared and pre-warmed to 37 °C. The RNA (100 nM final concentration) was renatured in buffer at 70 °C for 3 min then cooled to 37 °C prior to addition to the reaction solution. Immediately after the RNA was added, the fluorescence emission was measured every 2 min at 37 °C using the same plate-reader settings as for the ligand binding assays.

Deactivation assays were performed using buffer exchange to remove the cyclic di-nucleotide ligand. RNA (100 nM) was mixed with ligand (30 μM) and DFHBI (33 μM) at 37 °C in a buffer containing 40 mM HEPES, 125 mM KCl, and 3 mM $MgCl_2$ at pH 7.5. Once the reaction had reached maximum fluorescence, half of the reaction was passed through an Illustra MicroSpin G-25 Column (GE Healthcare) that had been equilibrated with DFHBI (33 μM) in buffer while the other half was passed through a column that had been equilibrated with ligand (30 μM), DFHBI (33 μM), and buffer. Immediately after elution of the RNA, the fluorescence emission was measured every 2 min at 37 °C using the same plate-reader settings as for the ligand binding assays.

In-Line Probing Assays

In vitro transcribed RNA was radiolabeled with γ-^{32}P ATP using T4 polynucleotide kinase (NEB) following standard procedures (Regulski and Breaker, 2008). After PAGE purification, RNAs were passed through an Illustra MicroSpin G-25 Column (GE Healthcare) and eluted with ddH_2O. In-line probing assays were performed as previously described (Regulski and Breaker, 2008) for the extended Gs1761 riboswitch with terminator construct. Dried gels were exposed on a phosphorimager screen for several days and scanned using a Typhoon laser-scanning system (GE Healthcare).

Liquid Culture Growth of *G. sulfurreducens* PCA

From a glycerol stock, a 10 mL starter culture of *G. sulfurreducens* PCA in fumarate acetate media alone or supplemented with 0.1% yeast extract was grown anaerobically at 30 °C for 5-7 days without shaking in anaerobic culture tubes sealed under nitrogen with 20 mm blue butyl rubber stoppers and aluminum crimps. Intermediate 50 mL cultures were inoculated at 1:10 dilution, then used to inoculate master 1 L cultures at 1:20 dilution in the same media. Cells were grown anaerobically in fumarate acetate media with or without yeast extract at 30 °C until an OD_{600} ~ 0.500 was reached, which took about 2-3 days. Cells were harvested in 50 or 100 mL aliquots by centrifugation at 10,000 rcf for 10 min at 4 °C, and pellets were stored at -80 °C.

The fumarate acetate media contained the following in 1 L: 4 g sodium fumarate dibasic (25 mM sodium fumarate final conc.), 1.64 g sodium acetate (20 mM final conc.), 0.49 g $NaH_2PO_4 \cdot 2H_2O$, 0.97 Na_2HPO_4, 0.25 g NH_4Cl, 0.1 g KCl, 10 mL 100x vitamin mix (Bruce et al., 1999), 1 mL 1000x NB minerals mix (Bruce et al., 1999), and 10 g yeast extract (Bacto brand, if used). The media was boiled, cooled, and degassed by bubbling under nitrogen gas for 30 minutes, then aliquoted, sealed under anaerobic conditions, and autoclaved.

Cell Extraction from *G. sulfurreducens* PCA and *E. coli*
Cyclic dinucleotides were extracted as described previously (Spangler et al., 2010) with the following modifications. A frozen cell pellet from 100 mL of liquid culture was thawed and resuspended in 600 µL extraction buffer (40% methanol, 40% acetonitrile, 20% ddH_2O). The cell solution was incubated at 4 °C for 20 min, then at ambient temperature for 20 min. After centrifugation at 4 °C for 20 min at 13,200 rpm, the supernatant was carefully removed and stored on ice. The remaining pellet was extracted twice more with 300 µL extraction solvent as described. The combined supernatants were evaporated to dryness by rotary evaporation, and the dried material was resuspended in 250 µL ddH_2O. The extract was filtered through a 10 kDa MWCO Amicon Ultra-4 Protein Concentrator (Millipore) and used immediately or stored in aliquots at -20 °C.

Direct LCMS Analysis of Cell Extracts
LC-MS analysis of *G. sulfurreducens* PCA cell extracts was performed using an Agilent 6120 Quadrupole LC-MS with an Agilent 1260 Infinity liquid chromatograph equipped with a diode array detector. Sample volumes of 20 µL were separated on a Poroshell 120 EC C18 column (50 mm length x 4.6 mm internal diameter, 2.7 µm particle size, Agilent) at a flow rate of 0.4 mL/min using a linear elution program of 0 to 10% B over 20 min. Solvent A was H_2O + 0.05 % TFA and solvent B was MeCN + 0.05 % TFA. Under these conditions, the cyclic dinucleotides in extracts were found to elute always in the order of cdiG (7.3 ± 0.3 min), cAG (7.6 ± 0.3 min), and cdiA (7.9 ± 0.4 min), although there was variability in the retention times between runs. Thus, assignment of cyclic dinucleotide identity was made through analysis of the mass spectra.

Extract samples were analyzed by MS in the positive ion mode using the range of *m/z* = 600 to 800. When a broader range of 100 to 1000 *m/z* was used, the expected mass for the corresponding cyclic dinucleotide is present, but is not the most abundant ion peak observed, even for the standards. This observation suggests that the relative ionization of cyclic dinucleotides is low under these conditions, and furthermore the cyclic dinucleotides may not be fully resolved from other small molecules present in the extract. Thus the UV absorbance peaks detected at 254 nm may not be solely attributable to the cyclic dinucleotides.

Live Cell Imaging by Fluorescence Microscopy and Flow Cytometry
Constructs for testing the Gm0970-Spinach biosensors *in vivo* were created as described previously (section 3.5) by inserting the aptamers into a tRNA scaffold encoded within the pET31b plasmid. GSU0895 and GSU1658 genes were amplified from *G. sulfurreducens* genomic DNA using primers that added NdeI and XhoI restriction sites and cloned into the pCOLADuet-1 vector. Biosensors and dinucleotide cyclase enzymes encoded in pET24a or pCOLA plasmids were coexpressed in *E. coli* BL21 (DE3) Star cells (Life Technologies). Fluorescence microscopy experiments and image analyses were carried out as described previously (section 3.5).

Preparation of cell samples for flow cytometry was carried out in a similar manner to the microscopy procedure. Briefly, after inoculating fresh LB/Carb/Kan cultures from

overnight starter cultures, cells were grown to an OD_{600} ~ 0.5, then induced with 1 mM IPTG at 37 °C for 2 hrs. Cells were pelleted at room temperature for 4 min at 3,700 rcf, washed once with M9 minimal media at pH 7.0, and then resuspended in M9 minimal media containing 25 μM DFHBI to a final concentration of ~400 cells/μL based on OD_{600}. Cellular fluorescence was measured for 12,000-50,000 cells using either a BD Influx v7 cell sorter with BD FACS Sortware (Version 1.0.0.650) or a Guava easyCyte 8HT flow cytometer (Millipore) equipped with a 488 nm laser. The BD Influx v7 cell sorter is located in the Flow Cytometry Core Facilities at UC Berkeley.

REFERENCES

Abel, S., Bucher, T., Nicollier, M., Hug, I., Kaever, V., Abel Zur Wiesch, P., and Jenal, U. (2013). Bi-modal distribution of the second messenger c-di-GMP controls cell fate and asymmetry during the Caulobacter cell cycle. PLoS Genet. *9*, e1003744.

Ablasser, A., Goldeck, M., Cavlar, T., Deimling, T., Witte, G., Röhl, I., Hopfner, K.-P., Ludwig, J., and Hornung, V. (2013). cGAS produces a 2′-5′-linked cyclic dinucleotide second messenger that activates STING. Nature *498*, 380–384.

Ahmad, I., Lamprokostopoulou, A., Le Guyon, S., Streck, E., Barthel, M., Peters, V., Hardt, W.-D., and Römling, U. (2011). Complex c-di-GMP signaling networks mediate transition between virulence properties and biofilm formation in Salmonella enterica serovar Typhimurium. PLoS One *6*, e28351.

Aklujkar, M., Coppi, M. V, Leang, C., Kim, B.C., Chavan, M.A., Perpetua, L.A., Giloteaux, L., Liu, A., and Holmes, D.E. (2013). Proteins involved in electron transfer to Fe(III) and Mn(IV) oxides by Geobacter sulfurreducens and Geobacter uraniireducens. Microbiology *159*, 515–535.

Alatossava, T., Jütte, H., Kuhn, A., and Kellenberger, E. (1985). Manipulation of intracellular magnesium content in polymyxin B nonapeptide-sensitized Escherichia coli by ionophore A23187. J. Bacteriol. *162*, 413–419.

Ausmees, N., Mayer, R., Weinhouse, H., Volman, G., Amikam, D., Benziman, M., and Lindberg, M. (2001). Genetic data indicate that proteins containing the GGDEF domain possess diguanylate cyclase activity. FEMS Microbiol. Lett. *204*, 163–167.

Bai, Y., Yang, J., Zhou, X., Ding, X., Eisele, L.E., and Bai, G. (2012). Mycobacterium tuberculosis Rv3586 (DacA) is a diadenylate cyclase that converts ATP or ADP into c-di-AMP. PLoS One *7*, e35206.

Block, K.F., Hammond, M.C., and Breaker, R.R. (2010). Evidence for widespread gene control function by the ydaO riboswitch candidate. J. Bacteriol. *192*, 3983–3989.

Blount, K.F., and Breaker, R.R. (2006). Riboswitches as antibacterial drug targets. Nat. Biotechnol. *24*, 1558–1564.

Boles, B.R., and Mccarter, L.L. (2002). Vibrio parahaemolyticus scrABC, a Novel Operon Affecting Swarming and Capsular Polysaccharide Regulation. J. Bacteriol. *184*, 5946–5954.

Bonanni, P.S., Bradley, D.F., Schrott, G.D., and Busalmen, J.P. (2013). Limitations for current production in Geobacter sulfurreducens biofilms. ChemSusChem *6*, 711–720.

Bruce, R.A., Achenbach, L.A., and Coates, J.D. (1999). Reduction of (per)chlorate by a novel organism isolated from paper mill waste. Environ. Microbiol. *1*, 319–329.

Burdette, D.L., Monroe, K.M., Sotelo-Troha, K., Iwig, J.S., Eckert, B., Hyodo, M., Hayakawa, Y., and Vance, R.E. (2011). STING is a direct innate immune sensor of cyclic di-GMP. Nature *478*, 515–518.

Butler, J.E., Young, N.D., and Lovley, D.R. (2010). Evolution of electron transfer out of the cell : comparative genomics of six Geobacter genomes. BMC Genomics *11*, 1–12.

Butler, S.M., Nelson, E.J., Chowdhury, N., Faruque, S.M., Calderwood, S.B., and Camilli, A. (2006). Cholera stool bacteria repress chemotaxis to increase infectivity. Mol. Microbiol. *60*, 417–426.

Chatterjee, D., Cooley, R.B., Boyd, C.D., Mehl, R. a, O'Toole, G. a, and Sondermann, H. (2014). Mechanistic insight into the conserved allosteric regulation of periplasmic proteolysis by the signaling molecule cyclic-di-GMP. Elife *3*, e03650.

Chen, Z., and Schaap, P. (2012). The prokaryote messenger c-di-GMP triggers stalk cell differentiation in Dictyostelium. Nature *488*, 680–683.

Chin, K.H., Lee, Y.C., Tu, Z.L., Chen, C.H., Tseng, Y.H., Yang, J.M., Ryan, R.P., McCarthy, Y., Dow, J.M., Wang, A.H., et al. (2010). The cAMP receptor-like protein CLP is a novel c-di-GMP receptor linking cell-cell signaling to virulence gene expression in Xanthomonas campest- ris. J. Mol. Biol. *396*, 646–662.

Christen, M., Christen, B., Folcher, M., Schauerte, A., and Jenal, U. (2005). Identification and Characterization of a Cyclic di-GMP-specific Phosphodiesterase and Its Allosteric Control by GTP. J. Biol. Chem. *280*, 30829–30837.

Christen, M., Christen, B., Allan, M.G., Folcher, M., Jenö, P., Grzesiek, S., and Jenal, U. (2007). DgrA is a member of a new family of cyclic diguanosine monophosphate receptors and controls flagellar motor function in Caulobacter crescentus. Proc. Natl. Acad. Sci. U. S. A. *104*, 4112–4117.

Christen, M., Kulasekara, H.D., Christen, B., Kulasekara, B.R., Hoffman, L.R., and Miller, S.I. (2010). Asymmetrical distribution of the second messenger c-di-GMP upon bacterial cell division. Science *328*, 1295–1297.

Corrigan, R.M., and Gründling, A. (2013). Cyclic di-AMP: another second messenger enters the fray. Nat. Rev. Microbiol. *11*, 513–524.

Corrigan, R.M., Abbott, J.C., Burhenne, H., Kaever, V., and Gründling, A. (2011). c-di-AMP is a new second messenger in Staphylococcus aureus with a role in controlling cell size and envelope stress. PLoS Pathog. *7*, e1002217.

Corrigan, R.M., Campeotto, I., Jeganathan, T., Roelofs, K.G., Lee, V.T., and Gründling, A. (2013). Systematic identification of conserved bacterial c-di-AMP receptor proteins. Proc. Natl. Acad. Sci. U. S. A. *110*, 9084–9089.

Danilchanka, O., and Mekalanos, J.J. (2013). Cyclic dinucleotides and the innate immune response. Cell *154*, 962–970.

Davies, B.W., Bogard, R.W., Young, T.S., and Mekalanos, J.J. (2012). Coordinated Regulation of Accessory Genetic Elements Produces Cyclic Di-Nucleotides for V. cholerae Virulence. Cell *149*, 358–370.

Deng, Y., Schmid, N., Wang, C., Wang, J., Pessi, G., Wu, D., Lee, J., Aguilar, C., Ahrens, C.H., Chang, C., et al. (2012). Cis-2-dodecenoic acid receptor RpfR links quorum-sensing signal perception with regulation of virulence through cyclic dimeric guanosine monophosphate turnover. Proc. Natl. Acad. Sci. U. S. A. *109*, 15479–15484.

Diner, E.J., Burdette, D.L., Wilson, S.C., Monroe, K.M., Kellenberger, C.A., Hyodo, M., Hayakawa, Y., Hammond, M.C., and Vance, R.E. (2013). The innate immune DNA sensor cGAS produces a noncanonical cyclic dinucleotide that activates human STING. Cell Rep. *3*, 1355–1361.

Ding, Y.-H.R., Hixson, K.K., Giometti, C.S., Stanley, A., Esteve-Núñez, A., Khare, T., Tollaksen, S.L., Zhu, W., Adkins, J.N., Lipton, M.S., et al. (2006). The proteome of dissimilatory metal-reducing microorganism Geobacter sulfurreducens under various growth conditions. Biochim. Biophys. Acta *1764*, 1198–1206.

Ding, Y.-H.R., Hixson, K.K., Aklujkar, M.A., Lipton, M.S., Smith, R.D., Lovley, D.R., and Mester, T. (2008). Proteome of Geobacter sulfurreducens grown with Fe(III) oxide or Fe(III) citrate as the electron acceptor. Biochim. Biophys. Acta *1784*, 1935–1941.

Düvel, J., Bertinetti, D., Möller, S., Schwede, F., Morr, M., Wissing, J., Radamm, L., Zimmermann, B., Genieser, H.-G., Jänsch, L., et al. (2012). A chemical proteomics approach to identify c-di-GMP binding proteins in Pseudomonas aeruginosa. J. Microbiol. Methods *88*, 229–236.

Fang, X., Ahmad, I., Blanka, A., Schottkowski, M., Cimdins, A., Galperin, M.Y., Römling, U., and Gomelsky, M. (2014). GIL, a new c-di-GMP-binding protein domain involved in regulation of cellulose synthesis in enterobacteria. Mol. Microbiol. *93*, 439–452.

Ferreira, R.B.R., Antunes, L.C.M., Greenberg, E.P., and McCarter, L.L. (2008). Vibrio parahaemolyticus ScrC modulates cyclic dimeric GMP regulation of gene expression relevant to growth on surfaces. J. Bacteriol. *190*, 851–860.

Fowler, C.C., Brown, E.D., and Li, Y. (2010). Using a Riboswitch Sensor to Examine Coenzyme B12 Metabolism and Transport in E. coli. Chem. Biol. *17*, 756–765.

Gao, A., and Serganov, A. (2014). Structural insights into recognition of c-di-AMP by the ydaO riboswitch. Nat. Chem. Biol. *10*, 787–792.

Gao, P., Ascano, M., Wu, Y., Barchet, W., Gaffney, B.L., Zillinger, T., Serganov, A.A., Liu, Y., Jones, R.A., Hartmann, G., et al. (2013a). Cyclic [G(2',5')pA(3',5')p] is the metazoan second messenger produced by DNA-activated cyclic GMP-AMP synthase. Cell *153*, 1094–1107.

Gao, P., Ascano, M., Zillinger, T., Wang, W., Dai, P., Serganov, A.A., Gaffney, B.L., Shuman, S., Jones, R.A., Deng, L., et al. (2013b). Structure-function analysis of STING activation by c[G(2',5')pA(3',5')p] and targeting by antiviral DMXAA. Cell *154*, 748–762.

Gomelsky, M. (2011). cAMP, c-di-GMP, c-di-AMP and now cGMP: bacteria use them all! Mol. Microbiol. *79*, 562–565.

Gomelsky, M., and Klug, G. (2002). BLUF: a novel FAD-binding domain involved in sensory transduction in microorganisms. Trends Biochem. Sci. *27*, 497–500.

Gray, P.M., Forrest, G., Wisniewski, T., Porter, G., Freed, D.C., Demartino, J.A., Zaller, D.M., Guo, Z., Leone, J., Fu, T.-M., et al. (2012). Evidence for cyclic diguanylate as a vaccine adjuvant with novel immunostimulatory activities. Cell. Immunol. *278*, 113–119.

Gu, H., Furukawa, K., and Breaker, R.R. (2012). Engineered Allosteric Ribozymes That Sense the Bacterial Second Messenger Cyclic Diguanosyl 5′-Monophosphate. Anal. Chem. *84*, 4935–4941.

Habazettl, J., Allan, M.G., Jenal, U., and Grzesiek, S. (2011). Solution structure of the PilZ domain protein PA4608 complex with cyclic di-GMP identifies charge clustering as molecular readout. J. Biol. Chem. *286*, 14304–14314.

Hansen, K., Prabakaran, T., Laustsen, A., Jørgensen, S.E., Rahbæk, S.H., Jensen, S.B., Nielsen, R., Leber, J.H., Decker, T., Horan, K. a, et al. (2014). Listeria monocytogenes induces IFNβ expression through an IFI16-, cGAS- and STING-dependent pathway. EMBO J. *33*, 1654–1666.

Hengge, R. (2009). Principles of c-di-GMP signalling in bacteria. Nat. Rev. Microbiol. *7*, 263–273.

Heppell, B., and Lafontaine, D.A. (2008). Folding of the SAM Aptamer is Determined by the Formation of a K-turn-dependent Pseudoknot. Biochemistry *47*, 1490–1499.

Ho, C.L., Chong, K.S.J., Oppong, J.A., Chuah, M.L.C., Tan, S.M., and Liang, Z.-X. (2013). Visualizing the perturbation of cellular cyclic di-GMP levels in bacterial cells. J. Am. Chem. Soc. *135*, 566–569.

Hobley, L., Fung, R.K.Y., Lambert, C., Harris, M.A.T.S., Dabhi, J.M., King, S.S., Basford, S.M., Uchida, K., Till, R., Ahmad, R., et al. (2012). Discrete cyclic di-GMP-dependent control of bacterial predation versus axenic growth in Bdellovibrio bacteriovorus. PLoS Pathog. *8*, e1002493.

Huang, C.-J., Wang, Z.-C., Huang, H.-Y., Huang, H.-D., and Peng, H.-L. (2013). YjcC, a c-di-GMP phosphodiesterase protein, regulates the oxidative stress response and virulence of Klebsiella pneumoniae CG43. PLoS One *8*, e66740.

Huang, H., Suslov, N.B., Li, N.-S., Shelke, S.A., Evans, M.E., Koldobskaya, Y., Rice, P.A., and Piccirilli, J.A. (2014). A G-quadruplex-containing RNA activates fluorescence in a GFP-like fluorophore. Nat. Chem. Biol. *10*, 686–691.

Kalia, D., Merey, G., Nakayama, S., Zheng, Y., Zhou, J., Luo, Y., Guo, M., Roembke, B.T., and Sintim, H.O. (2012). Nucleotide, c-di-GMP, c-di-AMP, cGMP, cAMP, (p)ppGpp signaling in bacteria and implications in pathogenesis. Chem. Soc. Rev.

Kamegaya, T., Kuroda, K., and Hayakawa, Y. (2011). Identification of a Streptococcus pyogenes SF370 Gene Involved in Production of C-Di-AMP. J. Med. Sci. *73*, 49–57.

Karns, K., Vogan, J.M., Qin, Q., Hickey, S.F., Wilson, S.C., Hammond, M.C., and Herr, A.E. (2013). Microfluidic Screening of Electrophoretic Mobility Shifts Elucidates Riboswitch Binding Function. *135*, 3136–3143.

Kazmierczak, B.I., Lebron, M.B., and Murray, T.S. (2013). Analysis of FimX, a phosphodiesterase that governs twitching motility in Pseudomonas aeruginosa. Mol. Microbiol. *60*, 1026–1043.

Kellenberger, C.A., and Hammond, M.C. In vitro Analysis of Riboswitch-Spinach Aptamer Fusions as Metabolite-Sensing Fluorescent Biosensors. Methods Enzymol. *in press*.

Kellenberger, C.A., Wilson, S.C., Sales-Lee, J., and Hammond, M.C. (2013). RNA-based fluorescent biosensors for live cell imaging of second messengers cyclic di-GMP and cyclic AMP-GMP. J. Am. Chem. Soc. *135*, 4906–4909.

Kim, B.-S., Jeon, Y.-S., and Chun, J. (2013). Current status and future promise of the human microbiome. Pediatr. Gastroenterol. Hepatol. Nutr. *16*, 71–79.

Krasteva, P.V., Fong, J.C., Shikuma, N.J., Beyhan, S., Navarro, M. V, Yildiz, F.H., and Sondermann, H. (2010). Vibrio cholerae VpsT regulates matrix production and motility by directly sensing cyclic di-GMP. Science *327*, 866–868.

Krasteva, P.V., Giglio, K.M., and Sondermann, H. (2012). Sensing the messenger: The diverse ways that bacteria signal through c-di-GMP. Protein Sci. *000*, 1–20.

Kulasekara, H., Lee, V., Brencic, A., Liberati, N., Urbach, J., Miyata, S., Lee, D.G., Neely, A.N., Hyodo, M., Hayakawa, Y., et al. (2006). Analysis of Pseudomonas aeruginosa diguanylate cyclases and phosphodiesterases reveals a role for bis-(3'-5')-cyclic-GMP in virulence. Proc. Natl. Acad. Sci. U. S. A. *103*, 2839–2844.

Kulshina, N., Baird, N.J., and Ferré-D'Amaré, A.R. (2009). Recognition of the bacterial second messenger cyclic diguanylate by its cognate riboswitch. Nat. Struct. Mol. Biol. *16*, 1212–1217.

Lauer, P., Chow, M.Y.N., Loessner, M.J., Portnoy, D.A., and Calendar, R. (2002). Construction Characterization and Use of Two Listeria monocytogenes Site-Specific Phage Integration Vectors. J. Bacteriol. *184*, 4177–4186.

Lee, V.T., Matewish, J.M., Kessler, J.L., Hyodo, M., Hayakawa, Y., and Lory, S. (2007). A cyclic-di-GMP receptor required for bacterial exopolysaccharide production. Mol. Microbiol. *65*, 1474–1484.

Li, T.-N., Chin, K.-H., Liu, J.-H., Wang, A.H.-J., and Chou, S.-H. (2009). XC1028 from Xanthomonas campestris adopts a PilZ domain-like structure without a c-di-GMP switch. Proteins *75*, 282–288.

Libanova, R., Becker, P.D., and Guzmán, C.A. (2012). Cyclic di-nucleotides: new era for small molecules as adjuvants. Microb. Biotechnol. *5*, 168–176.

Liu, N., Xu, Y., Hossain, S., Huang, N., Coursolle, D., Gralnick, J. a, and Boon, E.M. (2012). Nitric oxide regulation of cyclic di-GMP synthesis and hydrolysis in Shewanella woodyi. Biochemistry *51*, 2087–2099.

Lolicato, M., Bucchi, A., Arrigoni, C., Zucca, S., Nardini, M., Schroeder, I., Simmons, K., Aquila, M., DiFrancesco, D., Bolognesi, M., et al. (2014). Cyclic dinucleotides bind the C-linker of HCN4 to control channel cAMP responsiveness. Nat. Chem. Biol. *10*, 457–462.

Lonergan, D.J., Jenter, H.L., Coates, J.D., Phillips, E.J., Schmidt, T.M., and Lovley, D.R. (1996). Phylogenetic analysis of dissimilatory Fe(III)-reducing bacteria. J. Bacteriol. *178*, 2402–2408.

Lovley, D.R. (2008). The microbe electric: conversion of organic matter to electricity. Curr. Opin. Biotechnol. *19*, 564–571.

Lovley, D.R., and Coates, J.D. (1997). Bioremediation of metal contamination. Curr. Opin. Biotechnol. *8*, 285–289.

Lowden, M.J., Skorupski, K., Pellegrini, M., Chiorazzo, M.G., Taylor, R.K., and Kull, F.J. (2010). Structure of Vibrio cholerae ToxT reveals a mechanism for fatty acid regulation of virulence genes. Proc. Natl. Acad. Sci. U. S. A. *107*, 2860–2865.

Lu, X.-H., An, S.-Q., Tang, D.-J., McCarthy, Y., Tang, J.-L., Dow, J.M., and Ryan, R.P. (2012). RsmA Regulates Biofilm Formation in Xanthomonas campestris through a Regulatory Network Involving Cyclic di-GMP and the Clp Transcription Factor. PLoS One *7*, e52646.

Luo, Y., Zhou, J., Watt, S.K., Lee, V.T., Dayie, T.K., and Sintim, H.O. (2012). Differential binding of 2′-biotinylated analogs of c-di-GMP with c-di-GMP riboswitches and binding proteins. Mol. Biosyst. *8*, 772–778.

Lusk, J.E., Williams, R.J.P., and Kennedy, E.P. (1968). Magnesium and the Growth of Escherichia coli. J. Biol. Chem. *243*, 2618–2624.

Malone, J.G., Williams, R., Christen, M., Jenal, U., Spiers, A.J., and Rainey, P.B. (2007). The structure-function relationship of WspR, a Pseudomonas fluorescens response regulator with a GGDEF output domain. Microbiology *153*, 980–994.

Massie, J.P., Reynolds, E.L., Koestler, B.J., Cong, J.-P., Agostoni, M., and Waters, C.M. (2012). Quantification of high-specificity cyclic diguanylate signaling. Proc. Natl. Acad. Sci. U. S. A. *109*, 12746–12751.

Mehta, T., Coppi, M. V, Childers, S.E., and Lovley, D.R. (2005). Outer Membrane c-Type Cytochromes Required for Fe (III) and Mn (IV) Oxide Reduction in Geobacter sulfurreducens. Appl. Environ. Microbiol. *71*, 8634–8641.

Nakayama, S., Kelsey, I., Wang, J., Roelofs, K., Stefane, B., Luo, Y., Lee, V.T., and Sintim, H.O. (2011). Thiazole orange-induced c-di-GMP quadruplex formation facilitates a simple fluorescent detection of this ubiquitous biofilm regulating molecule. J. Am. Chem. Soc. *133*, 4856–4864.

Nakayama, S., Roelofs, K., Lee, V.T., and Sintim, H.O. (2012a). A C-di-GMP–proflavine–hemin supramolecular complex has peroxidase activity-implication for a simple colorimetric detection. Mol. Biosyst. *8*, 726–729.

Nakayama, S., Luo, Y., Zhou, J., Dayie, T.K., and Sintim, H.O. (2012b). Nanomolar fluorescent detection of c-di-GMP using a modular aptamer strategy. Chem. Commun. (Camb). *48*, 9059–9061.

Nausch, L.W.M., Ledoux, J., Bonev, A.D., Nelson, M.T., and Dostmann, W.R. (2008). Differential patterning of cGMP in vascular smooth muscle cells revealed by single GFP-linked biosensors. Proc. Natl. Acad. Sci. U. S. A. *105*, 365–370.

Nelson, J.W., Sudarsan, N., Furukawa, K., Weinberg, Z., Wang, J.X., and Breaker, R.R. (2013). Riboswitches in eubacteria sense the second messenger c-di-AMP. Nat. Chem. Biol. *9*, 834–839.

Nelson, J.W., Sudarsan, N., Phillips, G.E., Stav, S., Lünse, C.E., McCown, P.J., and Breaker, R.R. (2014). Control of Exoelectrogenesis in Geobacter spp. by c-AMP-GMP. *in press*.

Oppenheimer-Shaanan, Y., Wexselblatt, E., Katzhendler, J., Yavin, E., and Ben-Yehuda, S. (2011). c-di-AMP reports DNA integrity during sporulation in Bacillus subtilis. EMBO Rep. *12*, 594–601.

Paige, J.S., Wu, K.Y., and Jaffrey, S.R. (2011). RNA Mimics of Green Fluorescent Protein. Science *333*, 642–646.

Paige, J.S., Nguyen-Duc, T., Song, W., and Jaffrey, S.R. (2012). Fluorescence Imaging of Cellular Metabolites with RNA. Science *335*, 1194.

Pan, Y., Duncombe, T.A., Kellenberger, C.A., Hammond, M.C., and Herr, A.E. (2014). High-throughput electrophoretic mobility shift assays for quantitative analysis of molecular binding reactions. Anal. Chem. *in press*.

Plate, L., and Marletta, M.A. (2012). Nitric oxide modulates bacterial biofilm formation through a multicomponent cyclic-di-GMP signaling network. Mol. Cell *46*, 449–460.

Ponchon, L., and Dardel, F. (2007). Recombinant RNA technology: the tRNA scaffold. Nat. Methods *4*, 571–576.

Pukatzki, S., and Provenzano, D. (2013). Vibrio cholerae as a predator: lessons from evolutionary principles. Front. Microbiol. *4*, 384.

Rao, F., See, R.Y., Zhang, D., Toh, D.C., Ji, Q., and Liang, Z.-X. (2010). YybT Is a Signaling Protein That Contains a Cyclic Dinucleotide Phosphodiesterase Domain and a GGDEF Domain with ATPase Activity. J. Biol. Chem. *285*, 473–482.

Regulski, E.E., and Breaker, R.R. (2008). In-line probing analysis of riboswitches. Methods Mol. Biol. *419*, 53–67.

Ren, A., and Patel, D.J. (2014). c-di-AMP binds the ydaO riboswitch in two pseudo-symmetry-related pockets. Nat. Chem. Biol. *10*, 780–786.

Roelofs, K.G., Wang, J., Sintim, H.O., and Lee, V.T. (2011). Differential radial capillary action of ligand assay for high-throughput detection of protein-metabolite interactions. Proc. Natl. Acad. Sci. U. S. A. *108*, 15528–15533.

Roembke, B.T., Zhou, J., Zheng, Y., Sayre, D., Lizardo, A., Bernard, L., and Sintim, H.O. (2014). Molecular BioSystems a general fluorescent sensor for c-di-GMP and. Mol. Biosyst.

Römling, U., Galperin, M.Y., and Gomelsky, M. (2013). Cyclic di-GMP : the First 25 Years of a Universal Bacterial Second Messenger Cyclic di-GMP : the First 25 Years of a Universal Bacterial. Microbiol. Mol. Biol. Rev. *77*, 1–52.

Ross, P., Weinhouse, H., Aloni, Y., Michaeli, D., Weinberger-Ohana, P., Mayer, R., Braun, S., do Vroom, E., van der Marel, G.A., van Boom, J.H., et al. (1987). Regulation of cellulose synthesis in Acetobacter xylinum by cyclic diguanylic acid. Nature *325*, 279–281.

Ryjenkov, D.A., Simm, R., Römling, U., and Gomelsky, M. (2006). The PilZ domain is a receptor for the second messenger c-di-GMP: the PilZ domain protein YcgR controls motility in enterobacteria. J. Biol. Chem. *281*, 30310–30314.

Sadhu, M.J., Guan, Q., Sales-Lee, J., Iavarone, A.T., Hammond, M.C., Cande, W.Z., and Rine, J. (2013). Nutritional control of epigenetic processes in yeast and human cells. Genetics *195*, 831–844.

Schaap, P. (2013). Cyclic di-nucleotide signaling enters the eukaryote domain. IUBMB Life *65*, 897–903.

Seshasayee, A.S.N., Fraser, G.M., and Luscombe, N.M. (2010). Comparative genomics of cyclic-di-GMP signalling in bacteria: post-translational regulation and catalytic activity. Nucleic Acids Res. *38*, 5970–5981.

Shanahan, C.A., Gaffney, B.L., Jones, R.A., and Strobel, S.A. (2011). Differential Analogue Binding by Two Classes of c-di-GMP Riboswitches. J. Am. Chem. Soc. *133*, 15578–15592.

Simm, R., Morr, M., Remminghorst, U., Andersson, M., and Romling, U. (2009). Quantitative determination of cyclic diguanosine monophosphate concentrations in nucleotide extracts of bacteria by matrix-assisted laser desorption/ionization–time-of-flight mass spectrometry. Anal. Biochem. *386*, 53–58.

Smith, K.D., Lipchock, S. V, Ames, T.D., Wang, J., Breaker, R.R., and Strobel, S. a (2009). Structural basis of ligand binding by a c-di-GMP riboswitch. Nat. Struct. Mol. Biol. *16*, 1218–1223.

Smith, K.D., Lipchock, S. V, Livingston, A.L., Shanahan, C.A., and Strobel, S.A. (2010). Structural and biochemical determinants of ligand binding by the c-di-GMP riboswitch . Biochemistry *49*, 7351–7359.

Sommerfeldt, N., Possling, A., Becker, G., Pesavento, C., Tschowri, N., and Hengge, R. (2009). Gene expression patterns and differential input into curli fimbriae regulation of all GGDEF/EAL domain proteins in Escherichia coli. Microbiology *155*, 1318–1331.

Song, W., Strack, R.L., Svensen, N., and Jaffrey, S.R. (2014). Plug-and-Play Fluorophores Extend the Spectral Properties of Spinach. J. Am. Chem. Soc. *136*, 1198–1201.

Spangler, C., Böhm, A., Jenal, U., Seifert, R., and Kaever, V. (2010). A liquid chromatography-coupled tandem mass spectrometry method for quantitation of cyclic di-guanosine monophosphate. J. Microbiol. Methods *81*, 226–231.

Stelitano, V., Brandt, A., Fernicola, S., Franceschini, S., Giardina, G., Pica, A., Rinaldo, S., Sica, F., and Cutruzzolà, F. (2013). Probing the activity of diguanylate cyclases and c-di-GMP phosphodiesterases in real-time by CD spectroscopy. Nucleic Acids Res. *41*, e79.

Strack, R.L., Disney, M.D., and Jaffrey, S.R. (2013). A superfolding Spinach2 reveals the dynamic nature of trinucleotide repeat–containing RNA. Nat. Methods *10*, 1219–1224.

Sudarsan, N., Hammond, M.C., Block, K.F., Welz, R., Barrick, J.E., Roth, A., and Breaker, R.R. (2006). Tandem Riboswitch Architectures Exhibit Complex Gene Control Functions. Science *314*, 300–304.

Sudarsan, N., Lee, E.R., Weinberg, Z., Moy, R.H., Kim, J.N., Link, K.H., and Breaker, R.R. (2008). Riboswitches in eubacteria sense the second messenger cyclic di-GMP. Science *321*, 411–413.

Sun, L., Wu, J., Du, F., Chen, X., and Chen, Z.J. (2013). Cyclic GMP-AMP synthase is a cytosolic DNA sensor that activates the type I interferon pathway. Science *339*, 786–791.

Sureka, K., Choi, P.H., Precit, M., Delince, M., Pensinger, D. a., Huynh, T.N., Jurado, A.R., Goo, Y.A., Sadilek, M., Iavarone, A.T., et al. (2014). The Cyclic Dinucleotide c-di-AMP Is an Allosteric Regulator of Metabolic Enzyme Function. Cell *158*, 1389–1401.

Svindland, S.C., Pedersen, G.K., Pathirana, R.D., Bredholt, G., Nøstbakken, J.K., Jul-Larsen, A., Guzmán, C. a, Montomoli, E., Lapini, G., Piccirella, S., et al. (2012). A study of Chitosan and c-di-GMP as mucosal adjuvants for intranasal influenza H5N1 vaccine. Influenza Other Respi. Viruses 1–13.

Tarutina, M., Ryjenkov, D.A., and Gomelsky, M. (2006). An unorthodox bacteriophytochrome from Rhodobacter sphaeroides involved in turnover of the second messenger c-di-GMP. J. Biol. Chem. *281*, 34751–34758.

Tischler, A.D., and Camilli, A. (2004). Cyclic diguanylate (c-di-GMP) regulates Vibrio cholerae biofilm formation. Mol. Microbiol. *53*, 857–869.

Topp, S., Reynoso, C.M.K., Seeliger, J.C., Goldlust, I.S., Desai, S.K., Murat, D., Shen, A., Puri, A.W., Komeili, A., Bertozzi, C.R., et al. (2010). Synthetic Riboswitches That Induce Gene Expression in Diverse Bacterial Species. Appl. Environ. Microbiol. *76*, 7881–7884.

Tremblay, P., Summers, Z.M., Glaven, R.H., Nevin, K.P., Zengler, K., Barrett, C.L., Qiu, Y., Palsson, B.O., and Lovley, D.R. (2011). A c-type cytochrome and a transcriptional regulator responsible for enhanced extracellular electron transfer in Geobacter sulfurreducens revealed by adaptive evolution. *13*, 13–23.

Vargas, M., Malvankar, N.S., Tremblay, P., Amino, A., Required, A., Conductivity, P., Transport, L.E.E., This, S., Feeds, R.S.S., and Journal, A.S.M. (2013). Aromatic Amino Acids Required for Pili Conductivity and Long- Range Extracellular Electron Transport in Geobacter sulfurreducens.

Wallace, B.D., and Redinbo, M.R. The human microbiome is a source of therapeutic drug targets. Curr. Opin. Chem. Biol. *17*, 379–384.

Warner, K.D., Chen, M.C., Song, W., Strack, R.L., Thorn, A., Jaffrey, S.R., and Ferré-D'Amaré, A.R. (2014). Structural basis for activity of highly efficient RNA mimics of green fluorescent protein. Nat. Struct. Mol. Biol. *21*, 658–663.

Weber, H., Pesavento, C., Possling, A., Tischendorf, G., and Hengge, R. (2006). Cyclic-di-GMP-mediated signalling within the σS network of Escherichia coli. Mol. Microbiol. *62*, 1014–1034.

Weinberg, Z., Barrick, J.E., Yao, Z., Roth, A., Kim, J.N., Gore, J., Wang, J.X., Lee, E.R., Block, K.F., Sudarsan, N., et al. (2007). Identification of 22 candidate structured RNAs in bacteria using the CMfinder comparative genomics pipeline. Nucleic Acids Res. *35*, 4809–4819.

Welz, R., and Breaker, R.R. (2007). Ligand binding and gene control characteristics of tandem riboswitches in Bacillus anthracis. RNA *13*, 573–582.

Wilksch, J.J., Yang, J., Clements, A., Gabbe, J.L., Short, K.R., Cao, H., Cavaliere, R., James, C.E., Whitchurch, C.B., Schembri, M. a, et al. (2011). MrkH, a novel c-di-GMP-dependent transcriptional activator, controls Klebsiella pneumoniae biofilm formation by regulating type 3 fimbriae expression. PLoS Pathog. *7*, e1002204.

Wilson, S.C., Cohen, D.T., Wang, X.C., and Hammond, M.C. (2014). A neutral pH thermal hydrolysis method for quantification of structured RNAs. RNA *20*, 1153–1160.

Witte, C.E., Whiteley, A.T., Burke, T.P., Sauer, J.-D., Portnoy, D.A., and Woodward, J.J. (2013). Cyclic di-AMP Is Critical for Listeria monocytogenes Growth, Cell Wall Homeostasis, and Establishment of Infection. MBio *4*.

Witte, G., Hartung, S., Büttner, K., and Hopfner, K.-P. (2008). Structural biochemistry of a bacterial checkpoint protein reveals diadenylate cyclase activity regulated by DNA recombination intermediates. Mol. Cell *30*, 167–178.

Wood, S., Ferré-D'Amaré, A.R., and Rueda, D. (2012). Allosteric tertiary interactions preorganize the c-di-GMP riboswitch and accelerate ligand binding. ACS Chem. Biol. *7*, 920–927.

Woodward, J.J., Iavarone, A.T., and Portnoy, D.A. (2010). c-di-AMP secreted by intracellular Listeria monocytogenes activates a host type I interferon response. Science *328*, 1703–1705.

Wu, J., Sun, L., Chen, X., Du, F., Shi, H., Chen, C., and Chen, Z.J. (2013). Cyclic GMP-AMP is an endogenous second messenger in innate immune signaling by cytosolic DNA. Science *339*, 826–830.

Wu, X., Wu, F., Wang, X., Wang, L., Siedow, J.N., Zhang, W., and Pei, Z. (2014). Molecular evolutionary and structural analysis of the cytosolic DNA sensor cGAS and STING. *1*, 1–15.

Zhang, L., Li, W., and He, Z.G. (2013a). DarR, a TetR-like transcriptional factor, is a cyclic di-AMP-responsive repressor in Mycobacterium smegmatis. J. Biol. Chem. *288*, 3085–3096.

Zhang, X., Shi, H., Wu, J., Zhang, X., Sun, L., Chen, C., and Chen, Z.J. (2013b). Cyclic GMP-AMP containing mixed phosphodiester linkages is an endogenous high-affinity ligand for STING. Mol. Cell *51*, 226–235.

Zhou, J., Sayre, D.A., Zheng, Y., Szmacinski, H., and Sintim, H.O. (2014). Unexpected complex formation between coralyne and cyclic diadenosine monophosphate providing a simple fluorescent turn-on assay to detect this bacterial second messenger. Anal. Chem. *86*, 2412–2420.